A Functional Model for Primary Visual Cortex

Nastaran Hesam Shariati

A thesis submitted in partial fulfilment of the requirements for the degree of Doctor of Philosophy

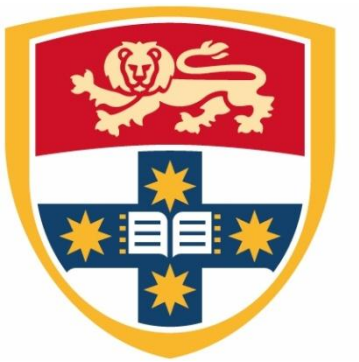

Discipline of Biomedical Science

Faculty of Medicine

The University of Sydney

Acknowledgements

My utmost gratitude goes to God, the Almighty, without whose mercy and blessing, this work would not have been possible. I would like to express my sincere gratitude to my supervisor Dr. Alan Freeman, for his invaluable guidance, many fruitful discussions and constant support in making this research possible over the years. I would like to thank my associate supervisor Dr. Aaron Camp for his guidance, and help during my thesis writing. My deep appreciation goes to my associate supervisor and friend Dr. Jin Huang for her continuous support, encouragement and advice during my stressful moment. I offer my regards to Prof. Fazlul Huq and Dr. Peter Knight for their valuable support and advices.

My special appreciation is extended to my beloved husband who was given me the reason, encouragement and inspiration to continue my work during the most stressful time of my life. To whom he was patient with me and understands my moodiness, allowing me to cover the whole house with my papers and books. To you, I dedicate this thesis.

I would like to express my respect and sincere gratitude to the lovely, and kind technical and admin staff at Bio – Felicia, Ruth, Ann, Gautham, Natasha, Helen and Tuyet – for creating a nice, helpful and supportive environment for students.

I am in debt to my lab mates, Munira, Padma and Elaine, for making the laboratory such an enjoyable environment to work in. My special thanks to my best friend, Paul, for his friendship and his constant technical support.

My heartfelt thanks are for my father and mother who keep supporting me from far by their precious encouragement. To my sisters and brother for their continuous support and encouragement throughout my study.

I would like to thank my angel daughter, Helia, who understood that I am under pressure especially during my thesis writing and tried to encourage me with her heartfelt hugs. To whom she was the initial reason to step on this path.

Brief Contents

Detailed Contents

Summary

Many neurons in mammalian primary visual cortex have properties such as sharp tuning for contour orientation, strong selectivity for motion direction, and insensitivity to stimulus polarity, that are not shared with their sub-cortical counterparts. Successful models have been developed for a number of these properties but in one case, direction selectivity, there is no consensus about underlying mechanisms. This thesis describes a model that accounts for many of the empirical observations concerning direction selectivity. The model comprises a single column of cat primary visual cortex and a series of processing stages. Each neuron in the first cortical stage receives input from a small number of on-centre and off-centre relay cells in the lateral geniculate nucleus. Consistent with recent physiological evidence, the off-centre inputs to cortex precede the on-centre inputs by a small interval (~4 ms), and it is this difference that confers direction selectivity on model neurons. I show that the resulting model successfully matches the following empirical data: the proportion of cells that are direction selective; tilted spatiotemporal receptive fields; phase advance in the response to a stationary contrast-reversing grating stepped across the receptive field. The model also accounts for several other fundamental properties. Receptive fields have elongated subregions, orientation selectivity is strong, and the distribution of orientation tuning bandwidth across neurons is similar to that seen in the laboratory. Finally, neurons in the first stage have properties corresponding to simple cells, and more complex-like cells emerge in later stages. The results therefore show that a simple feed-forward model can account for a number of the fundamental properties of primary visual cortex.

Chapter 1. Background

Light enters the eye and is detected by photoreceptors before passing through further cell layers in the retina. Axons from the ganglion cell layer bundle together to form the optic nerve and send visual information to the lateral geniculate nucleus (LGN) of the thalamus. Visual signals are then relayed to the primary visual cortex in the occipital lobe (Figure 1.1) and perceived as colour, form, movement, or a combination of these.

Cells in the primary visual cortex (V1) have emergent properties that distinguish them from cells in the sub-cortical visual pathway. For example, while cells in the LGN respond to many types of stimuli, cells in V1 respond to much more specific stimulus features (including orientation, direction of motion, spatial and temporal frequency). The mechanism underlying this stimulus specificity has been the subject of investigation for more than 50 years.

This chapter describes in detail the visual pathway from retina to the primary visual cortex and includes current models of visual stimulus selectivity. Discussion will primarily be focused on experimental findings in cat, since this animal is the most widely used in anatomical and physiological investigation of the visual cortex. First, the anatomical and functional structure of sub-cortical cells from the retina to the LGN will be reviewed. Second, the anatomical and functional properties of cortical cells in V1 along with existing models for each stimulus feature will be discussed.

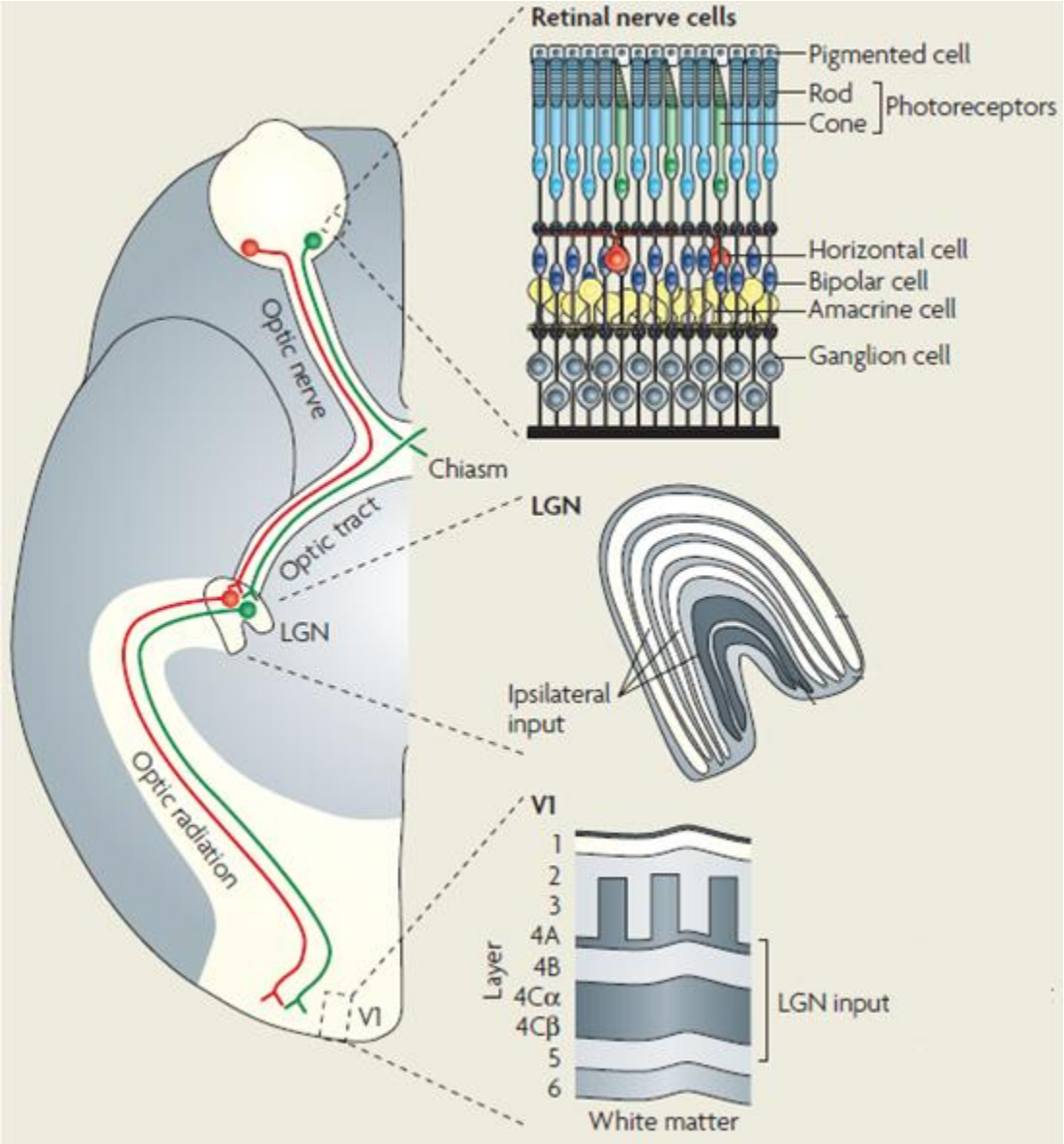

Figure 1.1: The direct visual pathway. The left panel shows the schematic visual pathway from retina to the primary visual cortex through the lateral geniculate nucleus (LGN). Ganglion cells from the temporal retina project to ipsilateral LGN (red lines) and those from the nasal retina project to contralateral LGN (green line). The right diagram (retinal nerve cells) shows the basic structure of the retina. Light entering the retina is absorbed by photoreceptors (rods and cones) and passes through bipolar cells to ganglion cells which provide the most direct visual pathway in the retina. Amacrine and horizontal cells mediate the lateral interactions. The axons of ganglion cells bundle together and form the optical nerve which synapses to the LGN of the thalamus. The axons of LGN neurons predominantly project to layer 4 of the primary visual cortex. The diagram applies to primates; details differ between primates and carnivores (Solomon & Lennie, 2007).

1.1. Retina

The retina is an intricate structure composed of at least five cell layers: photoreceptors, bipolar cells, horizontal cells, amacrine cells, and ganglion cells (Figure 1.1). Despite this, the most direct pathway for visual signals through retina is 1) photoreceptors, 2) bipolar cells, and 3) ganglion cells.

Once light enters the eye it passes through several retinal cell layers to stimulate photoreceptors located deep in the retina, beside the pigment epithelium (which absorbs the light not captured by the photoreceptors). Photoreceptors are divided into two subtypes: 1) rods that function mainly in the dim light and provide black and white vision, and 2) cones that are responsible for colour vision and associated high visual acuity in human. This research in this thesis focuses on the simulation of the visual properties of cat, given that the literature describing primary visual cortical function is richer for the domestic cat than for other species. Therefore, this chapter mostly reviews the cat's literature.

Unlike most other cells in the visual pathway rods and cones, do not fire action potentials. Instead, they respond to light with graded shifts in their membrane potential. Rods respond slowly to the light, that is, each photon of light summates over a long time, and allow detection of small changes in the light level. Cones, on the other hand, respond faster and provide greater temporal resolution of the visual image (Daw, 2012).

Bipolar cells transmit signals from the photoreceptors to ganglion cells directly or indirectly via amacrine cells. Like photoreceptors, bipolar cells respond to light with graded potentials rather than action potentials, and like photoreceptors, there are two types of bipolar cell: 1) rod bipolar cells that are associated with rods, and 2) cone bipolar cells that are associated with cones. Thus, each bipolar cell receives input from only one type of photoreceptor (Daw, 2012).

Unlike photoreceptors and bipolar cells, ganglion cells fire action potentials in response to light. As such, retinal ganglion cells are the output neurons of the retina, sending visual signals to the higher visual areas via the LGN (Daw, 2012).

Ganglion cells can also be characterized into one of two types based on the response to a spot of light applied to the receptive field (Figure 1.2). Kuffler (1953) described on-centre ganglion cells which fire action potentials in response to light directed to the centre of the receptive field, and off-centre ganglion cells which are excited when the light is turned off. Light extending beyond the centre of the receptive field attenuates the response of the cell.

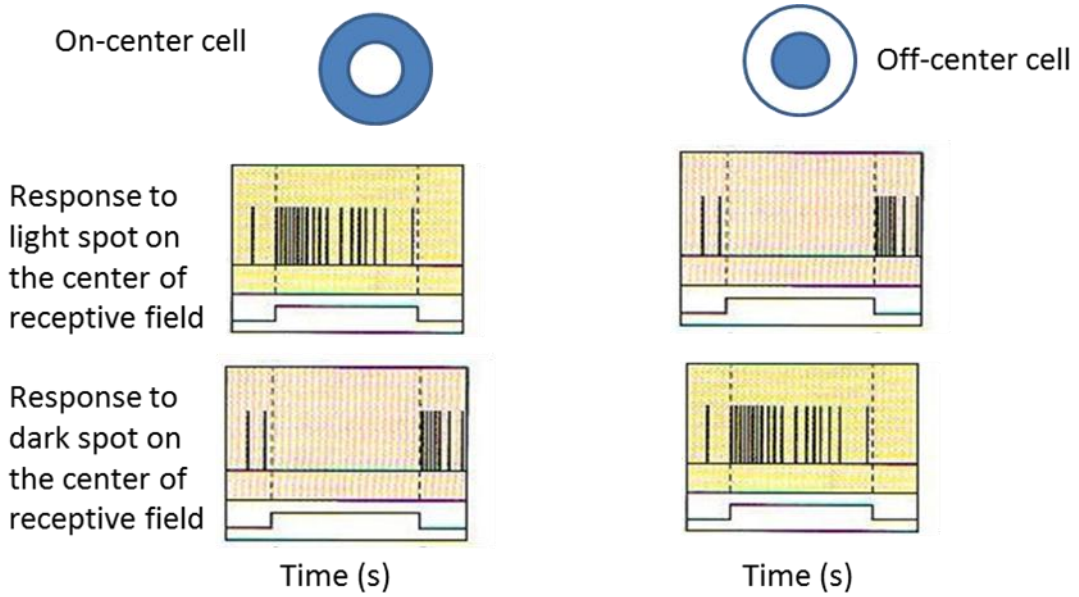

Figure 1.2: Retinal ganglion cell responses to a light or dark spot on the centre of the receptive field. On-centre cells fire vigorously in response to the light spot on the centre of the receptive field and reduce their firing for dark spot stimulus. Off-centre cells have the opposite reaction. (Adapted from http://retina.umh.es/webvision/GCPHYS1.HTM)

The characterization of ganglion cells was subsequently expanded in work by Kuffler (1953) and Enroth-Cugell and Robson (1966). They classified ganglion cells as either X- or Y-cells based on the spatial summation properties of the receptive field (X-cells summate linearly and Y-cells non-linearly), and showed that both X- and Y-cells display on- and off-centre characteristics. Later Stone and Hoffmann (1972) introduced another new physiological class of retinal ganglion cell called W cells, which have a slower conduction velocity than X and Y cells.

The properties of X and Y cells differ still further. X cells have longer latency (i.e. impulses take longer to travel from ganglion cells to the LGN), higher maintained

firing rate (40-70 spikes/s vs. 31 spikes/s) (Cleland & Levick, 1974, Enroth-Cugell & Robson, 1966, Kaplan, Purpura & Shapley, 1978), and behave like a low-pass filter in the temporal domain (Cleland, Dubin & Levick, 1971, Cleland & Levick, 1974).

Retinal ganglion cells are morphologically divided into three main types: 1) alpha, 2) beta, and 3) gamma (Boycott & Wässle, 1974). There is evidence (Boycott & Wässle, 1974, Levick, 1975) that morphologically classified alpha cells in cat are correlated with physiologically classified Y-cells, beta cells with X-cells, and gamma cells with W-cells (Boycott & Wässle, 1974).

Anatomically beta (X) cells have a small receptive field (0.5-3 deg) and are predominately located in the central region of the retina (Figure 1.3) with a lower density in peripheral regions. On the other hand, alpha (Y) cells have a larger receptive field (1-7 deg) (Boycott & Wässle, 1974, Enroth-Cugell & Robson, 1966, Levick, 1975, Stein, Johnson & Berson, 1996, Wässle, Boycott & Illing, 1981). Ultimately, these anatomical and morphological characteristics must serve to convey different information to the visual thalamus for subsequent integration.

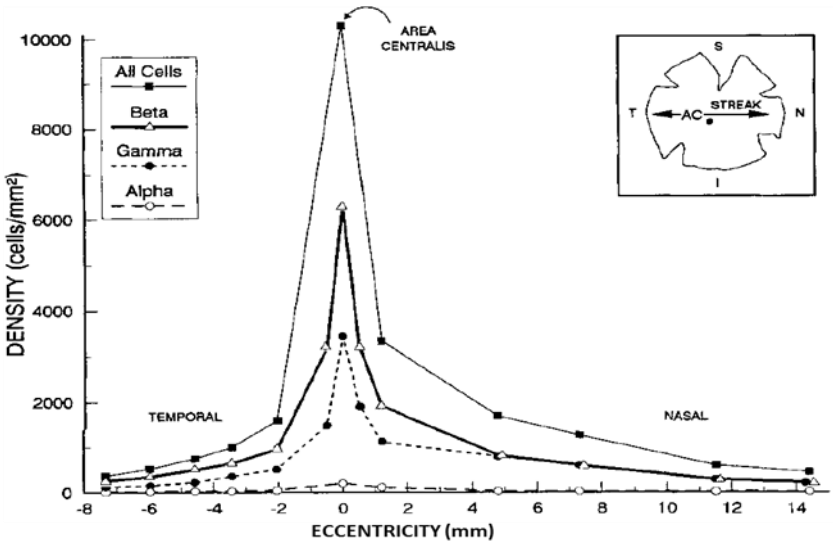

Figure 1.3: Retina ganglion cell density as a function of eccentricity (Stein et al., 1996). The density of all types of ganglion cells is high in the area centralis and reduces toward the periphery. Beta (X) cells have the highest density in the retina.

1.2. Lateral geniculate nucleus

As is the case for retinal ganglion cells, lateral geniculate nucleus neurons have concentric receptive fields with either on- or off-centres and antagonistic surrounds (Hubel & Wiesel, 1961, Kuffler, 1953). Based on their response, LGN neurons are classified as either X or Y cells. X cells, have high spatial resolution, sum their inputs linearly, and have sustained responses with longer latencies (time between the stimulus and the response). In comparison, Y cells have lower spatial resolution, non-linear spatial summation and a more transient response (i.e. shorter latencies) (Hubel & Wiesel, 1961, Saul & Humphrey, 1990). In addition to these differences, X and Y cells are divided into two sub-categories based on their timing response: 1) lagged 2) non-lagged. When compared with non-lagged cells, lagged cells generate a delayed response to the stimulus. For example, lagged X cells are delayed by about a quarter of cycle relative to non-lagged X cells at low temporal frequency (1 Hz), and this delay increases linearly with temporal frequency (Saul & Humphrey, 1990). Finally, since there is little difference between the response or size of receptive fields in the retina and those in the LGN, we can assume that LGN neurons inherit most of their spatial and temporal receptive field structure from the earlier parts of the visual pathway.

1.3. Retina to geniculate connection

Visual information is relayed from the retina to the primary visual cortex via two major channels: on, and off (Schiller, Sandell & Maunsell, 1986). The on and off pathways begin at the synapse between photoreceptors and bipolar cells, and converge on simple cells in the visual cortex. When a cone photoreceptor is illuminated, it becomes hyperpolarized and leads to the depolarization of an on-centre bipolar cell. Conversely, the off-centre bipolar cells are depolarized in response to the removal of stimuli. Each bipolar cell then makes synaptic connection with multiple ganglion cells of the same sign (i.e. on or off) (Figure 1.4). It has been shown that up to ten (average 2-3) retinal ganglion cells subsequently provide significant excitatory input to each geniculate neuron (Levick, Cleland & Dubin, 1972, Mastronarde, 1987b, Reid & Usrey, 2004, Usrey, Reppas & Reid, 1999), although some (Mastronarde, 1987a, Usrey et al., 1999) have shown that single neurons in the LGN receive strong input

from only one or two retinal ganglion cells and very weak inputs from others. The former data was obtained at eccentricities from 2 to 8 degrees while the latter result was acquired from 5 to 25 degrees eccentricity.

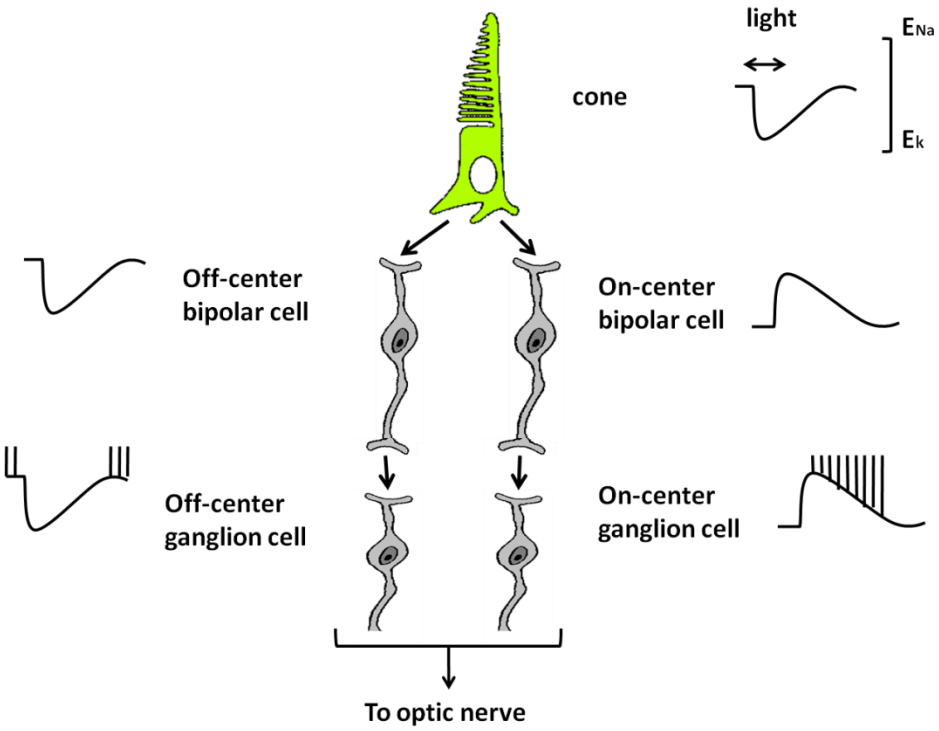

Figure 1.4: A light stimulus causes the hyperpolarisation of cone and depolarization of the on-centre bipolar cells which consequently results in firing on-centre ganglion cells. On the other hand, a light stimulus reduces impulse rate in the off-pathway (Kandel, Schwartz & T.M., 1991).

1.4. Simple and complex cells in the primary visual cortex

Cells in the primary visual cortex (V1) respond differently from retinal and geniculate cells. For example, a spot of light is a weak stimulus for cortical cells. Instead, these cells prefer more structured stimuli such as bars or lines and, as such, the excitatory and inhibitory regions of their receptive fields are arranged differently to cells earlier in the visual pathway.

Hubel and Wiesel (1962) identified two types of cells based on their receptive field structures: simple and complex cells. They made this identification by defining a

receptive field subfield as the area in which either dark or light stimuli yielded a response. Simple and complex cells were characterised based on two criteria: 1) subfield separation, and 2) summation within a subfield. Simple cells have two or more separate subfields with linear spatial summation across each subfield, while complex cells have overlapping on- and off-subfields with non-linear spatial summation.

Simple cells are similar to retinal ganglion cells and LGN neurons in that they have distinct excitatory and inhibitory regions. However, the spatial arrangement of excitatory and inhibitory regions is profoundly different (Figure 1.5). In simple cells, these regions are arranged side by side and are separated by straight-line boundaries rather than the circular ones observed earlier in the pathway. Essentially, simple cells have elongated excitatory (on) and inhibitory (off) subfields. To elicit an optimal response in a simple cortical cell, the stimulus must completely illuminate the subfield; therefore, the position and orientation of the stimulus is crucial (see Figure 1.6).

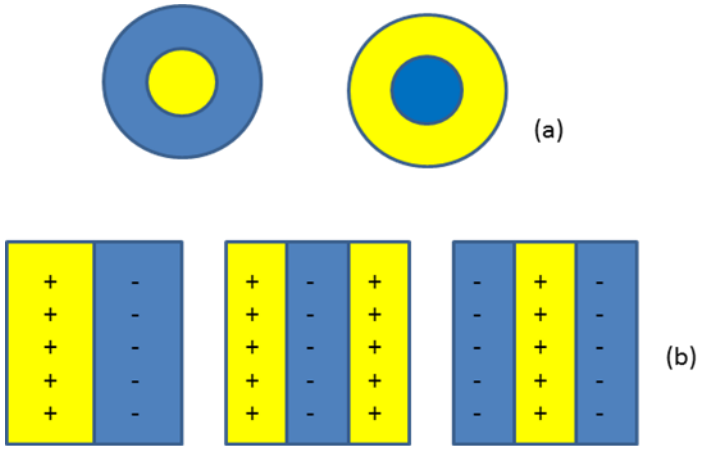

Figure 1.5: Schematic receptive field of (a) on- and off-centre LGN cells (b) simple cells. LGN cells have centre-surround organization while simple cells have elongated, separated subfields. Adapted from Hubel and Wiesel (1962).

Simple cells display linear spatial summation within each sub-region. That is, the response evoked by a bright bar presented in the excitatory region increases with the size or intensity of the stimulus. This property was implicitly described by Hubel and

Wiesel (1962) and explicitly explained by Movshon et al. (1978c) and Dean and Tolhurst (1983). The response of a simple cell to two stimuli presented simultaneously to an excitatory sub-field was equal to the sum of the individual responses to two stimuli presented individually. When stimuli extend beyond the excitatory sub-field the response of the cell was attenuated.

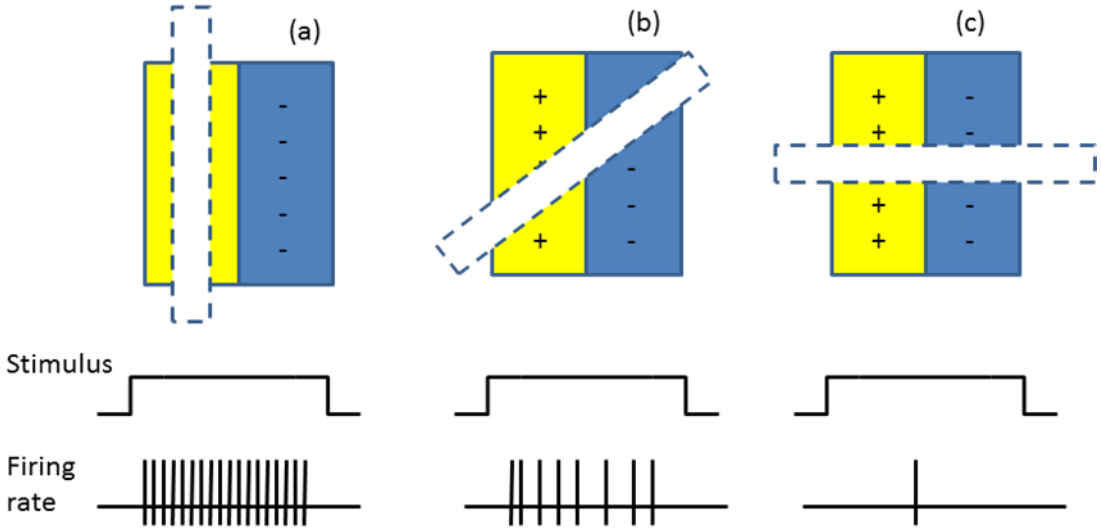

Figure 1.6: Response of a simple cell to a bright bar stimulus in different orientations. (a) The cell responds vigorously to a vertical stimulus at the same orientation as the on-subfield. b) Few impulses are evoked in response to a tilted stimulus (c) No impulse in response to an orthogonal stimulus. Adapted from Hubel and Wiesel (1962).

Complex cells, on the other hand, have predominately overlapping excitatory and inhibitory subfields (but see Martinez et al. 2005). They give 'on-off' responses to stimuli presented anywhere in their receptive field. This means that the geometry of the optimal spatial stimulus cannot be predicted purely from the arrangement of sub-regions. While the optimal stimulus for a simple cell is one that almost fills the most sensitive region of its receptive field, for complex cells it is usually significantly smaller than the receptive field. As such, complex cells summate inputs non-linearly.

1.4.1. Laminar location and synaptic connections

There is consensus that the majority of cells in layer 4 of the primary visual cortex are simple cells (Ferster & Lindstrom, 1983, Gilbert, 1977, Gilbert & Wiesel, 1979, Hirsch, Alonso, Reid & Martinez, 1998, Hubel & Wiesel, 1962, Martinez, Alonso,

Reid & Hirsch, 2002). As was predicted by Hubel and Wiesel (1962), simple cells receive monosynaptic inputs from LGN neurons (Bullier & Henry, 1979, Ferster & Lindstrom, 1983, Martinez, Wang, Reid, Pillai, Alonso, Sommer & Hirsch, 2005, Reid & Alonso, 1995, Tanaka, 1983). Recently, Martinez et al. (2005) proved by morphological and quantitative measurements that the simple cells found in upper layer 6 receive direct inputs from geniculate cells as well.

Layer 2 and 3 and layer 5 consist mainly of complex cells (Gilbert, 1977, Martinez et al., 2002). Cells in layer 2 and 3 receive their major inputs from simple cells in layer 4 and the majority of complex cells in layer 5 receive their inputs from layer 2 and 3 (Alonso & Martinez, 1998, Gilbert & Wiesel, 1979, Hirsch et al., 1998, Martinez et al., 2002). There is evidence that complex cells in layers 2 and 3 also get some direct inputs from LGN neurons instead of simple cells in layer 4 (Hammond & MacKay, 1975, Hoffman & Stone, 1971, Malpeli, 1983, Malpeli, Lee, Schwark & Weyand, 1986, Martin & Whitteridge, 1984, Tanaka, 1983).

1.4.2. Cortical responses

Cortical cells process the visual information within a localized region of space and over a restricted period of time. Temporal and spatial responses to different stimuli have been used to distinguish simple and complex cells. This section describes the temporal response; the next section explains the spatial aspect of the receptive field of cortical cells.

Extracellular recordings suggest that the responses of simple and complex cells to a drifting grating exhibit different spike rates. Simple cells respond to drifting gratings with a highly modulated response in synchrony with the temporal frequency of stimulation while complex cells produce elevated mean firing rates (Carandini & Ferster, 2000, Dean, 1981, Hamilton, Albrecht & Geisler, 1989, Movshon, 1978, Movshon, Thompson & Tolhurst, 1978a, Skottun, De Valois, Grosof, Movshon, Albrecht & Bonds, 1991, Thompson & Movshon, 1978).

Examples of extracellular recordings from simple and complex cells are shown in Figure 1.7 (Dean & Tolhurst, 1983). Simple and complex cells in this study were

classified based on the spatial summation ratio (ratio of width of one subfield of the receptive field to half of the period of the drifting grating at optimum spatial frequency). Simple cells with linear spatial summation show a ratio lower than one and complex cells have a ratio higher than one, indicating non-linear spatial summation.

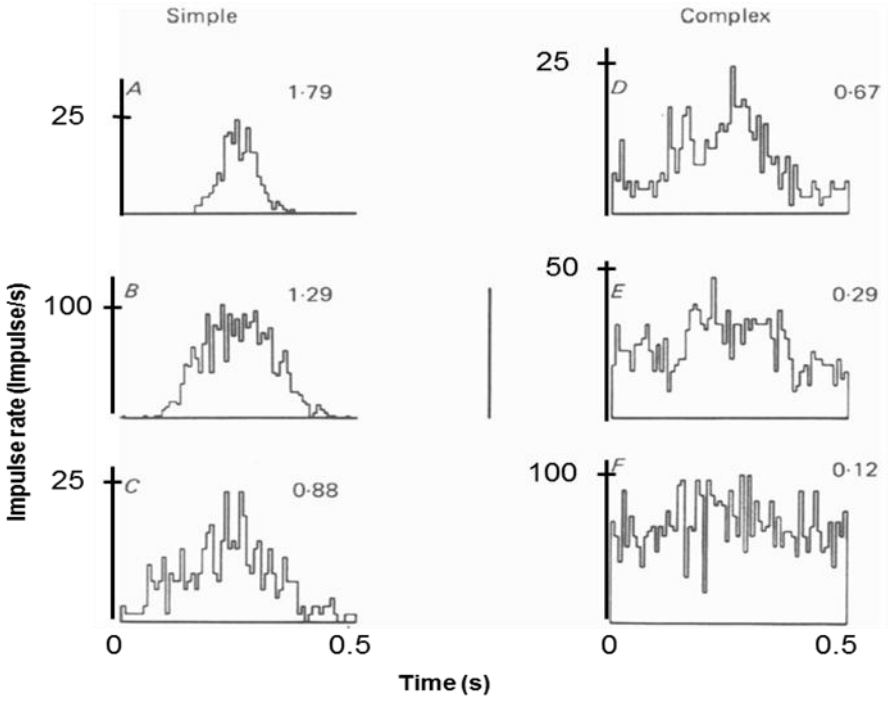

Figure 1.7: Firing rate of six simple and complex cells in response to a drifting grating of optimal spatial frequency. The number on the top right of each graph shows the ratio of Fourier fundamental frequency amplitude (AC) to the mean firing rate (DC) of the response. Complex cells show a significant mean firing rate compared to simple cells, therefore the ratio of AC to DC level is lower in the complex cells (Dean & Tolhurst, 1983).

Similar results have been recorded in other extracellular (Figure 1.8) and intracellular studies (Figure 1.9). The difference between simple and complex cells in extracellular recording is more apparent in the preferred direction. Simple cell have high modulation compared to complex cells, which have high mean firing rate (Figure 1.8). However, the difference between simple and complex cells is clearer in intracellular recording (Figure 1.9). The membrane potential of the simple cells is strongly modulated at the temporal frequency of the stimulus in the preferred direction. By

contrast, the membrane potential response of the complex cell consists of an elevation in the mean and weak modulation at the stimulus frequency.

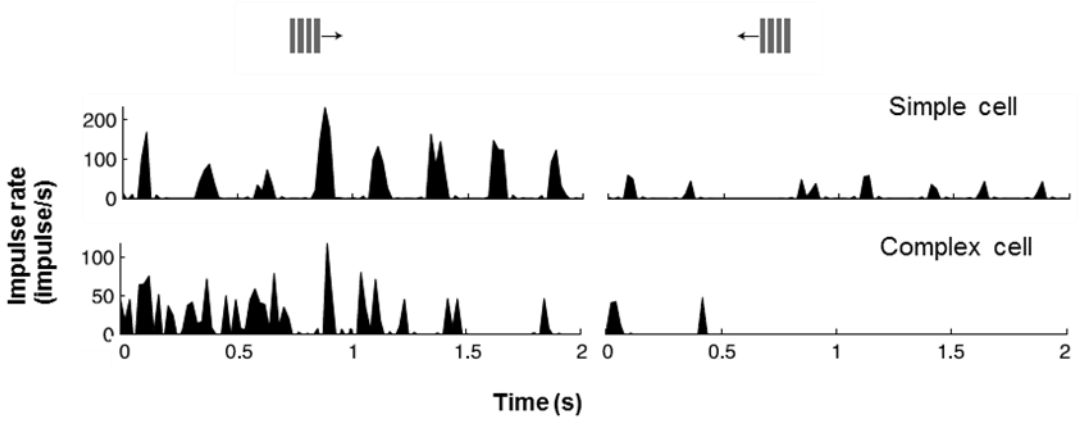

Figure 1.8: Impulse rate of a simple and a complex cell to a grating drifting in the preferred and anti-preferred directions. High modulation and low mean rate was observed in the simple cell while the complex cell shows high mean firing rate and lower modulation (Carandini & Ferster, 2000).

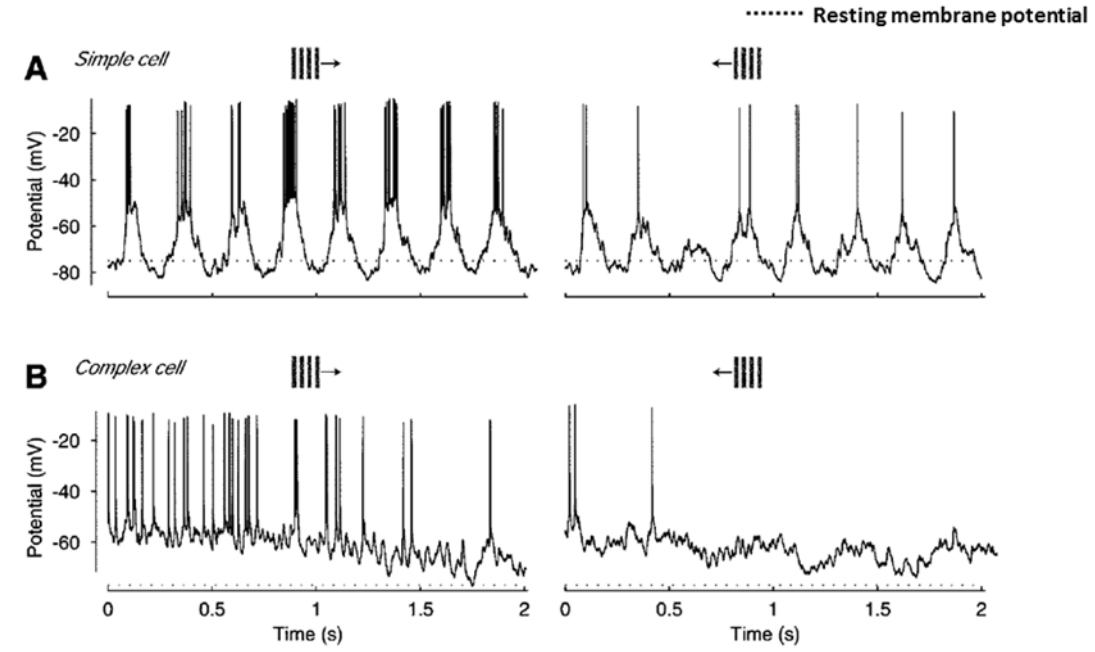

Figure 1.9: Membrane potential response of a simple and a complex cell in response to a grating drifting in the preferred and anti-preferred direction. The simple cell shows a high modulation compared to the complex cell which has a high mean firing rate (Carandini & Ferster, 2000).

1.4.3. Spatial receptive field

The visual receptive field is described as a region of space in which the presence of a stimulus will influence the firing of the neuron. Neurophysiologists used the receptive field to study the function of the cell, describing the transformation between the visual stimulus and neural activity.

Early studies used the manual approach, putting different shapes of stimuli in the receptive fields of the cells, for mapping and plotting the receptive field (Hubel & Wiesel, 1961, Kuffler, 1953). Receptive field mapping has been improved over the years by using a white noise mapping technique for faster recording (see (DeAngelis, Anzai, Ohzawa & Freeman, 1995) for review). In the white noise technique, brief light and dark stimuli are turned on and off in random locations within the receptive field. For example, each stimulus is presented for 50 ms in 20×20 positions in the x-y plane. The receptive field is then reconstructed as the average stimulus preceding spikes by a fixed interval. Responses to light and dark stimuli are analysed separately. The receptive fields of geniculate, simple and complex cells in Figure 1.10 were plotted using this technique (DeAngelis et al., 1995). As the Figure shows, geniculate cells have a concentric receptive field, simple cells have elongated and separated excitatory and inhibitory regions, and complex cells have overlapping on and off subfields (shown separately).

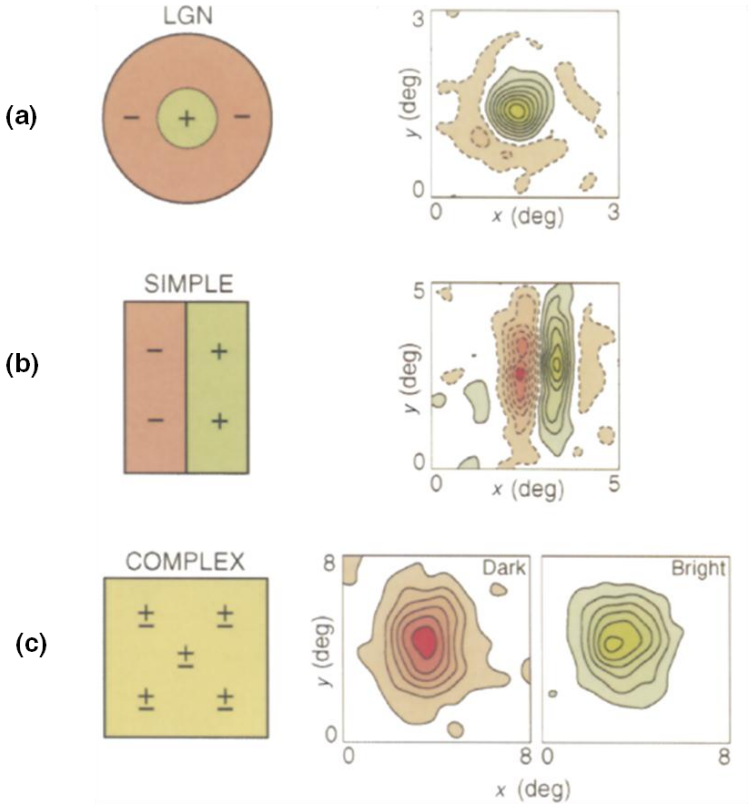

Figure 1.10: Schematic (left) and measured (right) contour map of the receptive field of a (a) geniculate, (b) simple and (c) complex cell. The spatial receptive field was measured using the reverse correlation technique. The excitatory and inhibitory subfields are shown by green and red respectively (DeAngelis et al., 1995).

Figures 1.11 and 1.12 are other receptive field mapping examples from a recent study by Martinez et al. (2005). A sparse white stimulus was used for contour mapping. Specifically, a spot of light of 0.85° to 1.7° size with contrast of 50 to 70% was flashed for 31-47 ms in 16×16 locations in a grid square. Membrane potential was measured, and the push (excitatory) and pull (inhibitory) response is indicated in each region with grey and black traces respectively.

The receptive fields of cells in layer 4, which receive the direct inputs from geniculate cells, have distinct on- and off- subfields. In these cells, the off-subfield is stronger and larger than the on-subfield. Within each subfield, there is a push-pull response meaning that the responses to bright and dark stimulus oppose each other.

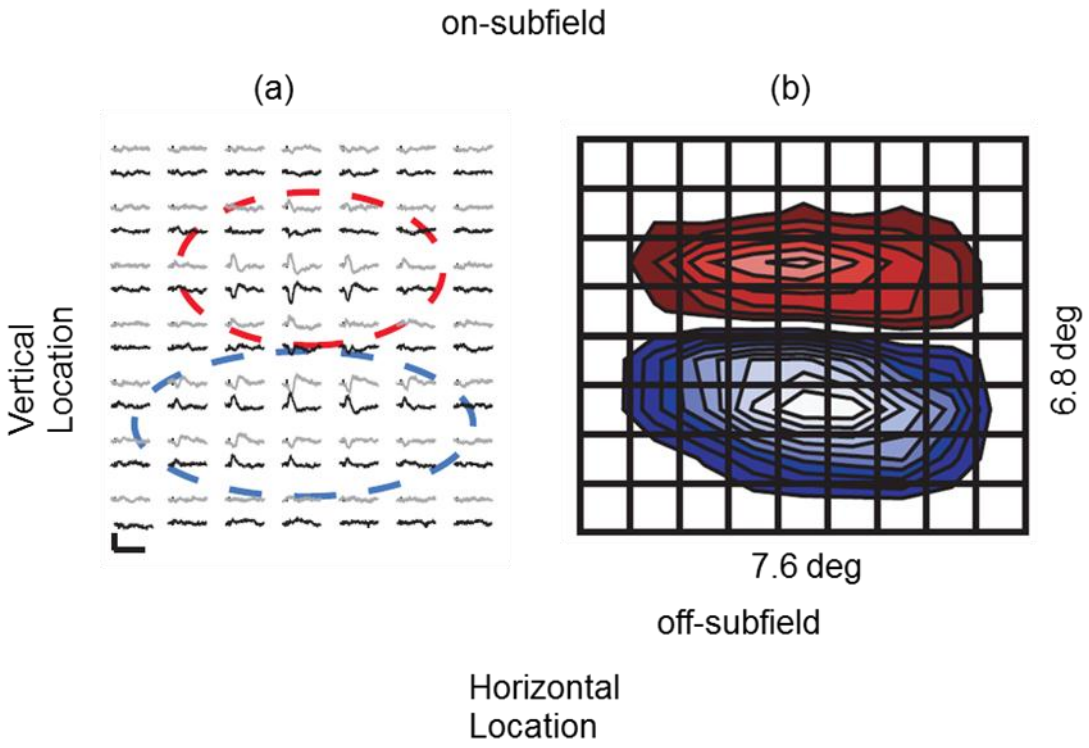

Figure 1.11: A simple cell receptive field in layer 4. (a) Each location in the receptive field is represented by grey and black traces for light and dark stimulus responses (push-pull response), respectively, and the dotted line indicates the receptive field of the cell. (b) Contour plot (Martinez et al., 2005).

Complex cells in this study, which were mostly located in layer 6, had overlapping on- and off- subfields. Synaptic responses in this type are push-push (same response from both dark and bright stimulus) rather than push-pull. Two examples of complex cells in this study are shown in Figure 1.12.

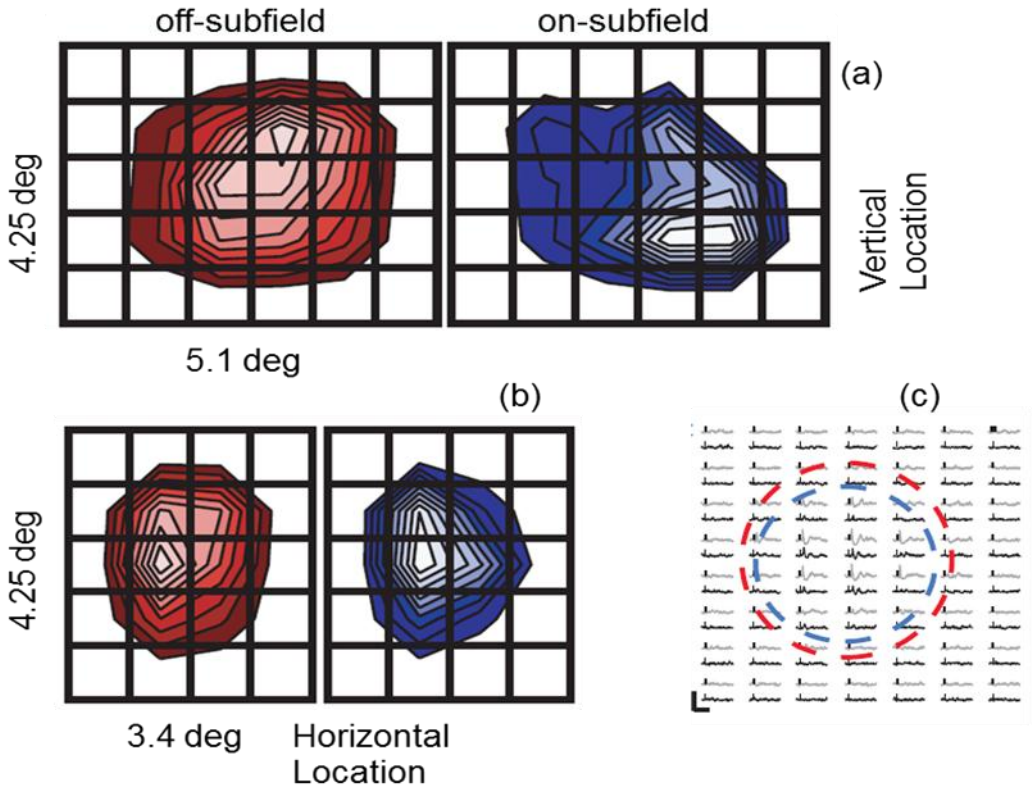

Figure 1.12: (a,b) are examples of contour receptive field maps of complex cells. (c) Complex cell traces with responses to dark and bright spot and are shown by black and grey impulses, respectively, in different locations. The opposite contrast evokes the same sign and same magnitude of responses (push-push response).

1.4.4. Quantitative measurements

Simple cells can be described qualitatively (Hubel & Wiesel, 1962) by:

1-Separate on- and off- subfields

2-Linear summation within each subfield

3-An antagonism between on- and off-subfields

4-Prediction of geometry of optimal spatial stimulus from region structure

Cells that cannot satisfy the above criteria are considered as complex cells. Since qualitative measurement is not consistent and the comparison between various laboratories is not reliable, many studies suggested quantitative methods as being more useful for discriminating between simple and complex cells.

Many neurophysiologists (De Valois, Albrecht & Thorell, 1982, Dean & Tolhurst, 1983, Movshon et al., 1978a, Movshon, Thompson & Tolhurst, 1978b, Movshon et al., 1978c, Ohzawa & Freeman, 1986a, Ohzawa & Freeman, 1986b, Skottun et al., 1991, Skottun & Freeman, 1984) used Fourier analysis of the response to a drifting grating for the classification of simple and complex cells. The preceding *cortical responses* section noted that simple cells usually respond to drifting grating with a pronounced modulation of activity in time whereas complex cells show little or no modulation. Therefore, relative modulation of the response can be used as a criterion for the classification. Relative modulation is defined as the ratio of the amplitude of the first harmonic (f1) to the mean response level (f0) (after removing the average maintained firing rate), that is, the ratio of the AC to DC response. This ratio varies from 0 to 2. A value of 0 indicates a cell without modulation and value 2 indicates that all impulses are confined to a single stimulus phase. This ratio (f1/f0) is typically bigger than one in simple cells and less than one for complex cells (Figure 1.13). Relative modulation is calculated using a drifting grating with optimal spatial frequency since many complex cells can generate a modulated response at lower frequencies (Hammond, Pomfrett & Ahmed, 1989). Skottun et al. (1991) combined the data of Figure 1.13 with data from 1061 cells from other laboratories in Figure 1.14 (a) and (b) respectively. They showed that cortical cells can be quantitatively categorized based on the relative modulation ranging from zero to two (Figure 1.14 a).

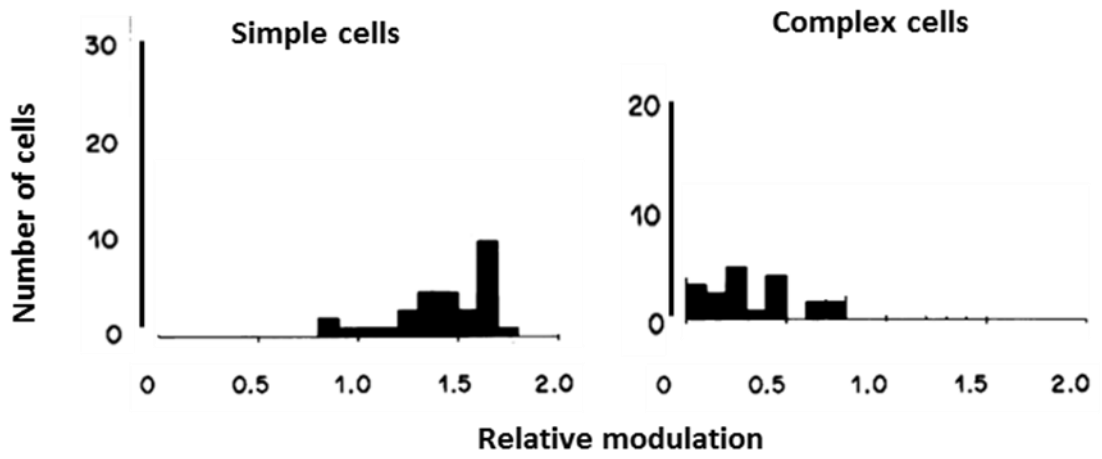

Figure 1.13: Distribution of relative modulation (f1/f0) to a drifting grating stimulus. The relative modulation in simple cells is usually higher than one and complex cells possess relative modulations lower than one (Dean & Tolhurst, 1983).

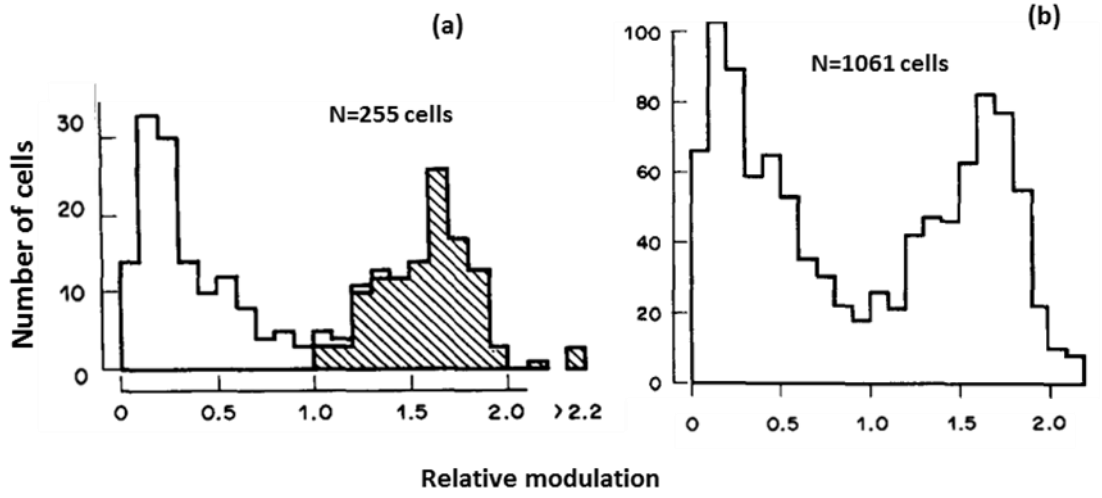

Figure 1.14: Distribution of cells with regard to modulation of response to drifting grating. (a) Data from Dean and Tolhurst (1983) and distribution analysis from Skottun et al. (1991). The hashed area shows the simple cells based on the separated on- and off-subfields. (b) Data collected from several laboratories (Skottun et al., 1991). The distribution of modulation ratio of the response is bimodal.

Dean and Tolhurst (1983) defined another quantitative criterion based on the separation between the on- and off-subfields. This new criterion, called discreteness, was defined as:

$$discreteness = \frac{\sum_{i=1}^{n} |(on(i) + off\ (i)|}{\sum_{i=1}^{n} |on(i)| + \sum_{i=1}^{n} |off\ (i)|} \tag{1.1}$$

where *i* is the number of location and *on(i)* and *off(i)* are the responses to the bright and dark stimulus in each location, respectively. This index is close to one for simple cells, which have no overlap, and close to zero for complex cells, which have substantial overlap. The distribution of this value over a population of cells indicated that there is a continuous range of overlap between subfields and the distribution is not bimodal (Figure 1.15).

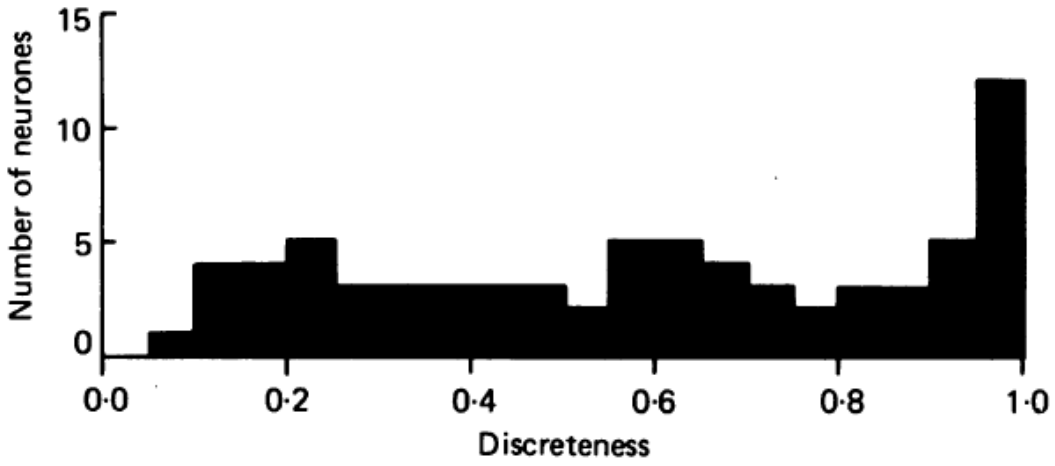

Figure 1.15: Distribution of discreteness of receptive field regions for 74 cells. The distribution of overlap between subfields is continuous from zero to one (Dean & Tolhurst, 1983).

Recently Martinez et al. (2005) introduced two more indices for quantifying simple and complex cells: 1) overlap index 2) push-pull index. The overlap index is defined in equation 1.2. W_p and W_n are the widths of on- and off-subfields and *d* is the distance between peak positions of each subfield. This value is less than zero for separated subfields and close to one for overlapping subfields. The histogram of the overlap index for the population of cortical cells in all layers of the primary visual cortex (33 cells) is shown in Figure 1.16. Simple cells have an index lower than zero due to separate on- and off-subfields and this index is higher than zero for complex cells because of the overlap of the excitatory and inhibitory subfields. The distribution of

overlap index gives similar results to the discreteness index of Dean and Tolhurst (1983).

$$Overlap\_Index = \frac{0.5W_p + 0.5W_n - d}{0.5W_p + 0.5W_n + d} \tag{1.2}$$

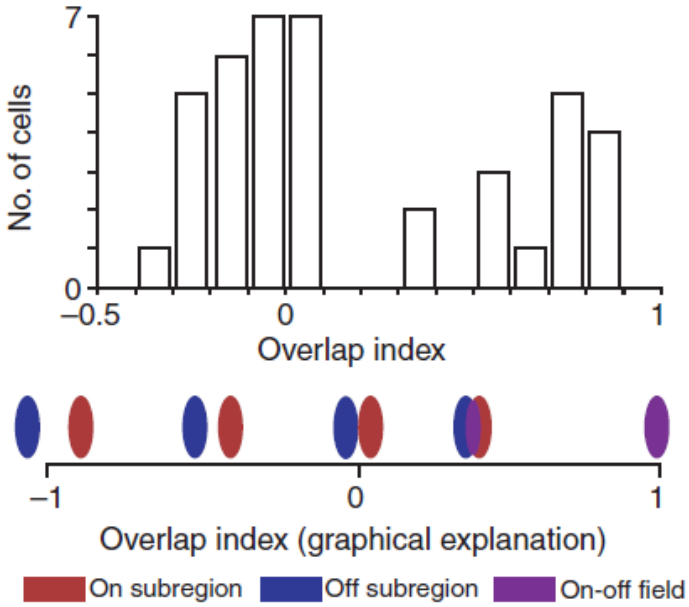

Figure 1.16: Overlap index explains the amount of overlap between subfield of receptive field. Receptive fields with separated subfields have an index of lower than zero and complete overlap of subfields produces an index value greater than one (Martinez et al., 2005).

The push-pull index is another quantitative method for discriminating between simple and complex cells and is defined as:

$$\text{Push} - \text{pull index} = \left| P + N \right| \tag{1.3}$$

where *P* represents synaptic responses to bright stimuli and *N* shows the response to dark stimuli. Therefore, when the stimulus of opposite contrast evokes the same magnitude of response with the opposite sign, the value is zero. After normalisation, a value of one shows that a stimulus of only one contrast produces a response and a value of two indicates that bright and dark stimuli generated the same sign and similar amplitude responses (Figure 1.17). Simple cells achieve a push-pull index close to

zero because opposite contrasts evoke excitatory and inhibitory responses with similar amplitude, whereas complex cells have the maximum push-pull index due to the excitatory response to opposite contrasts.

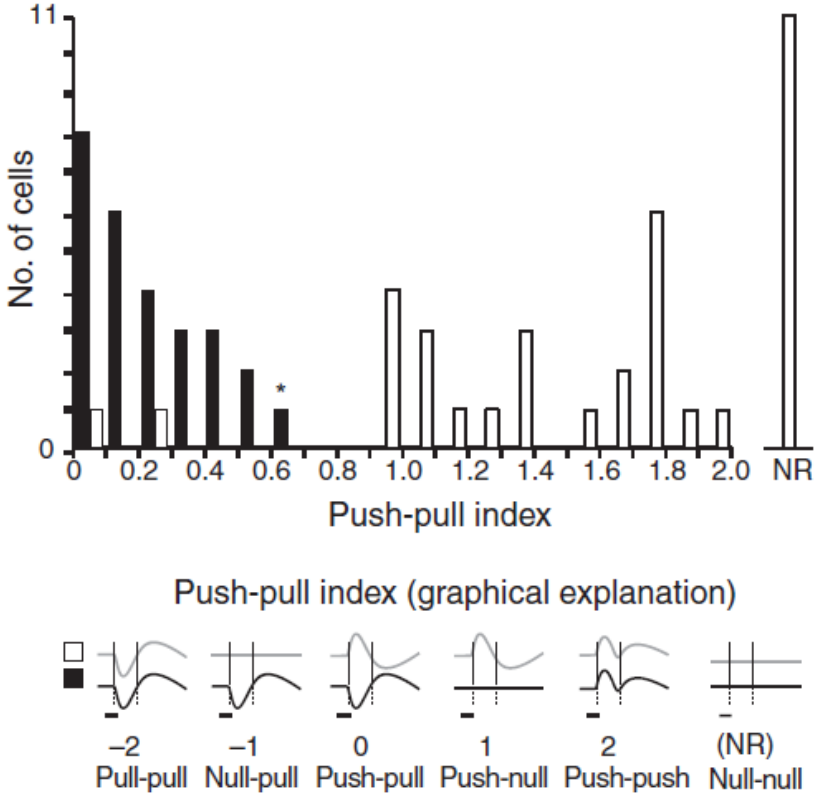

Figure 1.17: The push-pull index histogram of the population of cells in all layers of the primary visual cortex. Filled bars represent cells with separated on- and off-subfields and open bars show cells with overlapping on- and off-subfields. The bottom graph explains the meaning of each index value. When both bright and dark stimuli evoke the same response the push-pull index is two; the push-pull index is zero when different contrasts generate the opposite response (Martinez et al., 2005).

1.4.5. Models

Many models have been developed to describe the properties of simple and complex cells. Hubel and Wiesel (1962) described simple and complex cells with a hierarchical model with feed-forward inputs and no other intracortical inputs. Recent studies (Ben-

Yishai, Bar-Or & Sompolinsky, 1995, Somers, Nelson & Sur, 1995) debated the inability of this kind of model to completely explain the properties of the cortical cell. In this section, the plus and minuses of proposed models will be reviewed.

1.4.5.1. Feed-forward model

The earliest model describing simple cells was inspired by their receptive field properties (Hubel & Wiesel, 1962). In this model, simple cell receptive fields are constructed from the convergence of concentric geniculate inputs whose receptive fields are aligned in visual space. The aligned LGN cells converge to layer 4 in the primary visual cortex and generate the parallel on- and off-subfields of the simple cell (Figure 1.18).

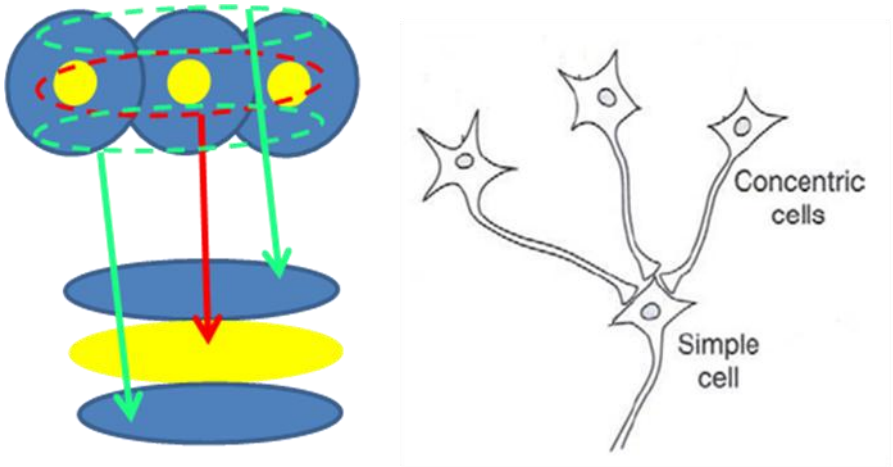

Figure 1.18: Proposed model for constructing the receptive fields of simple cells from converging concentric LGN cells. Each subfield of the simple cell is constructed from the summation of many LGN cells with centre-surround receptive field. On-centre inputs converge to the on-subfield and off-surround inputs converge to the off-subfield. Redrawn from Hubel and Wiesel (1962).

In addition, they proposed that complex cells can be constructed from the convergence of simple cells (Figure 1.19). Later, this hierarchical model received strong support from physiological studies. First, simple cells which are mostly present in layer 4 of the visual cortex (Hirsch et al., 1998, Hirsch, Martinez, Alonso, Desai, Pillai & Pierre, 2002, Hubel & Wiesel, 1962, Martinez et al., 2002) receive monosynaptic inputs from geniculate cells (Chung & Ferster, 1998, Reid & Alonso,

1995, Tanaka, 1983). Second, most simple cells in layer 4 project into layers 2 and 3, of which most are complex cells (Martinez et al., 2002). Martinez and Alonso (2001) showed that cells in layer 2 and 3 are visually inactive when the thalamic inputs to layer 4 are inactivated by injection of GABA in LGN. Their results suggested that inactivation of simple cells in layer 4 causes the inactivation of the complex cells in layer 2 and 3, confirming the feed-forward mechanism in the primary visual cortex.

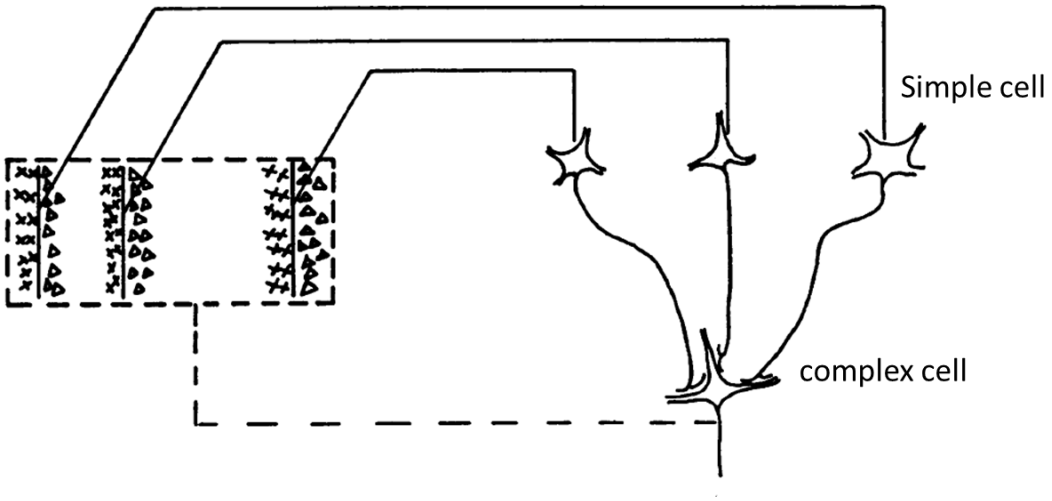

Figure 1.19: Proposed model for constructing complex cell receptive fields from convergent simple cells. The receptive fields of simple cells shown in blue and yellow ovals converge to a complex cell shown by yellow filling and blue lines since excitatory and inhibitory subfields overlapped each other. Redrawn from Hubel and Wiesel (1962).

Some recent studies, including Martinez et al. (2005), are in favour of a feed-forward model. They provide evidence of a spatial distribution of push and pull for thalamic cells and simple cells that is consistent with a feed-forward mechanism.

Hubel and Wiesel's (1962) model for complex cells has, however, been challenged by other studies. Hoffmann and Stone (1971) and Stone et al. (1979) found that some complex cells receive their inputs from geniculate neurons rather than simple cells. They suggested that linear cells in the retina and LGN cells (X cells) project to simple cells, and non-linear cells (Y-cells) project to complex cells since, unlike simple cells, complex cells have non-linear characteristics. Recent evidence indicates that only a

minority of complex cells receive direct inputs from geniculate cells (Martinez & Alonso, 2001). In addition, projection of X-cells to simple cells and Y-cells to complex cells is refuted by some studies (Ferster & Lindstrom, 1983, Tanaka, 1983).

1.4.5.2. Recurrent model

This group of models originates from the finding that the number of geniculate cells projecting to simple cells is small compared to the number of excitatory inputs from other cortical cells (Ahmed, Anderson, Douglas, Martin & Nelson, 1994, Peters & Payne, 1993). Cortical cells receive many excitatory and inhibitory inputs from other cortical cells (Binzegger, Douglas & Martin, 2004, Binzegger, Douglas & Martin, 2007). Some studies have therefore simulated cortical cell properties by including intracortical circuitry as well as geniculate inputs (Ben-Yishai et al., 1995, Somers et al., 1995). They used sophisticated models containing excitatory and inhibitory inputs from cortical cells to describe the properties of simple and complex cells, including orientation and direction selectivity.

However, Martinez et al. (2002) challenged these types of models using different experimental results. Whereas geniculate synapses onto cortical cells are fewer than intracortical synapses, geniculocortical connections are stronger due to larger synapses and dendritic synapses that are closer to the target cell (Ahmed et al., 1994), a bigger postsynaptic potential (Gil, Connors & Amitai, 1999) and the generation of simultaneous spikes by many geniculate projections to the target cortical cell (Alonso, Usrey & Reid, 1996). Other evidence, such as inactivation of cortical cells in layers 4, 2 and 3 after inactivation of LGN, also demonstrate the inadequacy of these types of models (Martinez & Alonso, 2001).

In addition, other studies (Anderson, Carandini & Ferster, 2000b, Martinez et al., 2002) showed that there is no difference between the excitatory and inhibitory orientation tuning of the cortical cells in layers 4, 2 and 3 while cortical cells in many feedback models (Ben-Yishai et al., 1995, Somers et al., 1995, Sompolinsky & Shapley, 1997) receive inhibitory inputs with broader orientation tuning than that of the target cell (orientation tuning is explained in the next section). As such, with no

difference between the excitation and inhibition parts of the orientation tuning curve, Figure 1.20 is good evidence for the feed-forward model.

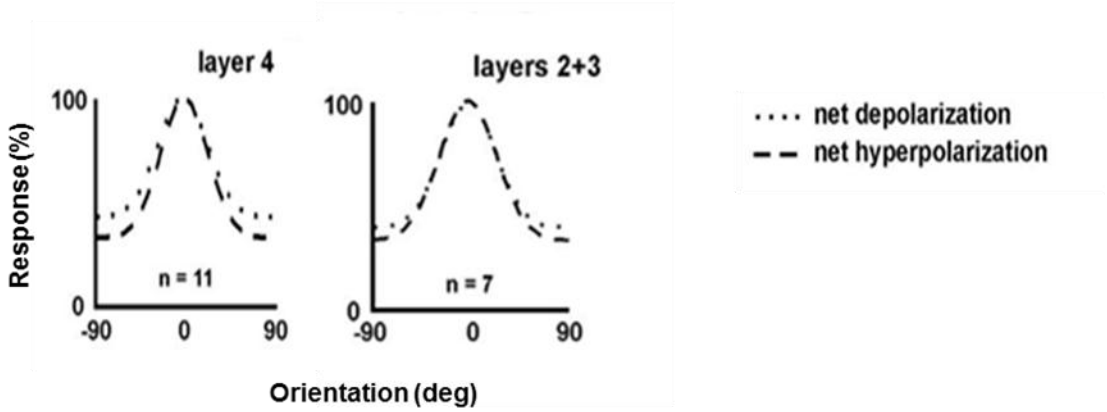

Figure 1.20: Depolarization and hyperpolarization of orientation selectivity of the cat cortical cells in different layers (Martinez et al., 2002). Most feedback models depend on broadening the inhibition for sharpening the orientation response, whereas the empirical orientation tuning curve of both excitation and inhibition indicates the same bandwidth.

1.5. Orientation selectivity

About 50 years ago, Hubel and Wiesel (1962) discovered that cortical cells in the primary visual cortex are sensitive to the orientation of a stimulus. Since then, many researchers have investigated this property in many species including cats, primates and ferrets. Some studies also attempted to determine the mechanism underlying this property. This section reviews this property as explored in many experimental and computational works.

1.5.1. Qualitative measurement

Hubel and Wiesel (1962), in their seminal paper, assessed orientation selectivity with a bar of light (or dark) in the cortical receptive field. They showed that cortical cells in the primary visual cortex fire impulses vigorously in response to stimuli with their preferred orientation and they generate few or no impulses for the orthogonal orientation. Both simple and complex cells respond to the stimulus in their preferred orientation and they produce little or no response in the other orientations (Figure 1.21). Following these studies, many scientists have investigated this property qualitatively and quantitatively with elongated visual stimuli in the primary visual cortex of several species (Bullier & Henry, 1979, Ferster & Miller, 2000, Gilbert, 1977, Hubel & Wiesel, 1962, Vidyasagar, Pei & Volgushev, 1996).

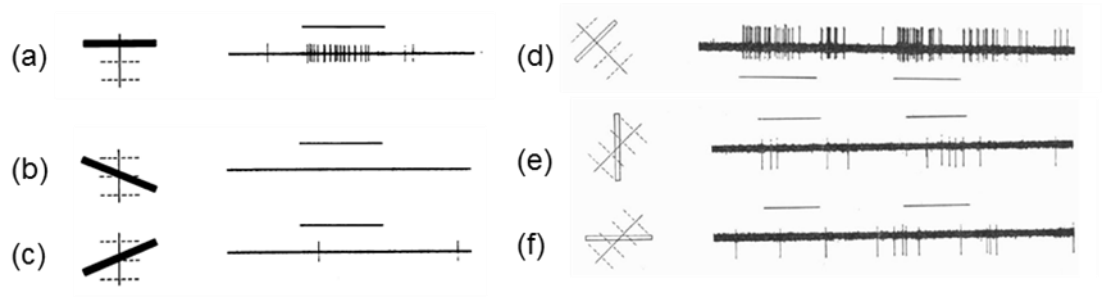

Figure 1.21: Response of a simple and a complex cell to oriented dark or light bar. (a) Simple cell response to a horizontal dark bar. (b,c) The same simple cell produces few spikes to a tilted bar. (d) Complex cell responds to a light bar in its preferred orientation. (e,f) The same complex cell generates few spikes in other orientations (Hubel & Wiesel, 1962).

1.5.2. Quantative measurements

Orientation selectivity can be assessed quantitatively using the orientation tuning curve. Campbell et al. (1968) were the first to introduce this method. The orientation tuning curve is a quantitative method for showing the response of a cell in different orientations. Typically, a neuron is stimulated with a drifting grating or elongated bar in a variety of orientations and the response of the cell is recorded for each orientation. The tuning curve is the plot of response of a cell for each orientation. As the literature indicates, the tuning curves of cortical cells are bell-shaped. The maximum response indicates the optimum orientation, and the bandwidth of the curve gives the precision of tuning (Figure 1.22).

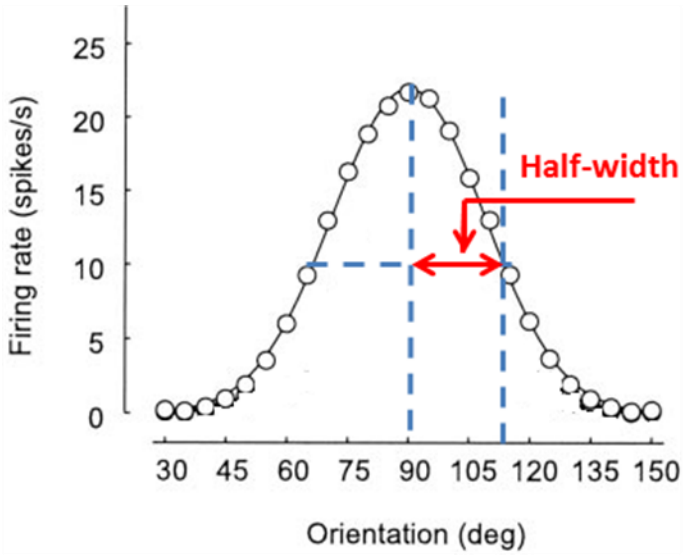

Figure 1.22: An example of the orientation tuning curve of a simple cell in response to a drifting grating stimuli with 80% contrast (Carandini, Heeger & Senn, 2002). The peak of the curve indicates the response of the neuron to the optimal orientation. The half-width at half-height provides the bandwidth of the orientation tuning curve.

Many studies have quantitatively assessed the orientation selectivity of cortical cells using the orientation tuning curve. There is consensus that cells in area 17 have a narrower bandwidth than those in area 18. In each area, simple cells have a narrower bandwidth than complex cells (Gizzi, Katz, Schumer & Movshon, 1990, Hammond & Andrews, 1978, Rose & Blakemore, 1974). The mean bandwidth for simple cells is 15° to 25° while the bandwidth of complex cells is 23° to 26° in the cat primary visual cortex (Carandini & Ferster, 2000, Gizzi et al., 1990, Hammond & Andrews, 1978) (Figure 1.23).

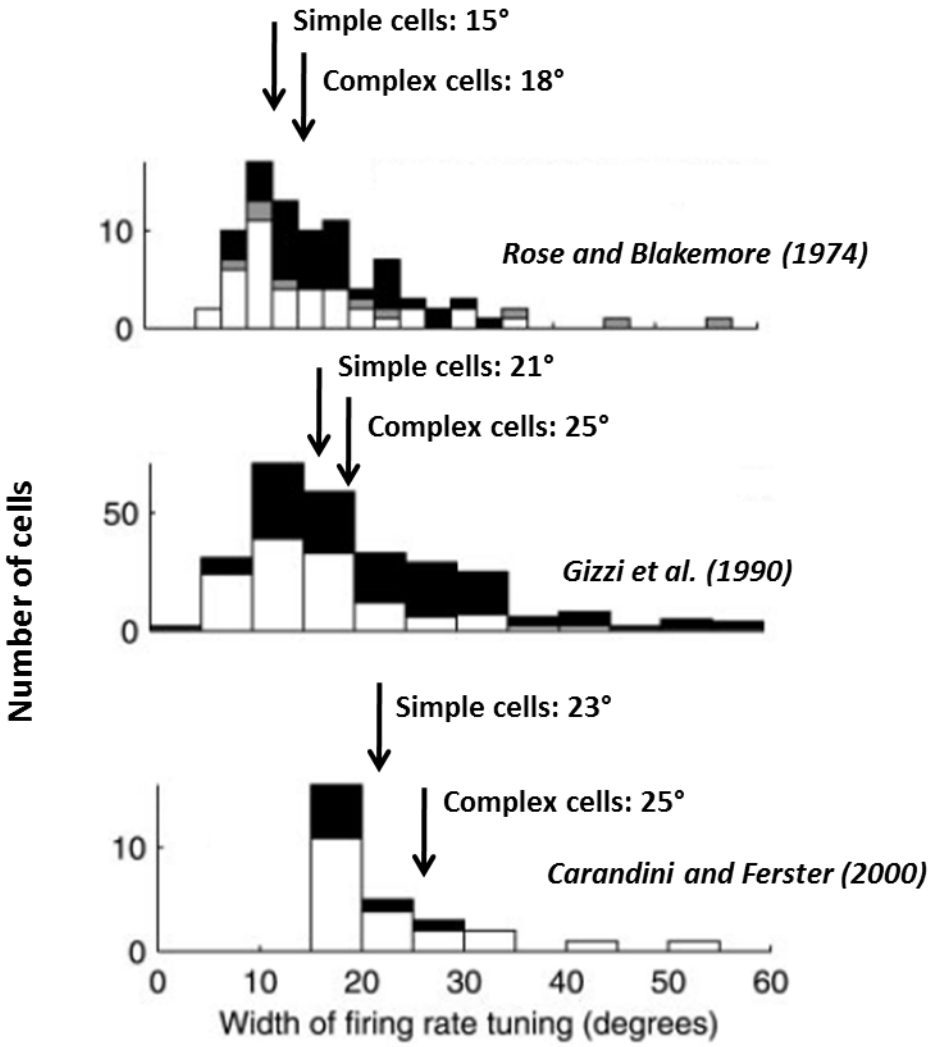

Figure 1.23: Orientation tuning half-width in simple and complex cells of the cat primary visual cortex. White shows simple cells, black shows complex cells and grey shows unclassified cells. Simple cells have an average bandwidth of about 20° whereas complex cells have a slightly broader bandwidth (Carandini & Ferster, 2000).

Further, Carandini and Ferster (2000) investigated the orientation tuning curve for the membrane potential and spike rate of simple cells in the cat primary visual cortex. These investigations indicated that bandwidths of the membrane potential are wider than bandwidths computed from spike rate. The average of bandwidth computed from the membrane potential was 38 ± 15° while this value for firing rate was 23 ± 8° using a drifting grating stimulus.

1.5.3. Orientation selectivity mechanism

The mechanism of orientation selectivity in cortical cells has been studied by many researchers. One striking observation about orientation selectivity is that the lateral geniculate neurons, which provide the major source of visual information to the cortical cells, are largely insensitive to the orientation of the stimulus. Instead, many researchers believe that cortical orientation selectivity is mainly due to the pattern of geniculocortical connections (Chung & Ferster, 1998, Ferster, Chung & Wheat, 1996, Reid & Alonso, 1995). Reid and Alonso (1995) studied the connection of the thalamic relay cells to simple cells by the cross-correlation approach. They found that there is a functional connection between geniculate cells and simple cells when the centres of the geniculate cell receptive field overlaps with a simple cell subfield of the same polarity. For example, the receptive fields of on-centre geniculate cells overlap with the on-subfields of the simple cells to which they connect. Their results imply that both the subfield organisation and orientation selectivity of simple cells are established by monosynaptic connection with lateral geniculate inputs, and simple cells are created solely by LGN cells inputs (Figure 1.24).

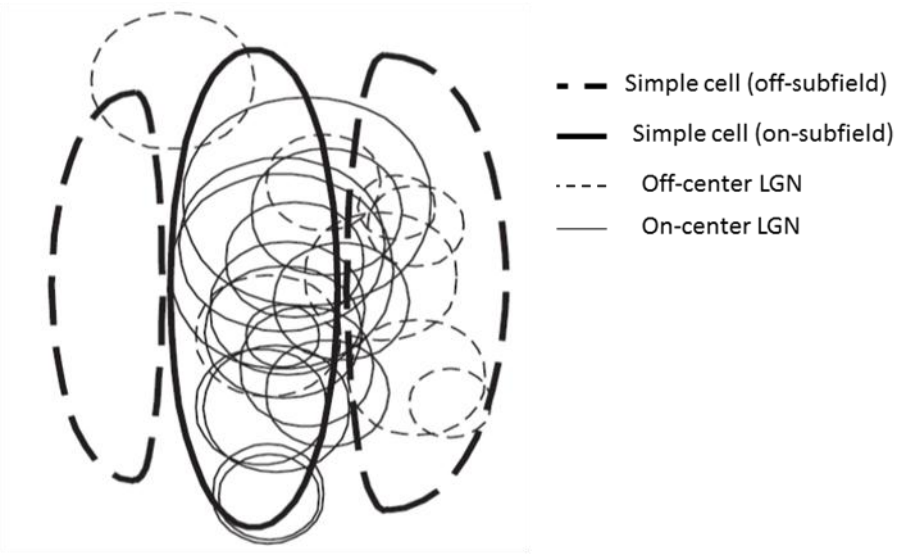

Figure 1.24: Spatial relation between simple and geniculate receptive fields of many functionally connected cell pairs. A receptive field of a simple cell is illustrated with the connected LGN receptive fields. There is a strong connection between an on-centre LGN cells overlapped with an on-subfield and off-centre LGN cells overlapped with an off-subfield (Reid & Alonso, 1995).

Ferster's laboratory (Chung & Ferster, 1998, Ferster et al., 1996) used intracellular recording to investigate the strength of the thalamic inputs and the contribution of these inputs to orientation selectivity and tuning of simple cells, while inactivating the cortical network. The first study inactivated cortical inputs to simple cells by cooling (Ferster et al., 1996). They compared orientation tuning before and after suppression of the cortical networks and showed that the orientation tuning bandwidth is the same in the two situations but that the amplitude of the cortical response decreased by about 63% after suppression. Figure 1.25 shows the orientation tuning curve of one simple cell for both warm and cool cortex.

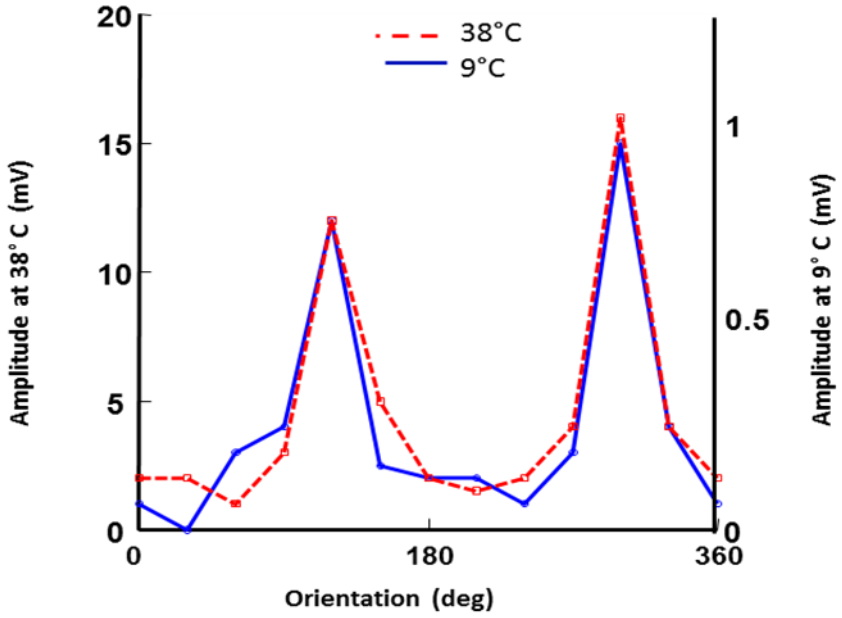

Figure 1.25: Membrane potential tuning curve of one simple cell before and after cortex cooling. Inactivating the cortical inputs doesn't change the bandwidth of the orientation tuning, it only reduces the amplitude of the response. Redrawn from Ferster et al. (1996).

In their subsequent study (Chung & Ferster, 1998), they eliminated the effect of cortical inputs to the simple cells by electrical stimulation of the nearby cortex. Intracellular recording of excitatory postsynaptic potential (EPSPs) during cortical suppression only reflects thalamic inputs since the cortical responses are inhibited by electrical stimulation. Suppression of cortex reduced the amplitude of response by 54% but didn't have any effect on the orientation tuning of the cells. The authors

concluded that 46% of the response of simple cells originates from thalamic inputs and the remaining parts come from other sources - presumably cortical neurons.

Together, these studies suggested that orientation selectivity and orientation bandwidth of simple cells originates from geniculate cells. Indeed, they suggest that thalamic inputs provide about one third to one half of the excitatory input to simple cells, with the remaining inputs originating from cortex.

However, some other studies suggested that cortical inputs have a significant role in sharpening the orientation tuning (Carandini & Ferster, 2000, Gardner, Anzai, Ohzawa & Freeman, 1999). For example, Carandini and Ferster (2000) determined from the relationship between the tuning curve computed from membrane potential and spike rate, that the orientation tuning originates from the thalamocortical inputs but sharpening of the orientation tuning is due to impulse generation within cortex. If only the lateral geniculate nucleus is considered for orientation, the tuning curve would be very broad.

1.5.4. Orientation selectivity model

The origin of orientation selectivity in cortical cells has been investigated extensively using a variety of different models and computational approaches. Three types of models have been proposed for describing and understanding the mechanism: 1) feed-forward model, 2) inhibitory model and 3) recurrent model. The feed-forward model suggests that selectivity arises simply from the arrangement of the thalamic inputs to the cortical cells. Some studies determined that the feed-forward model alone cannot explain the invariance of the orientation tuning to the changes of stimulus contrast. Hence, many studies attempted to explain this mechanism with some addition to the feed-forward model such as push-pull inhibition or adding the effect of other cortical neurons to the oriented cells.

1.5.4.1. Feed-forward models

The first orientation-selective model described the subfield arrangement of the cortical cells with a linear model, with direct inputs from the lateral geniculate nucleus (Figure 1.18). The model proposed to explain the orientation selectivity of

cortical cells in the cat primary visual cortex (Hubel & Wiesel, 1962). They suggested two possibilities: 1) On- and off-subfields result from on- and off-inputs respectively. 2) One of the subfields of simple cells arises from the centre mechanism of many same-sign LGN cells whose receptive field centres lie along the axis of the sub-field, and other subfields are produced by the surround mechanism of the LGN cells. In this model, thalamic inputs summed linearly to generate the orientation sensitivity of the simple cells. So, if a bar of light is put on the on-subfield at the orientation of the subfield axis, the cortical cell will be stimulated and generate spikes, and if a dark bar is presented at the preferred orientation on the off-subfield, the cell will fire spikes. This is due to spatial summation in each subfield. However, a bar perpendicular to the preferred orientation is not effective in generating a response due to antagonism between excitatory and inhibitory subfields. In this state, a bar stimulus excites both subfields together and the response would be small.

The evidence suggests the importance of the role of LGN cells in the orientation selectivity of simple cells. Further, cross-correlation studies (Reid & Alonso, 1995, Tanaka, 1983) and cortical inactivation experiments (Chung & Ferster, 1998, Ferster et al., 1996) confirmed this mechanism.

The next step in the feed-forward model is adding a threshold for producing a spike rate. This is critical for the generation of a sharp tuning response of simple cells and in removing the effect of low amplitude inputs. Carandini and Ferster (2000) proposed a rectification model for converting membrane potential to firing rate based on intracellular and extracellular recording. They suggested a linear relationship between membrane potential and firing rate. Firing rate grows linearly above threshold and is zero below threshold (Carandini & Ferster, 2000).

All experiments described above support the feed-forward model. The basic organisation of the simple cell receptive field such as subfields, orientation selectivity and preferred orientation can be predicted by the spatial organisation of connected LGN cells.

However, the feed-forward model cannot describe the invariance of simple cell orientation selectivity when stimulus contrast changes. The orientation tuning curve of

the feed-forward model broadens with increasing contrast whereas the orientation tuning of simple cells to drifting gratings indicated that tuning bandwidth doesn't change with stimulus contrast (Carandini et al., 2002, Sclar & Freeman, 1982, Skottun, Bradley, Sclar, Ohzawa & Freeman, 1987, Wehmeier, Dong, Koch & Van Essen, 1989). As Figure 1.26 shows, the height of the tuning curve increases with contrast but the tuning bandwidth is fixed at all contrast levels (Sclar & Freeman, 1982).

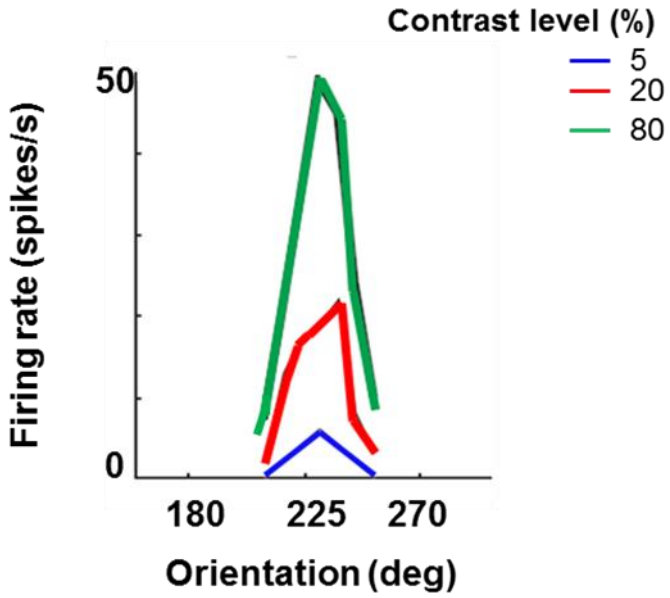

Figure 1.26: Orientation tuning curve of a simple cell in response to drifting gratings with three contrast levels. Increasing the contrast level increases the amplitude of response while the bandwidth is unchanged. Redrawn from Sclar and Freeman (Sclar & Freeman, 1982).

Sompolinsky and Shapley (1997) noted that even though LGN cells have a significant role in orientation selectivity of simple cells, the tuning bandwidth of the membrane potential is broadly tuned (half-width of 45°). The response amplitude due to linear spatial summation of geniculate inputs increases with stimulus contrast. In the feed-forward model, there is no mechanism for suppressing the excitatory inputs evoked by LGN when the orientation of the stimulus deviates from the preferred orientation. Adding the spike threshold doesn't have any effect on the tuning bandwidth. No matter where the threshold is, the tuning curve of the firing rate response will show significant broadening: More widely tuned excitatory input lies below the threshold

which would be disclosed by increasing contrast level in the feed-forward model. So, if the threshold is set too low, stimuli at high contrast elicit responses in all orientations, and if the threshold is too high, stimuli at low contrast elicit no response at all (Figure 1.27).

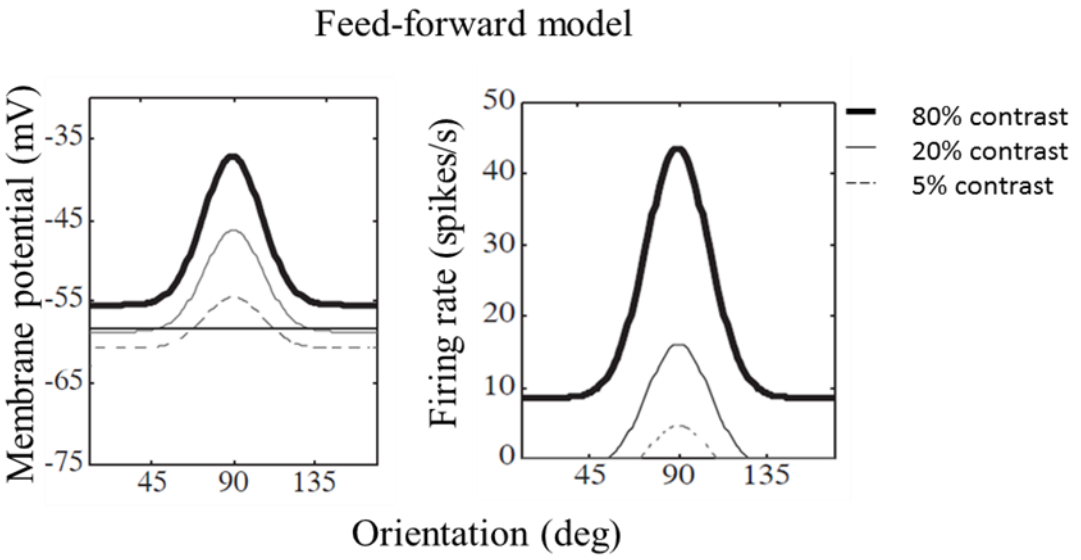

Figure 1.27: Orientation tuning curve for membrane potential and firing rate for the feed-forward model. Bandwidth of the tuning curve will increase by increasing the stimulus level, contradicting experimental results. Adding push-pull inhibition to the feed-forward model makes orientation selectivity contrast invariant in the feed-forward model (Ferster & Miller, 2000).

1.5.4.2. Inhibitory models

One simple solution for contrast invariance of response is a varying threshold level: threshold changes by changing contrast. This solution does not agree with experimental results because threshold level is invariant with contrast (Carandini & Ferster, 2000). Another possibility may be to include inhibition in the feed-forward model. Inhibition can provide contrast invariance as well as explaining some of the receptive field properties of inhibition in simple cells.

Typically, the tuning curve can be sharpened by adding inhibitory inputs from cortical cells (Ferster & Koch, 1987, Worgotter & Koch, 1991). In this nonspecific inhibition mechanism, a cortical cell receives a broadly tuned excitatory input from LGN and

broadly tuned inhibitory input from other cortical cells. The inhibitory inputs sharpen the orientation tuning and leave the bandwidth contrast invariant. Thus increasing inhibition with increasing contrast prevents broadening of the tuning curve.

However, the nonspecific inhibition model does have some drawbacks. First, this model predicts inhibitory inputs at non-optimal orientation, which is not confirmed by intracellular recording (Ferster & Lindstrom, 1983). In addition, strong inhibition significantly reduces the responsiveness of cortical cells and results in a smaller firing rate than is observed in the empirical data (Sompolinsky & Shapley, 1997).

Troyer et al. (1998) suggested a mechanism for contrast-invariant orientation selectivity of the feed-forward model based on push-pull inhibition. Many intracellular (Anderson, Lampl, Reichova, Carandini & Ferster, 2000a, Hirsch, Alonso & Reid, 1995) and extracellular (Palmer & Davis, 1981) studies have shown that simple cells receive off-inhibition in their on-subfields and on-inhibition in their off-subfields. Each on-subfield receives on-excitation and off-inhibition and each off-subfield receives off-excitation and on-inhibition. Using this inhibition scheme does not affect responses to a bar or grating in preferred orientation because excitation and inhibition responses are out of phase: peak excitation occurs at minimum inhibition and vice versa. Conversely, responses in the non-preferred orientation are affected. Orthogonally oriented bars or gratings activate on-inhibition in the off-subfield and cancel out the on-excitation in the on-subfield.

The push-pull inhibition in the Troyer et al. (1998) model is stronger than excitatory inputs from relay cells. If the excitatory and inhibitory inputs have equal strength, the tuning curve would be contrast variant: the amplitude of the tuning curve will increase with increasing contrast and so the portion of the peak above the threshold will broaden with contrast. Therefore, by assuming strong anti-phase inhibition, the baseline of the tuning curve of the membrane potential moves down with increasing contrast, and the width of the peak point above the threshold remains constant (Figure 1.27).

The Troyer et al. model (1998) is in accord with physiological experiments. Intracellular and extracellular recordings support push-pull inhibition being stronger

than excitation (Anderson et al., 2000a, Hirsch et al., 1995). Hirsch et al. (1995) demonstrated that the response of a light spot in one subfield of a simple cell is completely suppressed by moving the spot slightly to the neighboring subfield of opposite polarity. Larger inhibitory conductance than excitatory conductance is further evidence for stronger inhibitory inputs to simple cells. Recording conductance of excitation and inhibition evoked by drifting gratings demonstrated that the latter is 2-5 times larger than the former (Anderson et al., 2000a).

1.5.4.3. Recurrent model

This set of models also deals with the contrast sensitivity of orientation selectivity. In a recurrent model, LGN inputs have weaker roles and cortical cells play a more prominent role in establishing orientation selectivity. The orientation selectivity in this type of model comes from short-range excitation and longer-range inhibition in the cortex (Ben-Yishai et al., 1995, Somers et al., 1995).

The model proposed by Somers et al. (1995) comprises three layers: retinal ganglion cells, lateral geniculate nucleus and simple cells in layer 4 of the primary visual cortex (Figure 1.28). Simple cells receive excitatory and inhibitory inputs from cortical cells, along with thalamocortical inputs. LGN inputs create a columnar orientation basis but are not the basis for sharp tuning of the cortical cells. The orientation tuning sharpening is principally done by cortical excitatory inputs. Somers et al. (1995) extracted the number of the synapses to simple cells from experimental studies, that is 20% of the inputs provided by LGN, 20% from cortical inhibitory, and more than 50% from other excitatory cortical cells. Inhibition within the cortical column was drawn from a broader range of orientations than the excitatory inputs. The effective orientation range of inhibitory inputs was ±60° while the excitatory range was ±15°. According to this model, the cortical cells receive excitatory inputs from other cortical cells with similar orientation (same orientation column) and inhibitory inputs from a range of orientation columns. Cortical inputs integrated and amplified a weak thalamic orientation bias. In other words, the cortical interactions amplified the LGN excitatory input in the preferred orientation and suppressed it at non-preferred orientations. The combination of excitatory and inhibitory feedback substantially increased the initial orientation bias supplied by LGN input and results in a sharp

tuning response. The response from this model is contrast invariant: increasing the contrast increases positive feedback in the preferred orientation and also negative feedback in the non-preferred orientation.

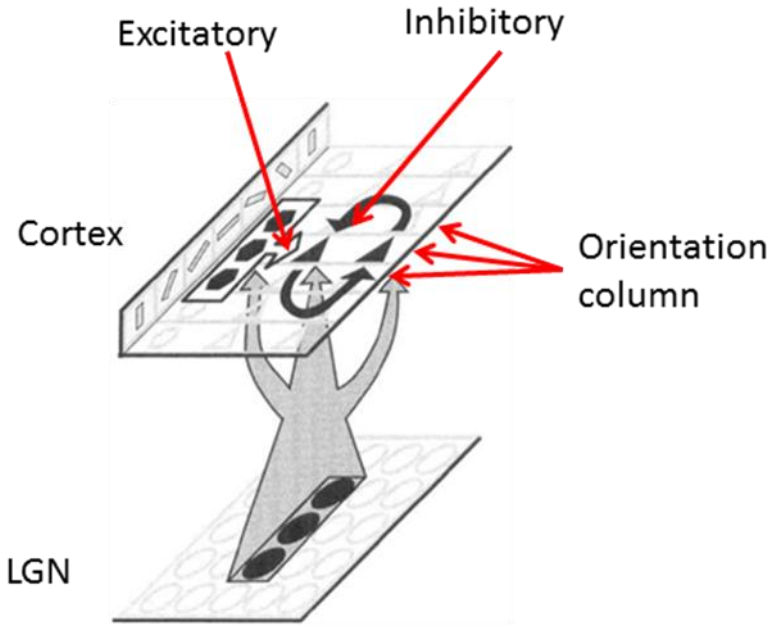

Figure 1.28: Recurrent model of orientation selectivity in cortical cells proposed by Somers et al. (1995). In this model, recurrent cortical excitation with the same orientation as the target cell is combined with cortical inhibitory inputs that have a broader orientation. This combination of excitatory and inhibitory intracortical inputs amplifies a weak thalamic orientation bias (hexagon: excitatory, triangle: inhibitory).

One of the drawbacks of this model is the insignificant role of LGN for orientation selectivity of the simple cells: many experimental studies have indicated that the LGN inputs determine the orientation of the cortical cell and that intracortical circuitry has only a sharpening role. Another issue with this model is that excitation and inhibition in cat cortex have similar orientation tuning (Martinez et al., 2002) but this is not the case in the Somers et al. model (1995).

1.5.4.4. Anisotropic LGN-driven recurrent model

Recently, another type of model has been developed based on this idea that LGN cells have orientation biases (Levick & Thibos, 1980, Vidyasagar & Heide, 1984, Xu,

Ichida, Shostak, Bonds & Casagrande, 2002). Recent computational model implemented this idea in a simple feed-forward model which get its inputs from biased oriented LGN cells and sharpens the orientation tuning with recurrent inputs from other cortical cells (Kuhlmann & Vidyasagar, 2011). In this model, simple cells are excited by orientation-biased LGN cells and inhibited by LGN cells with unoriented receptive field. The biased LGN inputs produce a weak orientation tuning response which sharpens further by recurrent cortical excitation and inhibition. This study further proposed that emergence of the full range of orientations from a restricted number of broadly tuned LGN cells can be the basis for the columnar organisation of the cortex. Considering the work of Thibos and Levick (1985) on orientation bias, there is a good evidence that orientation bias is sufficient to correctly cover all preferred orientations at each point in space.

1.6. Direction selectivity

Direction selectivity is one of the well-known and fundamental features of the cells in the visual system. This is accomplished in neurons of the primary visual cortex in animals with frontally-positioned eyes, such as cats (Hubel, 1959, Hubel & Wiesel, 1962, Hubel & Wiesel, 1963). The direction- selective cells such as simple cells of cat primary visual cortex respond vigorously to a moving stimulus such as a bar or grating moving in one direction (called the preferred direction) and little or not at all in the opposite direction (called the null, non-preferred, or anti-preferred direction).

1.6.1. Qualitative measurement

The mechanism of direction selectivity was firstly investigated in the insect's eye (Reichardt, 1961). Insect eyes are called compound eyes due to their repeating unit structure. The single visual unit, the ommatidium, functions as a separate visual receptor. The compound eye is an excellent structure for detecting motion. They respond far better to moving stimuli than to still ones.

Reichardt (1961) fixed an insect in a hollow cylinder with black and white stripes. The insect was glued to a stand and suspended in air but it was able to walk freely on a y-maze shape. Reichardt (1961) recorded the direction and intensity of the optomotor response (movement of eye, head or body in response to the optical stimulus) of insects in response to moving stimuli in order to identify the visual response in the central nervous system. This study suggested that the insect's reaction depends on the speed of the moving pattern and the pattern of light changes. The maximum reaction was elicited with a quarter-cycle phase delay between a stimulus to one ommatidium and another stimulus to the adjacent ommatidium.

Barlow and colleagues (Barlow, Hill & Levick, 1964, Barlow & Levick, 1965) discovered direction-selective cells by recording the response of rabbit ganglion cells to moving stimuli. These units discharged vigorously when the stimulus moved in one direction and responded with less or no discharge for the reverse direction. Receptive field mapping with the stationary spot stimulus established a centre-surround organisation for the direction-selective ganglion cells.

In another study, Hubel and Wiesel (1962) investigated the direction-selective cells in the cat primary visual cortex for the first time. They stimulated light-adapted eyes with stationary and moving stimuli of various shapes in anaesthetized cats and found that the most effective stimulus for the cortical cells was an orientated rectangle moving across the receptive field. This type of stimulus caused strong discharges of spikes in one direction and much less discharge in the non-preferred direction of the movement (Figure 1.29). Intracellular recording confirmed these results: Priebe and Ferster (2005) demonstrated that the modulation of membrane potential is larger in the preferred direction than in the non-preferred direction (Figure 1.30).

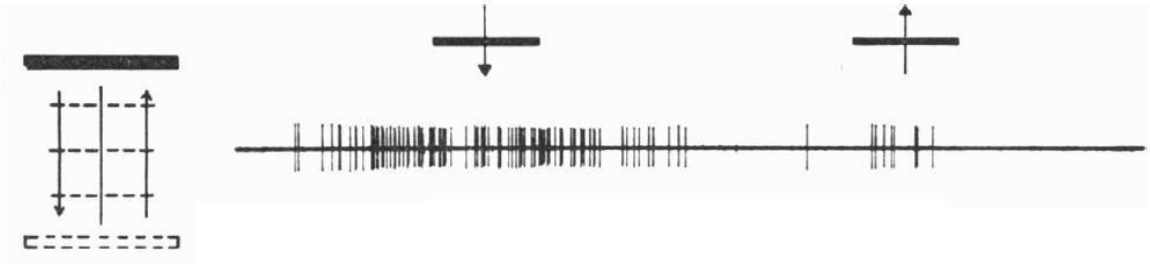

Figure 1.29: Response of a cell in cat primary visual cortex to an orientated bar moving in different directions. The cell fires many impulses to a moving bar in one direction and fires few impulses for the non-preferred direction (Hubel & Wiesel, 1962).

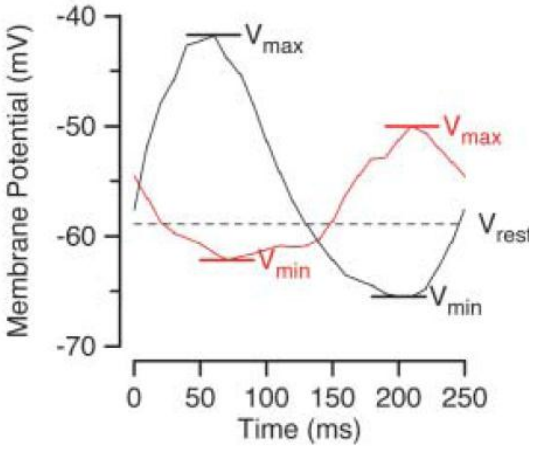

Figure 1.30: Direction selectivity can be observed in intracellular recordings. Membrane potential of simple cells for motion in the preferred (black) and non-preferred (red) direction shows that neuron respond with higher modulation in the preferred direction than in the non-preferred direction (Priebe & Ferster, 2005).

1.6.2. Quantative measurements

In addition to measuring the response of the neuron in the preferred and non-preferred direction, the direction selectivity can be assessed quantitatively using grating stimuli and the direction selectivity index (DSI). The direction selectivity index is calculated based on the fundamental Fourier component of the cell in the preferred and non-preferred direction. This index is close to one for highly direction-selective cells and is close to zero for non-directional cells. This method was introduced by Schiller et al. (1976) and has been used by many scientists (Gizzi et al., 1990, Orban, Kennedy & Maes, 1981, Reid, Soodak & Shapley, 1987) for studying the direction selectivity of cell populations.

Some studies (Carandini & Ferster, 2000, Reid et al., 1987) defined this index as the difference in the responses obtained with preferred and non-preferred directions of motion divided by the sum of those responses (equation 1.4) while some other studies defined this index as in equation 1.5 (Peterson, Li & Freeman, 2004).

$$DSI = \frac{R_p - R_{np}}{R_p + R_{np}} \tag{1.4}$$

$$DSI = 1 - \frac{R_{np}}{R_p} \tag{1.5}$$

where R_p and R_{np} are the responses to the preferred and non-preferred direction respectively. Cells with a DSI over 0.5 are considered as direction-selective cells and those below 0.5 counted as non-directional cells.

This method has been used by many studies to measure the distribution of the directionality in the primary visual cortex. Most studies estimated about 60 to 70% of the cells as direction selective (Carandini & Ferster, 2000, Gizzi et al., 1990, Hamilton et al., 1989, McLean, Raab & Palmer, 1994). Two studies (Humphrey & Saul, 1998, Peterson et al., 2004) determined that more than 70% of the simple cells are direction selective (Figure 1.31). Other studies suggested that fewer than 50% of simple cells are direction selective (Berman, Wilkes & Payne, 1987, Orban et al., 1981).

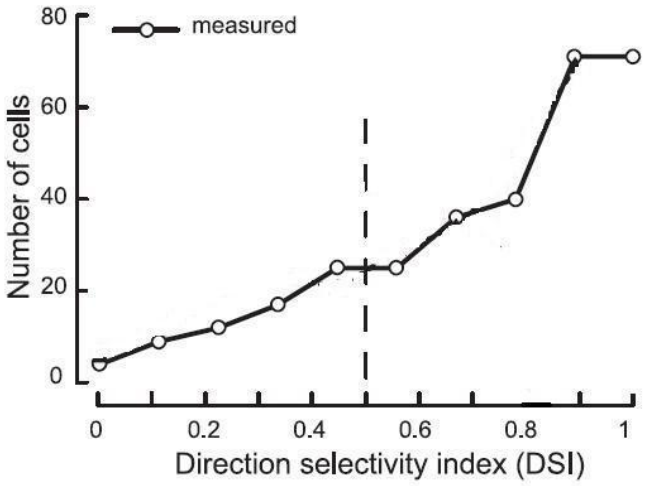

Figure 1.31: Direction selectivity index histogram for 310 simple cells of cat. The neurons were stimulated with a drifting grating at a temporal frequency of 2 Hz. About 75% of the simple cells have a DSI higher than 0.5 (Peterson et al., 2004).

1.6.3. Direction selectivity mechanism

Direction selectivity mechanisms in the visual system has been studied in different species and with a variety of techniques, from behavioral and psychophysical analysis to physiology. In all of the proposed mechanisms, the ability to detect the direction of motion depends on the interaction between responses from at least two points in the visual field at two times (Peterson et al., 2004, Priebe & Ferster, 2005, Reichardt, 1961).

Barlow and Levick (1965) suggested that direction selectivity is mainly due to suppression in the non-preferred direction rather than facilitation in the preferred direction. The anatomical structure in relation to functional organization for the sequence-discrimination is assigned to bipolar cells because the ganglion cell appears to pick up from subunits that are replicated in different parts of receptive field, and bipolar cells are the replicated anatomical elements that feed ganglion cells. Horizontal cells are known for lateral processes. So, these cells can inhibit the bipolar on one side and thus prevent them from responding in non-preferred direction. According to their analysis, the direction selectivity of movement is done in two steps. The first step is summation of the selected excitatory influences and the second step is

the inhibitory interaction of another element that has the power of veto. These two steps occur in bipolar and ganglion layers. A ganglion cell does not pool from all the bipolar cells in its receptive field, but it picks up selectively from those cells responding to a moving stimulus in a particular direction. This is followed by an inhibitory interaction which makes the response more specific.

For a long time, it was assumed that simple cells sum their inputs linearly. Some studies suggested that linear spatial summation (Reid et al., 1987) or linear temporal summation (Ganz & Felder, 1984) is mostly responsible for direction selectivity. However, recent studies have shown that direction selectivity contains a non-linear component and that linear prediction underestimates the direction selectivity index (Heeger, 1993, Jagadeesh, Wheat & Ferster, 1993, Jagadeesh, Wheat, Kontsevich, Tyler & Ferster, 1997, Peterson et al., 2004, Priebe & Ferster, 2005, Reid & Usrey, 2004). Reid et al. (1991) showed that the direction selectivity index of the linear prediction was 3 times smaller than the measured one, a result confirmed by later studies. For example, Priebe and Ferster (2005) provided evidence that the direction selectivity index of the spike rate was at least 3 times larger than the index calculated from membrane potential.

Reid et al. (1991) found that linear spatial summation of non-directional X and Y LGN cells of the cats usually underestimates the direction selectivity. The response of simple cells to drifting grating and stationary grating stimuli showed that there is a significant non-linear component to direction selectivity. A linear mechanism can estimate the response of the cell in the preferred direction but overestimates the non-preferred response because there is a significant amount of non-linear suppression in the non-preferred direction. Goodwin and his colleagues (1975) also observed the same mechanism in the cat cortical cells: direction selectivity of the simple striate cells is the result of inhibition in non-preferred direction.

Following the discovery of lagged and non-lagged cells (Mastronarde, 1987a, Mastronarde, 1987b), Saul and Humphrey (1990) proposed that lagged and non-lagged LGN cells respond a quarter-cycle apart at low temporal frequency and that their response timing difference is the source of the direction selectivity in cat visual cortex. It is worth noting that a good rationale for the role of lagged geniculate cells

has yet to be providedforthcoming. In their next study (Saul & Humphrey, 1992), they showed that cortical cells are more selective at lower temporal frequencies and direction selectivity declines with temporal frequency. The optimal temporal frequencies for direction selectivity were 1- 2 Hz and above this frequency range, the response of the cell in the non-preferred direction increased. They claimed that losing direction selectivity at higher temporal frequency was due to the loss of temporal quadrature difference between geniculate inputs.

However, later studies suggested that neither inhibition (Peterson et al., 2004, Priebe & Ferster, 2005) nor the quadrature difference (Peterson et al., 2004) contribute to the direction selectivity of simple cells. Analysis of the minimum temporal phase difference between inputs of direction-selective simple cells indicated that there is no quadrature difference between inputs and that a quarter-cycle temporal difference is not necessary to produce direction-selective cells (Peterson et al., 2004). A phase difference between inputs which is less than 90° followed by static non-linearity can makes a highly direction-selective cell. Various degrees of direction selectivity can be achieved by summing the inputs with different phase.

Priebe and Ferster (2005) used intracellular measurements to investigate the role of inhibition (shunting and hyperpolarisation) in cortical direction selectivity. They showed that both excitatory and inhibitory synaptic inputs to simple cells were modulated by a grating moving in the preferred direction, but with almost 180° phase difference (Figure 1.32). In the non-preferred direction, the excitation and inhibition were smaller and still at nearly opposite phases. They suggested, therefore, that inhibitory inputs cannot shunt the excitatory inputs as Barlow and Levick (1965) proposed. Therefore, integration of synaptic inputs is linear and threshold increases the directional difference between spike rate and membrane potential responses (iceberg effect).This non-linear step, the transformation between membrane potential and firing rate, happens after synaptic integration of inputs (Figure 1.33). Previous studies also showed that threshold can account for the non-linear transformation between membrane potential and firing rate (Jagadeesh et al., 1993, Jagadeesh et al., 1997, Priebe & Ferster, 2005).

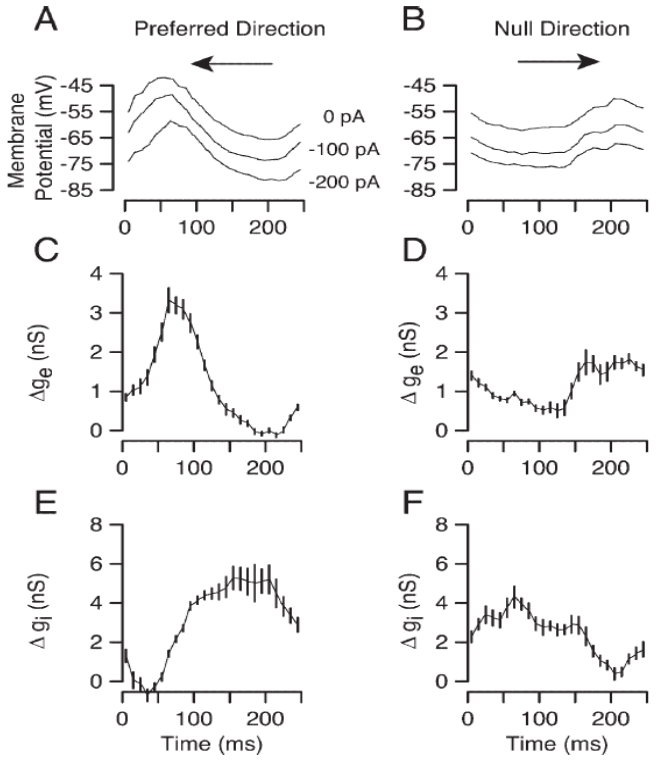

Figure 1.32: Inhibitory and excitatory inputs to directional cells in the preferred and non-preferred direction. The inhibitory and excitatory inputs have the same amplitude with a 180° phase difference between the two directions (Priebe & Ferster, 2005).

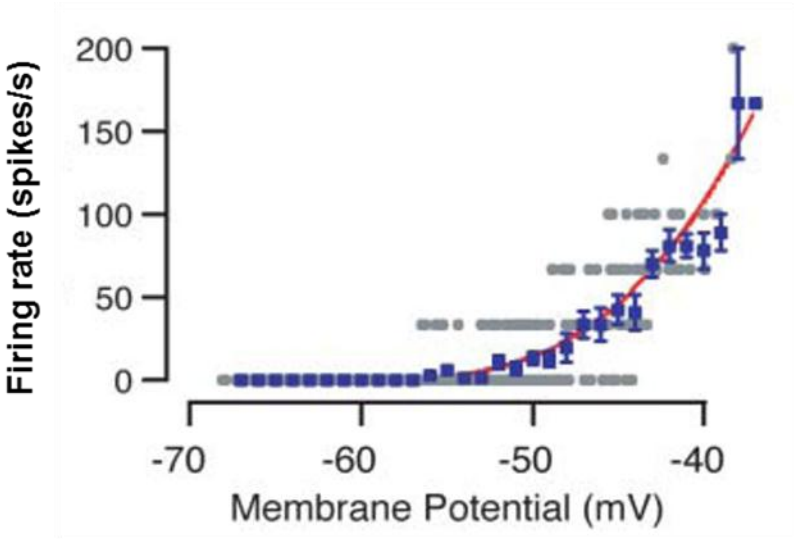

Figure 1.33: Direction selectivity in cortical cells is enhanced by the non-linear relationship between membrane potential and firing rate. The relationship between membrane potential and firing rate was fitted by a power law function with a power of 0.74 (Priebe & Ferster, 2005).

1.6.4. Direction selectivity model

Many studies have attempted to model direction selectivity in order to detect its mechanism. A temporal asymmetry is a vital part of any direction-selective detector (Borst & Egelhaaf, 1989, Soodak, 1986). The temporal asymmetry could come from a temporal delay filter (Barlow & Levick, 1965, Reichardt, 1961) or in the form of a phase difference between two filters (Adelson & Burgen, 1985).

Figure 1.34 and 1.35 show early models for motion detection in insects and rabbit retina, respectively. Both models assumed the existence of two types of channels with different conduction properties. Channel 1 and 2 in the Reichardt model (Figure 1.35) are low pass filters with different time constants while in the Barlow and Levick model (Figure 1.35), only one channel goes through a delay.

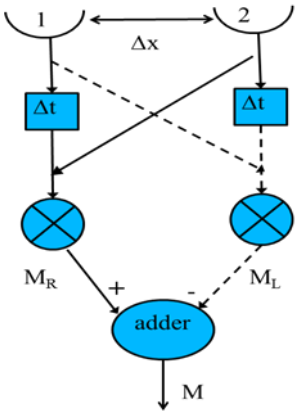

Figure 1.34: Reichart model for motion detection (Reichardt, 1961). For motion to the right the delayed response at position 1 is multiplied by the undelayed response at position 2. The strength of the final motion (M) is evaluated by subtracting the leftward motion signal, M_L, from the rightward motion signal, M_R. A positive result indicates rightward motion energy whereas a negative result shows leftward motion energy. Δt is fixed in both pathways, so the optimal response of this model occurs when the stimulus travels a distance Δx over time Δt (stimulus speed (Δx/Δt)).

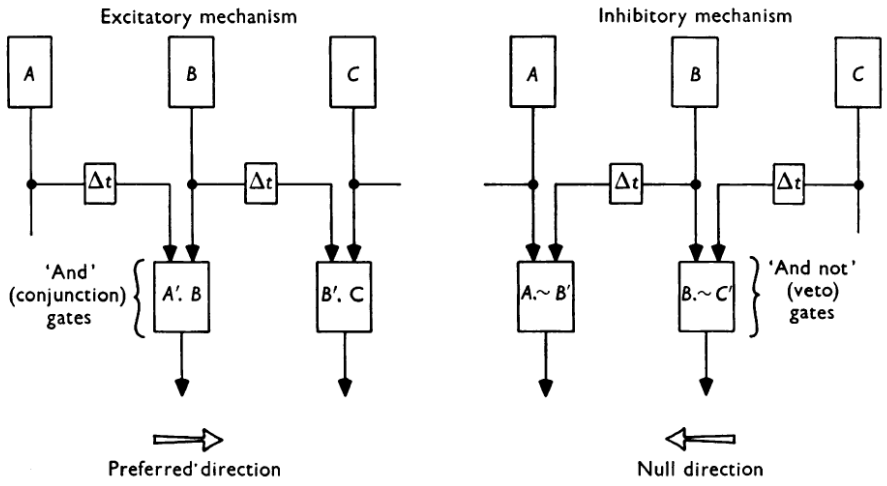

Figure 1.35: Direction selectivity model of Barlow and Levick (1965). The output is the spike rate of ganglion cells. In the non-preferred direction, the activity from B and C has an inhibitory action at the units in the next layer. That means the inhibition prevents activity from A and B from passing through the gate. In the preferred direction, the activities from groups of receptors of A and B are delayed before they pass through the next layer gate. So, action in the preferred direction is delayed and received synchronously with B.

The elementary motion detector (Reichardt, 1961) is based on encoding the motion by two spatially separated detectors where one is fed to a comparator through a slower channel than the other. When the transit time of the stimulus from the first to the second detector matches the delay associated with the first detector, the two signals will reach the comparator at the same time and motion will be detected. Note that if an object moves in the non-preferred direction then no motion signal will occur because the two signals from the detectors will arrive at different times. On the other hand, the Barlow and Levick (1965) model is based on suppression in the non-preferred direction rather than facilitation in the preferred direction.

A few years later, Torre and Poggio (1978) proposed a model based on electrical characteristics of membrane channels (Na and Cl channels). This study used a plausible mechanism of physiological synapses, which consisted of two inputs with linear inhibitory interaction followed by a threshold (Figure 1.36). The concept of the model was based on a delay between two presynaptic cells and low-pass filtering consistent with the Reichart and Barlow and Levick models (Barlow & Levick, 1965,

Reichardt, 1961). The electrical circuit of resistors-capacitors (R-C) implemented the low-pass filtering of the inputs to the direction-selective cell.

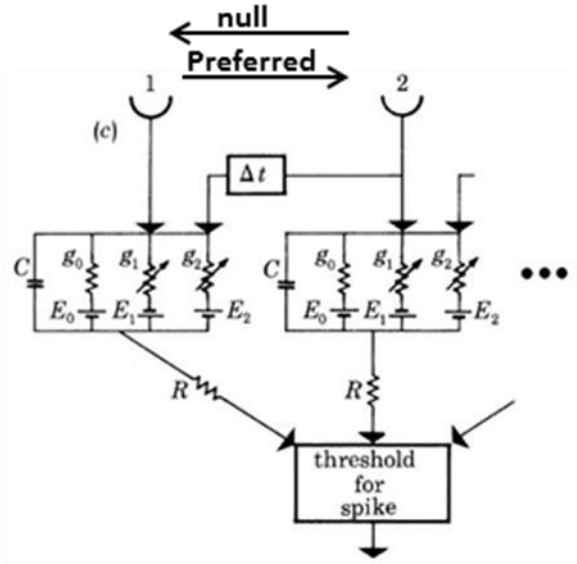

Figure 1.36: Electrical circuit of a synaptic mechanism in direction-selective cells. Channel one has a delay and this temporal difference together with the spatial separation of the channels, causes the direction-selective response. The R-C circuits are for producing a low-pass response (Torre & Poggio, 1978).

The spatial and temporal properties of the input channels were examined in more detail in later models (Adelson & Burgen, 1985, Watson & Ahumada, 1985). According to the Adelson and Bergen (1985) model, a pair of inputs with quadrature spatial and temporal phase differences can generate a direction-selective receptive field (Figure 1.38). Two quadrature filters are sensitive to the same direction with 90° phase difference. The response of these two units (directionally selective filters) are squared and summed to extract motion energy in one direction. The resulting response is always positive, so the energy response is sensitive to the direction of motion but insensitive to the sign of stimulus contrast. That means the response will be the same for a moving white-black edge as for a black-white moving edge in the same direction. The difference between rightward and leftward motion energy produces the motion detector part of this model, which expresses the motion regardless of the

direction of motion. Figure 1.37 provides a complete block diagram of the Adelson and Burgen (1985) motion detector.

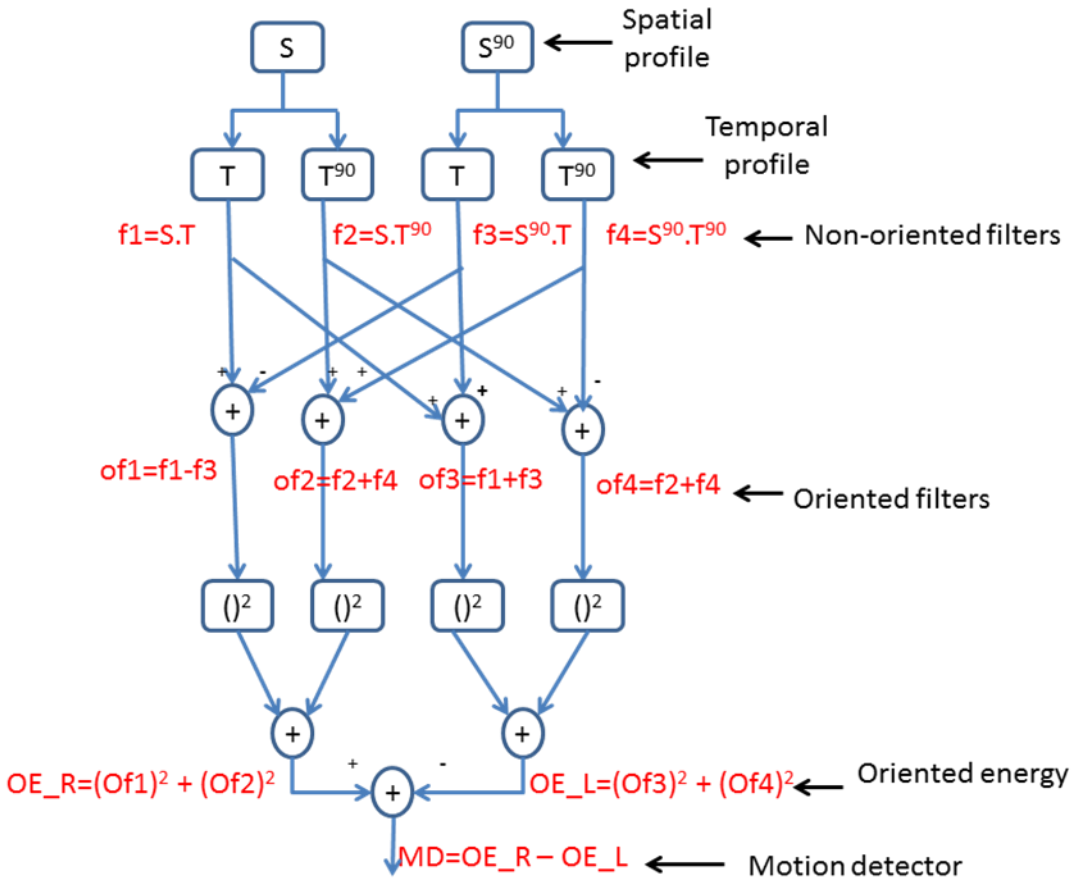

Figure 1.37: Motion detector of Adelson and Bergen (1985). S is the spatial profile and S^{90} is the same profile with a 90° phase shift. T is the temporal profile and T^{90} is the quadrature of this profile. Multiplication of these profiles produces the separable and non-oriented filters (f1 to f4). Addition and subtraction of these separable filters builds oriented filters which are sensitive to direction of motion (Of1 to Of4). Squaring and summation of two oriented filters in one direction with 90 degree phase difference (e.g. Of1 and Of2) produces an oriented energy model in one direction (OE_R) and the same action with the other two filters makes energy model in the opposite direction (OE_L). Summation of these oriented energy responses can make a motion detector which is sensitive to motion of objects regardless of their direction.

Recently, Ursino et al. (2007) developed a model to simulate the direction-selective cells in the primary visual cortex. This model consists of feed-forward inputs from geniculate cells combined with intracortical circuitry. Both feed-forward inputs and

intracortical mechanism have important roles: while the feed-forward inputs set the basis of direction selectivity, the intracortical mechanism sharpens the response. The basis of this model is the convergence of 15 lagged and non-lagged geniculate cells to the cortical cells. Each subfield of the cortical cell is constructed from the convergence of five geniculate cells in one row (Figure 1.38a) and direction selectivity originates from the time lag between lagged and non-lagged cells. Simple cells in this model have three subfields because of the convergence of the three rows of LGN. There is no time delay between LGN cells in one row, but the optimum time lag between lagged and non-lagged cells is 40 ms (Figure 1.38b). There is no time delay in the intracortical circuitry. The width and length of each subfield in cortical cells is 0.5° and 0.7° respectively.

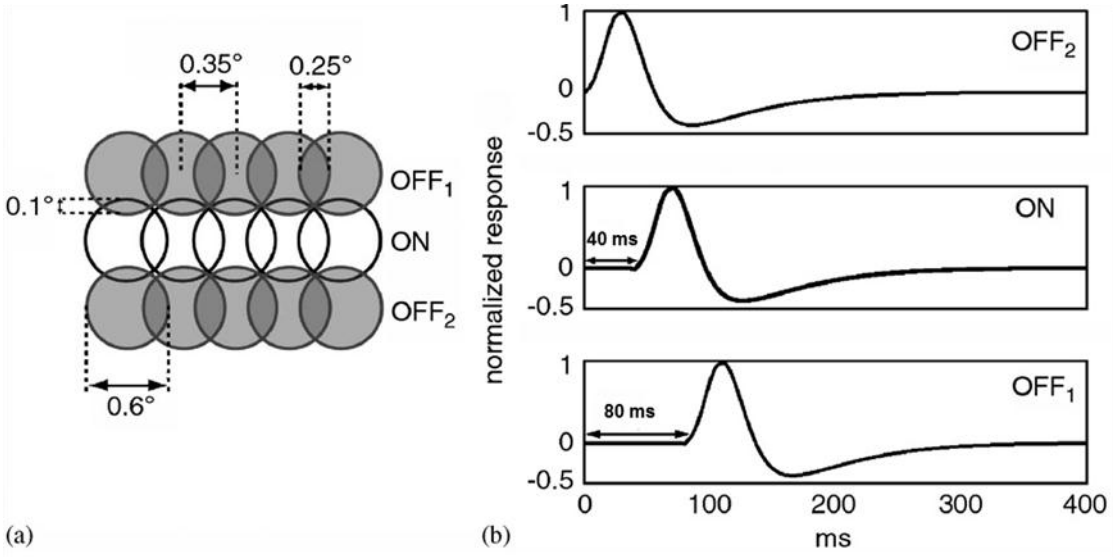

Figure 1.38: (a) Arrangement of thalamic inputs to the cortical cells, and (b) temporal impulse response of the geniculate cells, in the model proposed by Ursino et al. (2007)

The feed-forward convergence of the geniculate cells generated direction-selective cells with big response when the drifting grating was moving from the subfield with the shorter time lag to the subfield with the longer time lag, and a smaller response in the non-preferred direction. Due to the small direction selectivity index (about 0.35) with the feed-forward model, two intracortical circuitries (anti-phase and in-phase inhibitory and excitatory inputs) were added to the base model. These improved the direction selectivity of the cell to over 0.7. The intracortical circuitry consisted of

excitatory feedback from other cortical cells and inhibitory feed-forward input from interneurons. The excitatory and inhibitory strength were modulated across orientation to other orientation columns by a Gabor function. The intracortical circuitry enhanced the responses with similar direction and orientation via short-range excitatory feedback and suppressed the other responses in the long-range orientation and direction via feed-forward inhibition. In this model, anti-phase excitation and inhibition produced a higher DSI than an in-phase one.

One of the problems with this model is that it had an optimum response at high temporal frequency (4-8 Hz) while experimental results shows that cells are direction-selective at low temporal frequencies, between 1 to 4 Hz (Saul & Humphrey, 1992). Another problem is the big time delay between inputs to the cortical cells (40 ms) while recent experimental results observed a 3-6 ms time difference between the inputs to cortical cells (Jin, Wang, Lashgari, Swadlow & Alonso, 2009, Jin, Wang, Lashgari, Swadlow & Alonso, 2011a). Jin et al (Jin et al., 2011a) established this time delay from experiments on cats in similar conditions such as contrast level, background luminance (mean: 61 cd/m^2) and anaesthetic level.

1.7. Spatial frequency selectivity

Another fundamental cortical property is selectivity for spatial frequency. Cortical cells are typically narrowly tuned, with many having sharp cutoffs for both low and high spatial frequencies and average half-amplitude bandwidths of 1.5 octaves (Movshon et al., 1978c). Empirically, this property is examined by drifting an optimally oriented grating across the receptive field at a variety of spatial frequencies and measuring the fundamental Fourier amplitude of the impulse rate. The typical result (Movshon et al., 1978c), is that the neuron has an optimal spatial frequency, and that the response falls away rapidly on either side of the optimal value. The bandwidth of the spatial frequency curve is measured at half height of the curve and expressed in octaves.

$$BW_{sf} = log_2(\frac{f_{max}}{f_{min}}) \tag{1.6}$$

where

BW_{sf} is the bandwidth of the curve (octaves)
f_{max} is the upper frequency at the half height of the curve (cycle/degree)
f_{min} is the lower frequency at the half height of the curve (cycle/degree)

Figure 1.39 shows the spatial tuning curve of a simple and a complex cell in area 17. The simple cell has a lower optimum spatial frequency and narrower bandwidth than the complex cell (Movshon et al., 1978c).

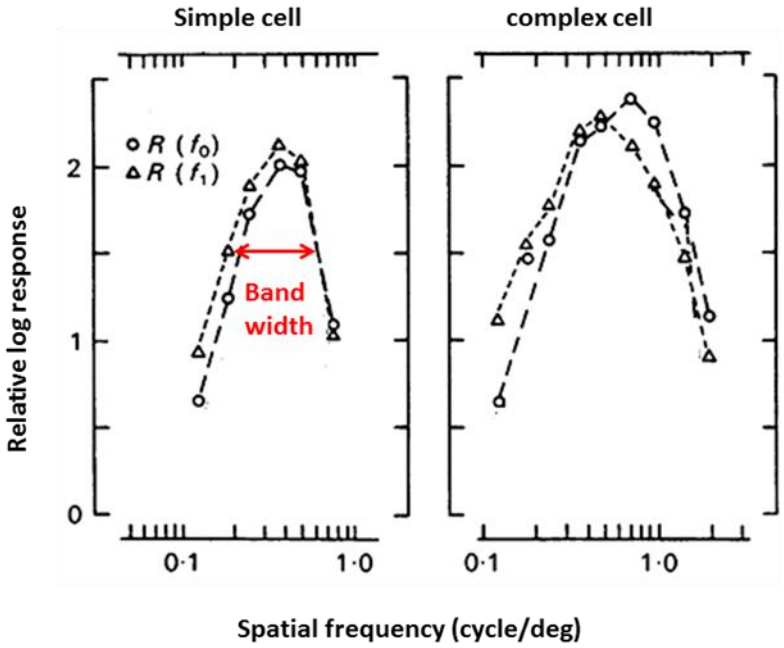

Figure 1.39: Spatial frequency tuning curve of a simple and a complex cell. Triangles give the fundamental frequency response and circles the mean firing rate of the cells. The simple cell shows a lower optimal spatial frequency than the complex cell (Movshon et al., 1978c).

Movshon et al. (1978c) assessed the spatial selectivity response over a populations of 149 cells within 5° of the area centralis in the primary visual cortex (Figure 1.40). The preferred range of spatial selectivity for both simple and complex populations was between 0.3 and 3 cycle/deg and the spatial frequency bandwidth varied between 0.7 and 3.2 octaves. On average, the tuning bandwidth of the spatial frequency in simple cells was found to be 1.5 octaves (Andrews & Pollen, 1979, Bauman & Bonds, 1991, Movshon et al., 1978c).

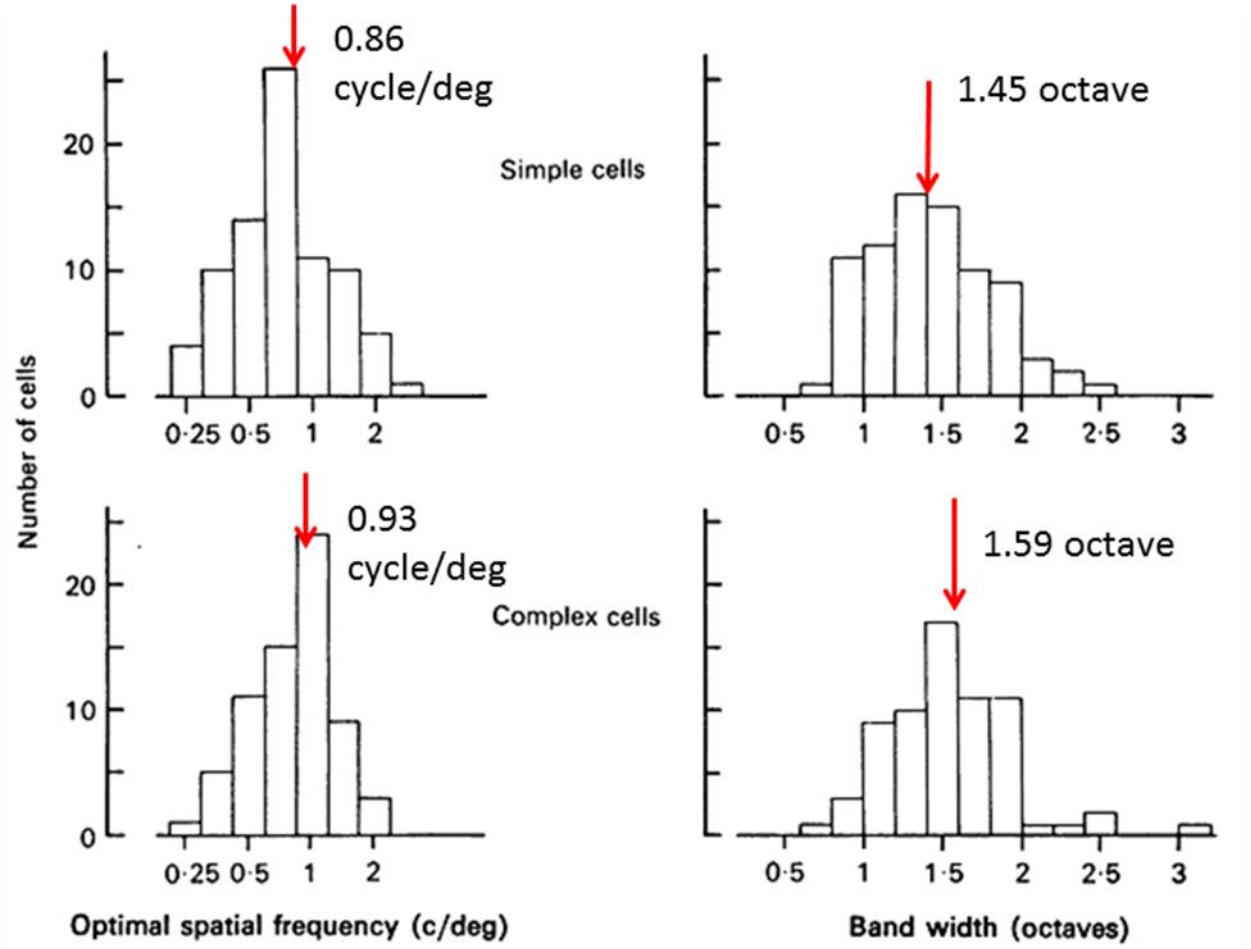

Figure 1.40: Population histograms of the optimal spatial frequency and bandwidth of the spatial frequency selectivity for simple and complex cells in area 17 of the cat cortex. Simple cells are slightly more narrowly tuned than complex cells (Movshon et al., 1978c).

1.7.1. Spatial selectivity mechanism

There are few models for the underlying mechanism of cortical selectivity for spatial frequency. One approach is to assume that spatial frequency selectivity derives from the orientation selectivity mechanism proposed by Hubel and Wiesel (1962). They hypothesized that the receptive field of a simple cell is generated by excitatory summation of signals from a linear array of geniculate receptive fields, which would yield greater activity from a bar oriented parallel to the array. An alternate model (Bauman & Bonds, 1991, Bonds, 1989) assumes that selectivity is shaped instead by intracortical inhibition. Spatial frequency selectivity has been explored with superimposed sinusoidal gratings (Bauman & Bonds, 1991, De Valois & Tootell,

1983). In this approach, one of the gratings is presented at the optimal spatial frequency of the cell and another is presented at different spatial frequencies to test the effect of suppression and facilitation on this selectivity. Observing spatial frequency-dependent responses in these studies suggested that suppression has a cortical source rather than a geniculate origin because no spatial frequency suppression has been observed in the geniculate fibers. However, Carandini and Heeger (2002) recently proposed that cortical responses such as spatial frequency selectivity can be controlled by thalamocortical synaptic depression instead of intracortical inhibition.

Chapter 2. Aims

2.1. Objectives of the research

Fifty years of research has provided detailed and rich information about signal processing in the visual pathway, including the primary visual cortex. Cells in the primary visual cortex are classified into two main groups; 1) simple cells, and 2) complex cells. These cells have characteristic properties which differentiate them from cells in the sub-cortical pathways. For example, individual neurons are known to be sensitive to the direction and orientation of moving stimuli, the spatial frequency of grating stimuli, as well as other stimulus features.

The mechanisms underlying these characteristic properties have been investigated using both physiological and computational approaches. As such, a number of models have been described to account for the emergence of a given stimulus feature (e.g. direction selectivity, orientation selectivity, and simple and complex responses). However, a major shortfall of most of these models is that only a single property is modelled in each. In addition, there have been few attempts to describe the diversity of the properties across the neural population.

The first aim of my research is to model the direction selectivity, orientation selectivity, spatial frequency selectivity, and complex responses of the cortical cells using the simplest possible model. The second aim is to simulate the diversity of these properties across the neuronal population.

For simplicity, the model is built initially from two sub-cortical inputs to the cortical cells in a single cortical column and is purely feed-forward. The sub-cortical portion contains four stages for simulating the visual pathway from retina to lateral geniculate cells. The geniculate inputs converge to cortical cells by a Gaussian weighting. Three consecutive cortical stages are considered, and the convergent excitatory inputs for each neuron in a stage come from the neurons in the preceding stage. The inputs are weighted with a Gaussian function centred on the recipient neuron. There are no connections between neurons in the same stage. This allows the assessment of how far

a purely feed-forward model can be pushed to predict cortical response properties. Where necessary, the model is enhanced by the addition of extra sub-cortical inputs, or cortical columns.

To make the task manageable, the scope of the model is limited in three ways. First, given that the literature describing primary visual cortical function is richer for the cat than for other species, the cat's visual pathway has been chosen for modelling. Second, there are several parallel sub-cortical pathways in the cat's visual system (Stone & Dreher, 1982); the model is restricted to the pathway with the highest spatial resolution, the X-cell pathway. Third, whereas primary visual cortex extends over more than one area in the cat, only area 17 is considered here because that is the major target for the X-cell pathway.

2.2. Organization of the thesis

Chapter 1 reviewed the visual pathway from retina to the primary visual cortex. In the first section, anatomical and functional properties of retinal and lateral geniculate cells were described. Following this, cortical cells and their properties were reviewed. I described the quantitative and qualitative measurements of each stimulus parameter as well as the existing models for each property.

Chapter 2 describes the aim of the research and the organization of the thesis.

Chapter 3 explains the design and development of the model, defines the parameters of the model, and describes the stimulus for testing the model.

Chapter 4 shows the receptive field and describes the orientation selectivity response of the model. This property will be demonstrated by the elongated receptive field and tuning curve.

Chapter 5 illustrates the direction selectivity of the model. The response of the cell to a moving stimulus and the direction selectivity index of the population of the cells will be evaluated in this chapter.

Chapter 6 describes the responses of simple and complex cells in the model, as well as the diversity of the response across the population of cells.

Chapter 7 shows the spatial frequency selectivity of the model. This chapter illustrates the spatial frequency tuning curve and the diversity of this property over a population of cells.

Chapter 8 discusses the research results.

Chapter 3. Methods

This thesis describes a model for simulating the fundamental properties of the cortical cells in the primary visual cortex. This model is designed to describe the simplest possible structure that can reproduce the direction selectivity, orientation selectivity, and spatial frequency selectivity of simple and complex cells in area 17 of visual cortex. The model can also simulate the diversity of these properties across a population of cells.

3.1. Model structure

A block diagram of the model's structure is shown in Figure 3.1. The model consists of four sub-cortical stages. Subcortical stages in the model simulate the most direct pathway of the visual signal, which is photoreceptors, bipolar cells, ganglion cells and relay cells in the lateral geniculate nucleus.

Sub-cortical stages consist of two pathways in the "basic model", as a motion-sensitive model needs two inputs. The two inputs are assumed to be nearest-neighbour X-cell pathways. As described in Chapter 1, the morphological correlates of X-type ganglion cells are beta cells. Wässle et al. (1981) have shown that nearest-neighbour beta cells are almost always of different sign. Accordingly, the two subcortical pathways of the model pass through an on-centre and an off-centre X-cell that are nearest neighbours. The basic model, with just two subcortical pathways, therefore uses the simplest possible structure.

There are three cortical stages. The first stage represents simple cells in layer 4 since this stage receives monosynaptic inputs from the lateral geniculate nucleus. The model doesn't specify the location of the later stages, but possibly include complex cells in layer 2 and 3. Each stage consists of an array of cells, with one at each node of a square grid. Each square in Figure 3.1 represents a single neuron, and each neuron receives convergent excitatory inputs from neurons in the preceding stage, where the inputs are weighted with a Gaussian function centred on the recipient neuron. There are no inhibitory connections and also no connections within a stage.

As shown in Figure 3.2, each neuron in the model is simulated as a linear low-pass temporal filter to produce a generator potential. Synaptic inputs are summed together over time to produce a generator potential. For all cells other than photoreceptors and bipolar cells, this potential is rectified to obtain the action potential rate.

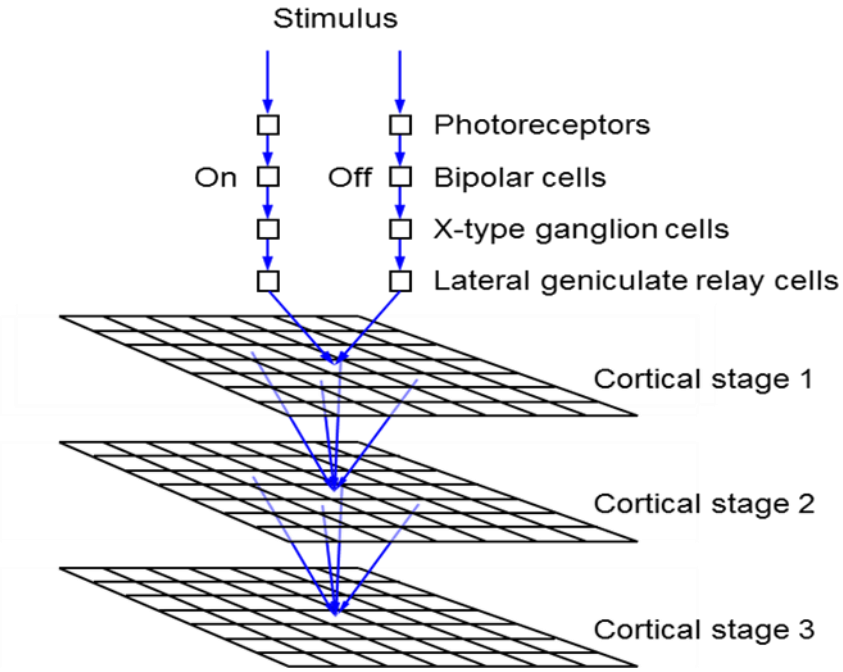

Figure 3.1: Block diagram of the basic model. This model consists of 4 stages of sub-cortical cells from photoreceptors to LGN and 3 stages of cortical cells, to mimic the visual pathway from retina to the primary visual cortex.

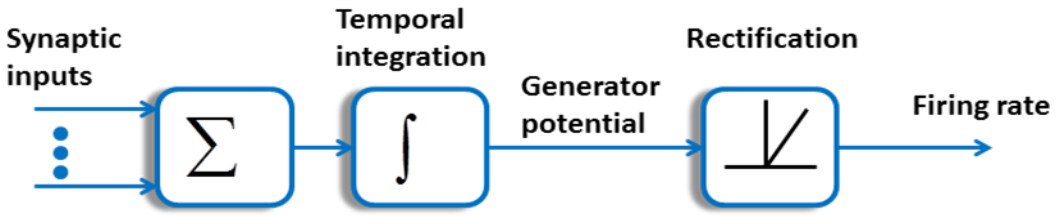

Figure 3.2: Block diagram of signal processing in a single neuron. Synaptic inputs are summed together and go through a temporal integration to produce a generator potential. For all neurons except photoreceptors and bipolar cells, the generator potential is rectified to produce the firing rate.

The conversion between generator potential and firing rate is shown in Figure 3.3. The shape and gradient are taken directly from the work of Carandini and Ferster

(2000). For different stimuli, different contrast level and different adaptation states, they found that there was a linear relationship between membrane potential and action potential rate. Firing rate is zero at potentials below threshold and it grows linearly with the potential above threshold. This linear gain between generator potential and firing rate was 7.2 impulse/ (s.mV) (the slope of the line in the Figure 3.3).

The dots on the diagram in Figure 3.3 indicate the generator potential in the absence of a stimulus for three groups of cells. Sub-cortical stages (ganglion cells and LGN neurons here) are assumed to have a generator potential greater than threshold in order to account for their relatively high spontaneous impulse rates (Kaplan et al., 1978, Stone & Fukuda, 1974). It will be shown in the Results section that neurons in cortical stage 1 are simple cells and neurons in later stages are more complex-like. Given that simple cells have little or no spontaneous impulse rate and that most complex cells have a non-zero rate (Rose & Blakemore, 1974), the stage 1 cells are assumed to be hyperpolarised relative to threshold and later stages to be moderately depolarized. The model's defining equations are as follows, and the derivation of these equations are provided in Appendix A.

$$\tau_i \frac{dp_i(t,z)}{dt} = \begin{Bmatrix} n_i g(x_i,y_i,z) * s(t,x_i,y_i,z) + p_s(z) - p_i(t,z) & z=1 \\ p_i(t,z-1) - p_i(t,z) & z=2,3 \\ [p_i(t,z-1)]^+ - p_i(t,z) & z=4 \end{Bmatrix}$$

$$\tau_{cort} \frac{dp_i(t,x,y,z)}{dt} = g(x,y,z) * [p(t,x,y,z-1)]^+ + p_s(z) - p(t,x,y,z) \quad z=5,6,7 \qquad (3.1)$$

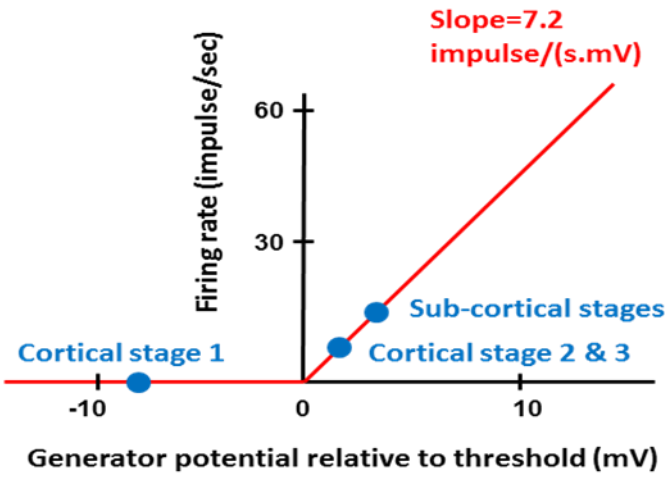

Figure 3.3: Relation between generator potential and firing rate, adapted from Carandini and Ferster (2000). They found a linear relationship between membrane potential and firing rate in cat primary visual cortex. The dots show the membrane potential in the absence of the stimulus. Cortical stage 1 (considered as simple cells due to monosynaptic inputs from LGN) is hyperpolarised since they don't have spontaneous activity. Sub-cortical stages (ganglion cells and LGN) are depolarized because they have high spontaneous activities. Cortical stage 2 and 3 (considered as complex-like cells due to receiving inputs from simple cells) are depolarized, reflecting their spontaneous activity.

3.2. Stimuli

Stimulus parameters matched published values as far as possible. Neurons in primary visual cortex are typically broadly tuned for temporal frequency, and 2 Hz is often used in published work; this value is used for the temporal frequency in this thesiswork.. Each of the quoted studies used a range of grating contrast, typically 0.25 – 0.5. Unless otherwise stated, grating contrast of 0.3 is used for the grating contrast here. Spot and bar contrasts are usually not stated in the literature; the contrast of light stimuli is set to 1 and to -1 for dark stimuli.

3.3. Implementation

Each neuron in the model is represented by a single nonlinear differential equation, and time courses in the model were obtained by simultaneous numerical integration of the equations for all neurons. The model was implemented in MATLAB (The MathWorks, Inc, R2008b). The differential equations of the model were solved using

MATLAB's *ode45* function. Appendix A derives the equations describing the model, and Appendix B describes how the model parameters were set. Table B.1 provides a summary of the model's parameters and their values. The risk of coding errors was reduced in two ways. First, my supervisor and I implemented the model equations independently before comparing results. Second, for low stimulus contrasts the model's equations are linear up to the production of impulses in cortical stage 1 neurons. I solved these equations analytically (see appendix A) and ensured that the numerical and analytical solutions agreed.

When compiling population statistics I needed some way of deciding which neurons should be excluded because of insufficient activation by the stimulus. This process of exclusion has a correlate in the laboratory: the experimenter encounters a new cell with the electrode and decides not to study it if it is insufficiently active. The criterion is as follows. A grating with optimal orientation and spatial frequency was drifted across the receptive field at 2 Hz. A neuron was excluded from analysis if the resulting elevation of its mean impulse rate was less than a criterion level. Following Romo et al. (2011) the criterion is set at 5 Hz.

Chapter 4. Receptive Fields and Orientation Selectivity

4.1. Aim

Neurons in the primary visual cortex are orientation selective. They fire impulses to a bar or line stimulus in an optimal orientation and they fire few or no impulses for the perpendicular orientation. This property, in physiological measurements, is shown by the sharpness of the orientation tuning curve obtained when the fundamental frequency response of the cell is plotted against the orientations of a drifting grating.

Some physiological studies suggested that orientation selectivity depends on the receptive field structure, an arrangement of on- and off-subfields with an antagonistic effect on each other (Hubel & Wiesel, 1962, Jones & Palmer, 1987, Palmer & Davis, 1981). This effect was observed by presenting visual stimuli at different positions in the visual field. For example, a bright bar stimulus aligned with the on-subfield generated a strong response while it generated a weaker response when the stimulus was rotated toward the orthogonal position.

This chapter explains the spatial distribution of excitatory and inhibitory subfields of cortical receptive fields in the model, and its relation to orientation selectivity. In addition, the orientation tuning of the population response will be compared with empirical results.

4.2. Receptive field

The most recognizable characteristic of a cell in the visual system is probably its receptive field, which is the map of the response to small stimuli placed at a variety of visual field locations. Receptive fields of model cells were mapped by placing a spot stimulus at different locations of the visual field. Figure 4.1 illustrates the visual field patch and the location of the on-centre and off-centre inputs in the basic model (Figure 4.1a) and the six-channel model (Figure 4.1b). In this Figure, the grey square represents the stimulated patch of the visual field (2°×2°), and the plus and minus signs indicate the receptive field centres of the on- and off-centre channels (though not to scale), respectively. The white square in the visual field represents a bright spot

stimulus. The location of a cortical cell is shown in the visual field patch as a numbered circle, where the number gives the cortical stage. For example, the circle in the middle of Figure 4.1a represents the middle cell in the first cortical stage.

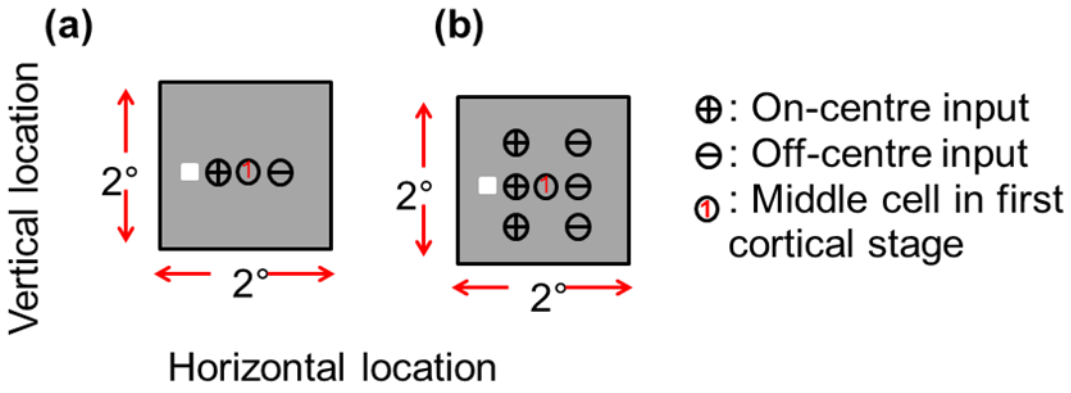

Figure 4.1: The grey square portrays the visual field patch (2°×2°). The plus and minus signs illustrate the receptive field centre of the on- and off-centre cells, respectively, in the subcortical stages (though not to scale). The circle with the number 1 represents the middle cell in the first cortical stage. The white square represents a bright spot stimulus.

Before plotting and explaining the receptive field, the impulse response of the subcortical cells and the middle cell in the first cortical stage to a bright spot stimulus is shown in Figure 4.2. The stimulus was located to the left of the on-channel, as shown by the bright spot in the visual field patch. Figure 4.2a shows the time course of neuronal responses in the on-channel; only the time-varying component of the response is shown and the time course of the photoreceptors, which hyperpolarize for light increments, is inverted for ease of comparison with the other responses. The peak response of each neuron is delayed relative to that of its predecessor, as expected of a cascade of low-pass filters. Responses of off-centre cells are shown on Figure 4.2b.

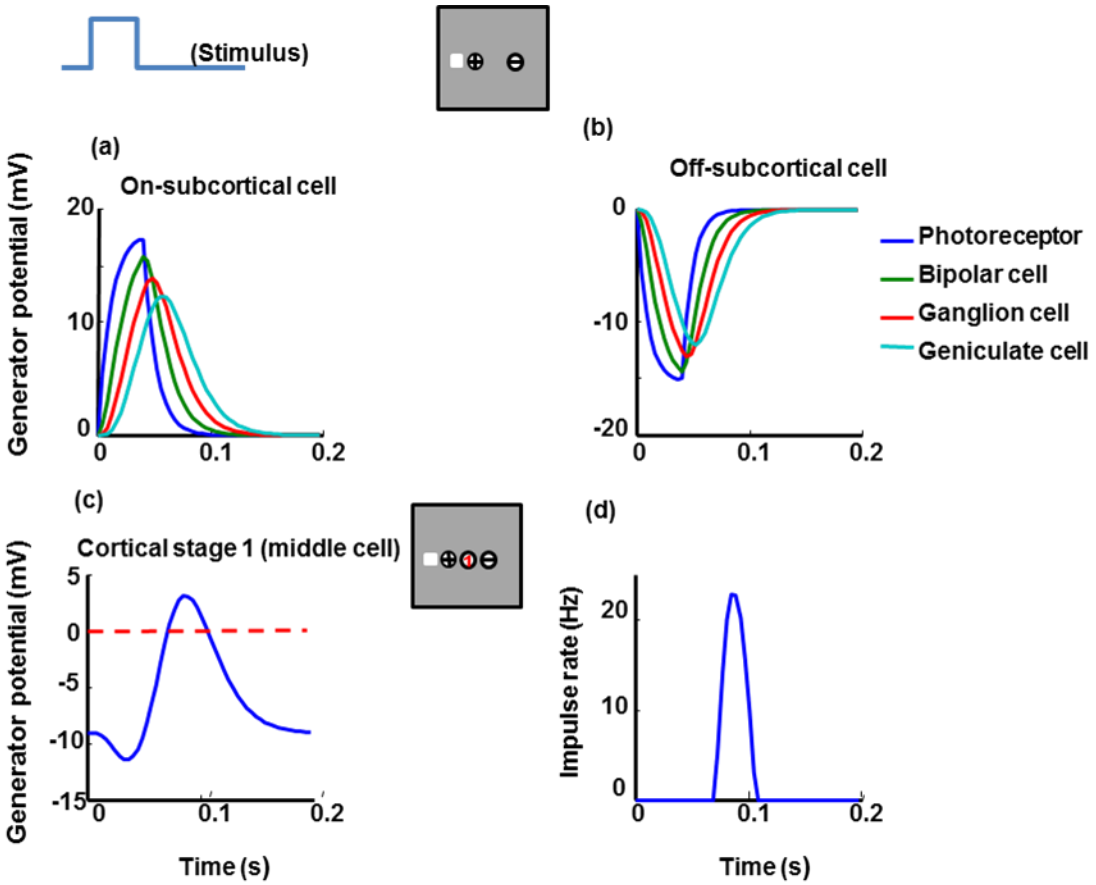

Figure 4.2: Responses of the subcortical cells, and the middle cell in the first cortical stage, to a spot stimulus. The grey square represents the stimulated visual field patch (2°×2°), and the plus and minus signs indicate the receptive field centres of on- and off-centre channels respectively (though not to scale). The white spot in the visual field patch represents a bright stimulus with a length of 0.38° and with its centre located 0.2° from the middle of the visual field patch. The rectangular waveform at the left indicates its time course. (a) Response of the on-centre cells and (b) the off-centre cells in all subcortical stages. Only time-varying responses are shown and the photoreceptor response on the left is inverted for easy comparison with the other traces. The time course in each stage is delayed relative to earlier stages because of the low-pass filtering action of all the cells. Due to the different time constant in the on- and off-pathway, there is a small difference in the amplitude of the generator potential of these two responses. (c) The membrane potential response of the middle cell in the first cortical stage (the location of the cell is shown in the visual field patch with a numbered circle) computed from the summation of the geniculate inputs and weighting factors. (d) The resulting impulse rate of the middle cortical cell after thresholding of the generator potential.

Responses in the on-channels are larger than those in the off-channels due to the closeness of the bright stimulus to the on-channel (Figure 4.2a,b). As such, the generator potential of the middle cortical cell (Figure 4.2c) is dominated by the on-channel input. Figure 4.2d depicts the impulse rate of the cortical cell after rectification of the generator potential; impulse rate is non-zero only when the generator potential rises above threshold. The initial value of the potential, at the left side of the graph, is less than threshold (shown by the dashed line) as required by the iceberg effect in cortical cells (Creutzfeldt and Ito, 1968).

Figure 4.3 illustrates the receptive field of the middle cortical cells in all three cortical stages. Maps such as these have been measured in the laboratory by presenting a spot stimulus at a succession of random locations and averaging the stimuli that precede impulses by a fixed delay (Jones and Palmer, 1987). I used a similar approach, with a delay – 85 ms – equal to the interval between stimulus onset and the peak of the response. Consistent with previous modelling work (Soodak, 1987; Ringach, 2004), two subfields can be seen in the resulting receptive field. One is produced by light increments and is dominated by signals from the on-channel. The other is produced by light decrements and derives primarily from the off-channel.

Physiological measurements have shown that the cortical receptive field has on- and off-subfield. The subfields of simple cells are separated and complex cells have overlapped subfields. The model's cortical cells have two subfields: one on and the other off. The on-subfield, the contour on the left of each plot, results from bright stimuli and the off-subfield from dark stimuli. Cells in cortical stage 1 have clearly separated on- and off-subfields whereas cells in stage 2 and stage 3 have partially overlapped subfields. Cells in the first cortical stage are therefore simple in character, corresponding to the finding that cortical cells connected monosynaptically to the geniculate are simple (Reid & Alonso, 1995). Cells in stages 2 and 3 are more complex-like.

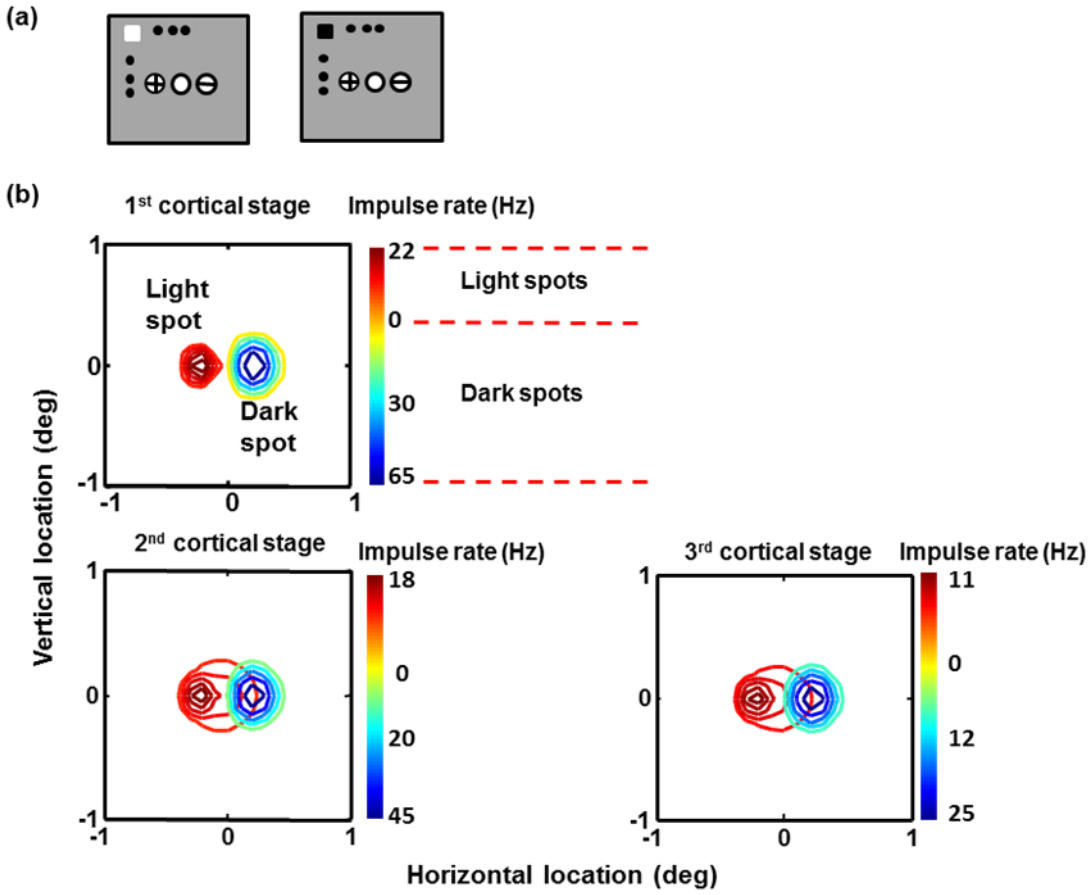

Figure 4.3: Receptive field spatial structure of the middle cells in the three cortical stages of the model. (a) The grey square shows the visual field patch. Bright and dark spots were presented in different locations of the visual field. The spot stimulus was 0.25° wide and presented at 16 locations evenly distributed across the visual field patch. The duration of the stimulus was 40 ms. (b) The spatial receptive field of the middle cells in the three cortical stages. The orange-red contour on the left of each graph is the on-subfield and the blue-green on the right is the off-subfield. The color bar on the right side of each graph shows the impulse rate to the two spot polarities.

The on-subfield in the first cortical stage has a smaller size than the off-subfield, similar to physiological measurement (Jin et al., 2011a, Jin, Weng, Yeh, Gordon, Ruthazer, Stryker, Swadlow & Alonso, 2008). This is due to the longer latency in the on-channel compared to the off-channel. As shown in Figure 4.4a, when a bright stimulus is presented close to the on-channel, the bigger response belongs to the on-channel. But since this channel is slower than the off-channel, the response of the cortical cell (which weighs, sums and integrates its inputs) is relatively small. On the

other hand, when a dark stimulus is presented close to the off-channel, the response in the off-channel is bigger and the response of the cortical cell is dominated by the big response from the off-channel (Figure 4.4b).

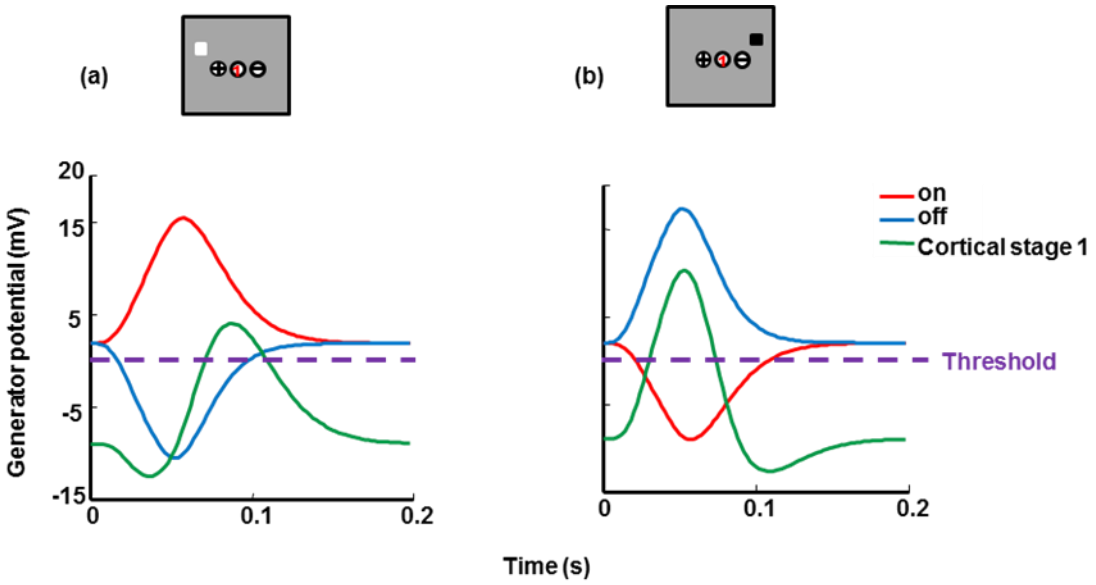

Figure 4.4: (a) Generator potential of the on- and off-geniculate cells and the middle cell of the first cortical stage in response to a bright stimulus with a side length of 0.38° and with its centre 0.2° from the middle of the visual field patch located near on-channel (x = -0.2°, y = 0.2°). On-geniculate cell produces larger response due to close location of the bright stimulus to the on-channel. The response of the cortical cell which is the weighted integral of on- and off-geniculate responses is small. (b) The response of the cells for a dark stimulus presented near the off-channel (x = 0.2°, y = 0.2°). Response of the cortical cell is large due to faster processing time in off-channel and the closeness of the dark spot to the off-channel

The basic model produces a cortical receptive field with on- and off-subfields. However, there are some deficiencies in the spatial receptive field of the model. First, cells in the first cortical stage have confined and insufficiently elongated subfields (Martinez et al., 2005). This deficiency will be addressed with a six-channel model, described below. Second, cortical cells in stage 2 and 3 have partial overlapped subfields while complex cells have completely overlapped subfields in physiological measurements. This issue will be further considered in chapter 6.

4.3. Orientation tuning

The model is designed to reproduce several fundamental properties of primary visual cortex, including sharp orientation selectivity. The receptive field in Figure 4.3a shows that the model must be at least coarsely orientation selective. The spatial subfield provides the basis for orientation selectivity of the cortical cells. In this example, when a bright bar stimulus is presented vertically on the on-subfield, the cell fires and a similar response is elicited when a dark bar is presented vertically on the off-subfield. However, if a horizontal bar is presented, the cell generates little response since it covers both on- and off-subfields. Orientation selectivity of the cortical response is checked quantitatively with an orientation tuning curve. The curve is obtained by presenting grating stimuli with orientations from -180 to 180 degree and plotting the fundamental frequency response of the cell versus orientation. Figure 4.5 shows orientation tuning curves of the middle cells in the three cortical stages. The bandwidth (half-width at half-height) of these cells is about 50°, which is very broad compared to physiological half-widths. Mean of bandwidth for cat simple cells is about 17° and for complex cells is about 25° (Carandini & Ferster, 2000, Gizzi et al., 1990, Hammond & Andrews, 1978).

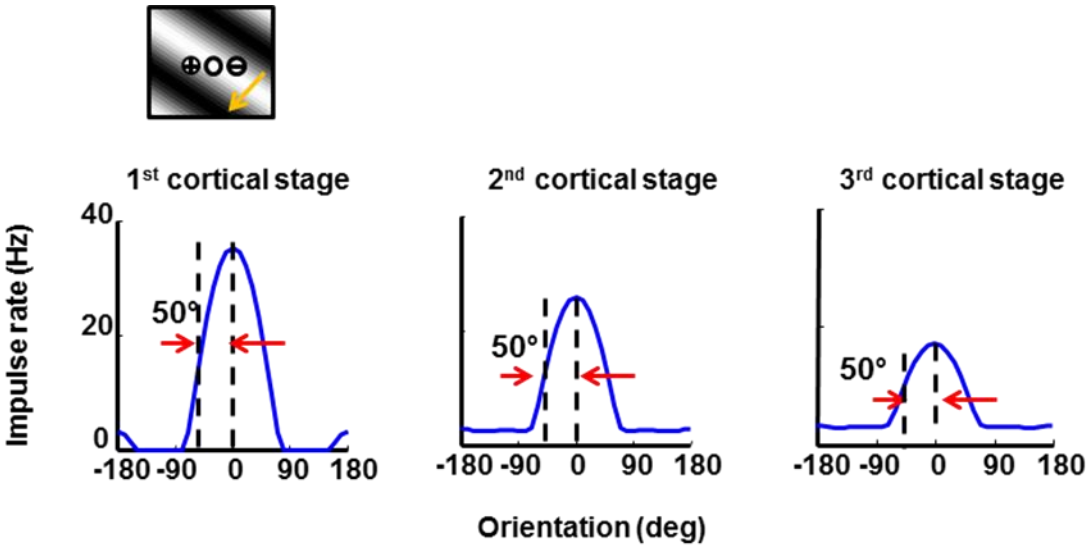

Figure 4.5: Orientation tuning curve for the middle cells in the three cortical stages of the model. Grating stimuli in different orientations were drifted across the visual field of the cells, and the fundamental component frequency response plotted against orientation. Optimal orientation is, by definition, that which evokes the peak response. Cells produce smaller responses at the other orientations and little response for the stimulus perpendicular to the optimal orientation. Half-width of the tuning curve for cells in all three stages is about 50°, which is broader than the physiological value.

A histogram of the orientation bandwidth for all active cells in the first cortical stage is plotted in Figure 4.6 (see Chapter 3 for the definition of *active*). Neurons in the basic model (2 sub-cortical channels) have half-widths clustered around 50°, a value substantially larger than for their empirical counterparts (Carandini and Ferster 2000, Gizzi et al. 1990). The distribution of the bandwidth also shows that the basic model has poor orientation selectivity compared to its empirical counterpart.

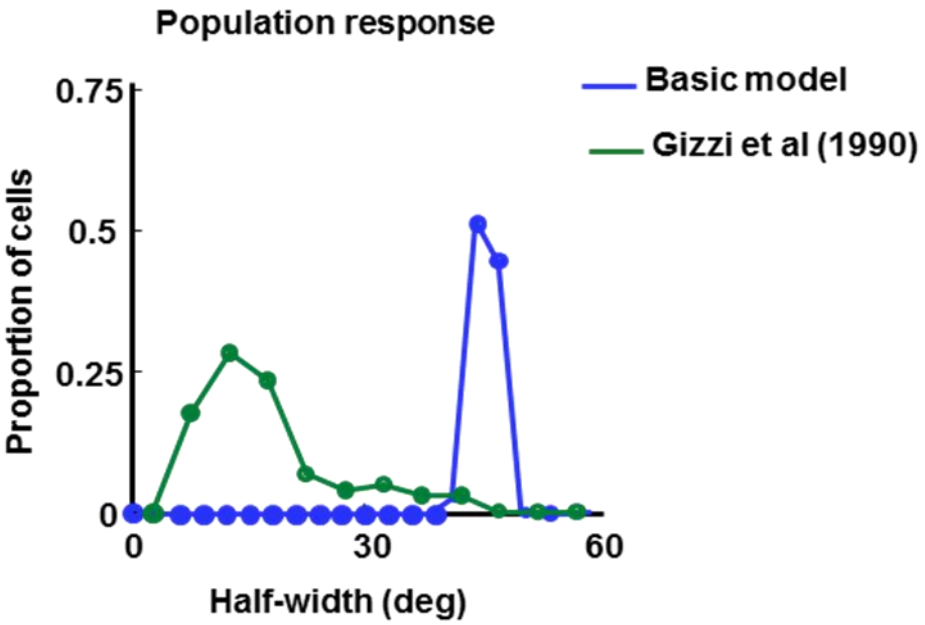

Figure 4.6: Comparison of the orientation bandwidth histogram of the basic model with its empirical counterpart. The method is chosen to mimic those used by Gizzi et al. (1990). The half-width of active cells in cortical stage one is shown by the blue curve and compared with the data of Gizzi et al. (green curve). Clearly, the basic model has poorer selectivity than the measured counterpart in the laboratory.

4.4. Six-channel model

Calculation of the orientation tuning as well as the receptive field shape showed that the basic model is only coarsely orientation selective. This limitation comes from using just two subcortical inputs to the cortical cells. To improve the results, another four subcortical channels were added in the sub-cortical stages as illustrated in Figure 4.7a. Therefore, the cortical cells receive inputs from six subcortical inputs with this new arrangement. The distance between same-sign cells was set to 0.75° and the distance between opposite-sign cells remained at 0.1°. The distance between ganglion cells of the same-sign can be as small as 0.2°, as described in appendix B, but it can be much larger, as indicated by the radius of the cortical cell receptive field. I chose a compromise distance of 0.75°: this produces an elongated subfield that largely fits into the 2° × 2° visual field patch.

Figure 4.7b shows that adding 4 extra sub-cortical channels creates elongated cortical subfields . As well as the elongation of the subfields of the cortical cells, bandwidth of the orientation tuning curve is reduced to 20° for the middle cortical cells (Figure 4.8). The histogram of the bandwidth over the population of cells is now much closer to its empirical counterpart (Figure 4.9).

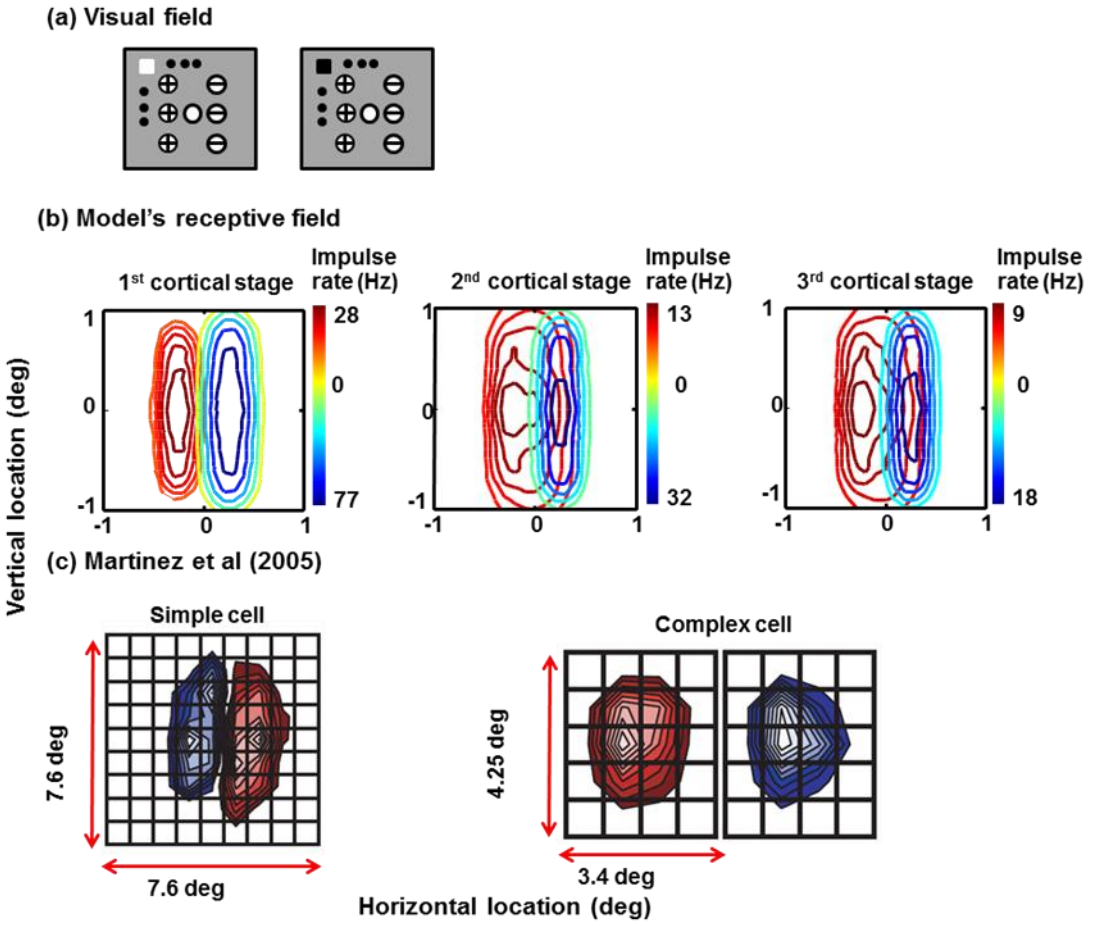

Figure 4.7 : Receptive field spatial structure of the middle cells in the three cortical stages of the model for the six-channel model. (a) Grey square shows the visual field patch. Six plus and minus signs in the visual field patch represent the location of the on-subcortical and the off-subcortical cells respectively. The circle in the middle represents the location of the middle cells in the cortical stages. The bright and dark spot put in different locations of the visual field and the response of the middle cells to these stimuli is mapped to obtain the receptive field of the cells. The spot stimulus was 0.6° wide and presented at 16 × 16 locations evenly distributed across the visual field patch. Duration of the stimulus was 40 ms. (b) the spatial receptive field of the middle cortical cells has elongated subfields compared to the basic model in Figure 4.3. The orange-red contour on the left of each graph is the on-subfield and the blue-green contour on the right is the off-subfield. The color bar on the right side of each graph shows the action potential rate for each color. (c) Simple and complex cell receptive fields measured by Martinez et al. (2005). The on- and off-subfields measured for the complex cell are spatially coincident (they are separated here for ease of comparison).

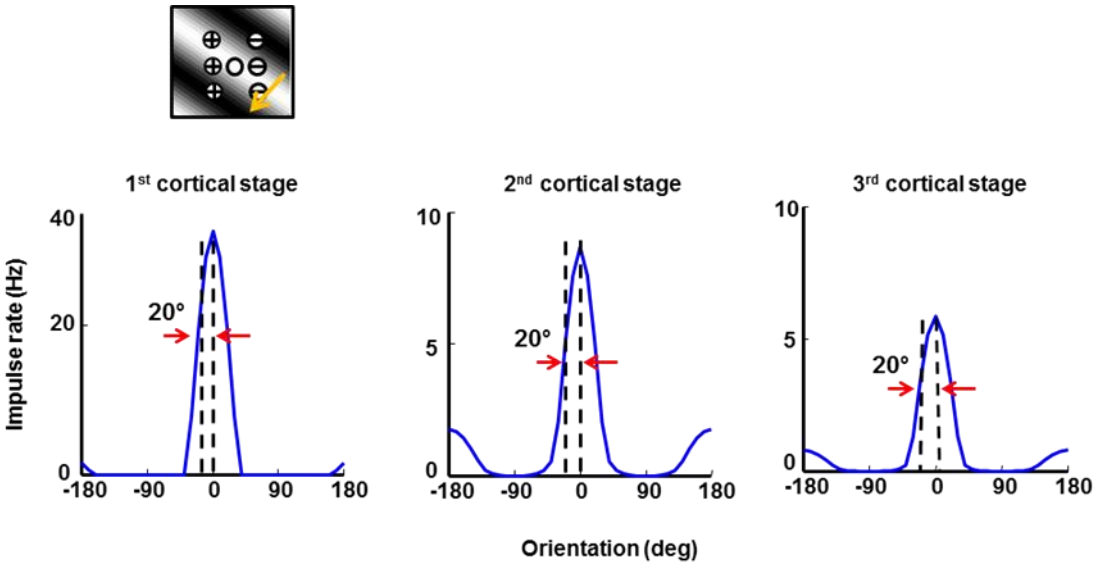

Figure 4.8: Tuning curve of the middle cell in all three cortical stages for the model with six subcortical channels. Increasing the number of subcortical inputs causes narrowing of the half-bandwidth to 20°.

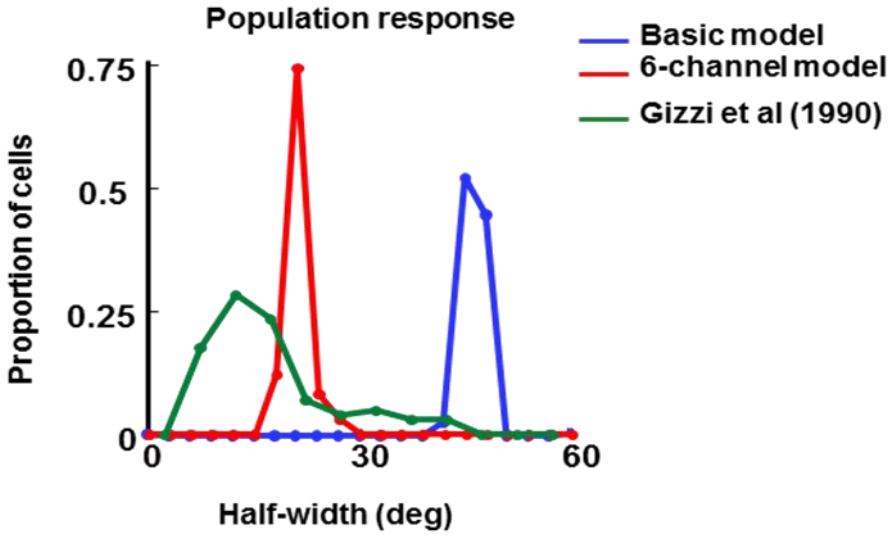

Figure 4.9: Histogram of half-width of the tuning curve for the model with six subcortical channels. The six-channel model (red curve) has a narrower bandwidth, similar to physiological data (green curve) (Gizzi et al., 1990) and has a narrower bandwidth than that at the basic model (blue curve).

4.5. Discussion and conclusions

The aim of this chapter was to simulate both the receptive fields and the orientation selectivity in the primary visual cortex with a simple model. I investigated the role of the thalamic inputs in determining orientation selectivity in a single cortical column. I showed that the basic organisation of the simple cells such as subfield structure, orientation selectivity, and preferred orientation, can be predicted by the spatial organisation of the thalamic inputs. The work tested the original hypothesis of Hubel and Wiesel (1962) with a computational model in which the parameters were obtained from physiological and morphological studies of the cat's visual system.

To this end, I started the simulation of the orientation selectivity of the cortical cells with only two thalamic inputs. I observed that this can produce coarse orientation selectivity with a broad tuning curve and confined receptive field. The modelling is consistent with the idea that thalamic inputs are the basis for orientation selectivity (Chung & Ferster, 1998, Reid & Alonso, 1995). This modelling however did not yield sharp orientation tuning and an elongated receptive field. Alonso et al. (2001) showed that cortical cells received their inputs from many thalamic cells, so the model was modified by adding extra subcortical inputs. Recalculating the results for a six-channel model showed a sharper orientation tuning curve and elongated subfields. These results are computational confirmation that geniculate inputs, rather than intracortical circuitry such as recurrence, are sufficient to produce much of the observed orientation selectivity.

The two-channel model produced a confined receptive field with a broad tuning curve, while the six-channel arrangement generated an elongated receptive field with high length-to-width ratio and sharp tuning curve. My results confirmed the correlation between the aspect ratio of simple cells subfields and the orientation tuning curve. The six thalamic inputs produced the elongated receptive field and sharp tuning curve similar to physiological evidence (Chung & Ferster, 1998, Ferster et al., 1996, Jones & Palmer, 1987, Reid & Alonso, 1995).

Moreover, I have examined the diversity of orientation tuning over a population of cells in the first cortical stage. The basic model generally had broad tuning, unlike

physiological neurons. However, increasing the number of inputs of the cortical cells reduced the population half-width, in better agreement with its empirical counterpart. Since the parameters of the model are fixed and no optimisation was done, not much variability can be seen in the histogram (Figure 4.6). Some variability in this histogram is due to the Gaussian convergence of the inputs to the cortical layers, so cells closer to the centre of cortical layer receive a bigger effect from geniculate inputs and further cells receive a smaller input from the Gaussian distribution.

Nevertheless, increasing the contrast level in the current model will increase the half-width of the orientation tuning curve (Figure 4.10). This is one of the weaknesses of the model. Physiological evidence (Ferster & Miller, 2000, Sclar & Freeman, 1982, Sompolinsky & Shapley, 1997) showed that orientation selectivity is invariant with contrast level. There is much evidence that inhibition results in sharpening of the orientation tuning curve when contrast is increasing (Anderson et al., 2000b, Ferster & Miller, 2000). There are a variety of models addressing the contrast-invariance of orientation selectivity, some of which rely on intracortical inhibition (Somers et al., 1995, Troyer et al., 1998), others of which do not (Finn, Priebe & Ferster, 2007). How should the model be modified to give this contrast-invariance? One possibility is intracortical inhibition. While the model emphasises the thalamocortical role for generating the visual properties, it is highly likely that the hyperpolarisation in the first cortical stage comes from the intracortical inhibition. Evidence that is more direct comes from intracellular recordings of simple cells, which show a hyperpolarised membrane potential in the absence of a stimulus (Carandini & Ferster, 2000). The addition of dynamic inhibition may rectify this limitation. In particular, adding lateral inhibitory connections within each stage would introduce a hyperpolarisation that increases with stimulus contrast. This would help to preserve the iceberg effect.

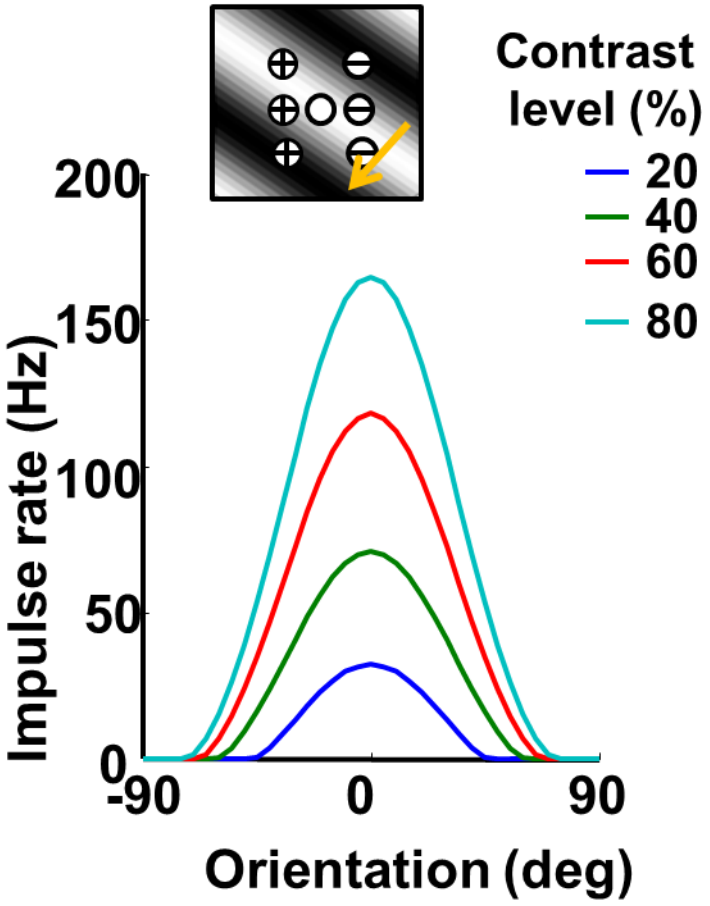

Figure 4.10: Orientation tuning curve of the model with variant contrast level. The half-width of the response increases with contrast level. The variant bandwidth is probably due to a lack of inhibition in the model as some models (Somers et al., 1995, Troyer et al., 1998) addressed this effect.

Chapter 5. Direction Selectivity

5.1. Aim

Direction selectivity is another key property of neurons in the primary visual cortex. In the primary visual cortex of cats, most of the cells in all layers are direction selective, responding strongly to a stimulus moving in one direction across their receptive field and weakly or not at all to movement in the non-preferred direction (Albrecht & Geisler, 1991, Hubel & Wiesel, 1962, Reid et al., 1987). A moving stimulus, by definition, is at one location at a given time and in another location at a later time. Therefore, the moving object can be identified by a cell that combines inputs which are different from each other in both space and time.

The basic hypothesis to test is that convergence of thalamic inputs with different locations in space and different delays can produce direction-selective cells. The mechanism of direction selectivity in the cat's visual cortex is addressed and simulated by showing the response of cortical cells in both preferred and non-preferred direction. To be more useful, the diversity of the directionality over a population of neurons using the direction selectivity index is also reproduced. To examine this question further, the spatio-temporal receptive field of the directional cells is studied and compared with non-directional cells and physiological recordings. In the case of any discrepancy between the model results and the empirical data, the model is modified to produce a better match.

5.2. Direction selectivity mechanism of the model

To generate a direction-selective unit, the model receives at least two asymmetric sub-cortical pathways. The inputs to directional-selective cells have two important characteristics: 1) there must be two or more inputs that are dissimilar from each other in spatial location and 2) the inputs must have different latencies or temporal phase. The spatial dissimilarity comes from two subcortical inputs (on- and off-pathway) and the temporal asymmetry comes from different latencies in the responses in those pathways. In my model, the off-pathway has a shorter time constant compared to the

on-pathway. This is consistent with recent evidence indicating that off-centre LGN response precede on-centre LGN response by 3-6 ms (Jin et al., 2009, Jin et al., 2011a). The time constant is set to 9 ms and 11 ms for off-centre cell and on-centre cells, respectively, as explained in Appendix B.

The mechanism for direction selectivity is depicted in Figure 5.1. The on-pathway has a longer processing time than the off-pathway. Moving a stimulus from right to left produces a big response and moving in the opposite direction (from left to right) produces a small response. How does this happen? In the preferred direction, when the stimulus is moving from the off- to the on-pathway, there is no stimulus delay and minimal processing delay in the off-pathway (Figure 5.1a). On the other hand, in the on-pathway, there is a stimulus delay and longer processing time. The output of the on-pathway, therefore lags that of the off-pathway and as such there is little cancellation of the two outputs. This results in a big response in the preferred direction.

On the other hand, moving the stimulus from the on- to the off-pathway (Figure 5.1b) leads to strong cancellation: the two subcortical responses are almost in phase because the extra processing delay in the on-pathway matches the stimulus delay in the off-pathway.

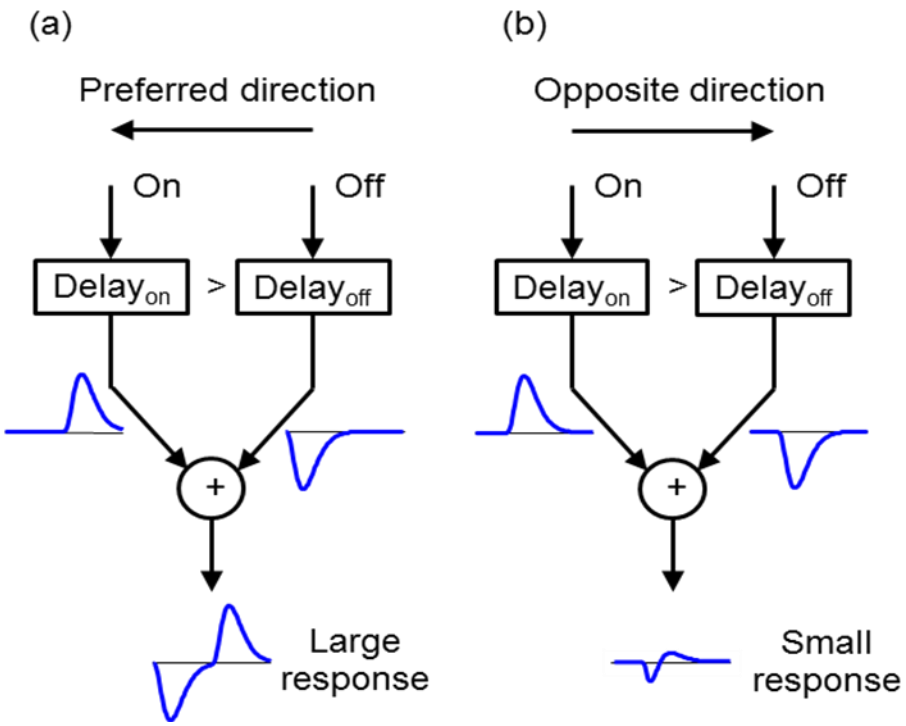

Figure 5.1: Schematic overview of the direction selectivity mechanism. The spatial and temporal differences between the two pathways are important factors to generating directional cells. There is a big response in one direction and a small response in the opposite direction.

5.3. Direction selectivity response: moving stimuli

Figure 5.2 shows the generator potential in both on- and off-geniculate cells of the basic model for a single cycle of a grating stimulus. The mean potential is set to zero and the off-signal is inverted to better compare these two signals. The graph at the left indicates the response of the cells in the preferred direction: the off-signal leads the on-signal because of its shorter processing time and the absence of a stimulus delay. The graph at the right, illustrating responses in the opposite direction, shows a much smaller phase difference between the two signals. Thus the sum of the on- and off-signals, which approximates the weighted sum formed by a cell in the first cortical stage, is smaller at the right that at the left. The reason for the directional difference is that for motion in the non-preferred direction, the time taken for the stimulus to travel from the middle of the on-centre receptive field to the middle of the off-centre field is

almost equal to the extra signal-processing time in the on-channel relative to the off-channel. Cancellation of the two inputs to the cortical cell is therefore almost complete, as shown by the sum curve.

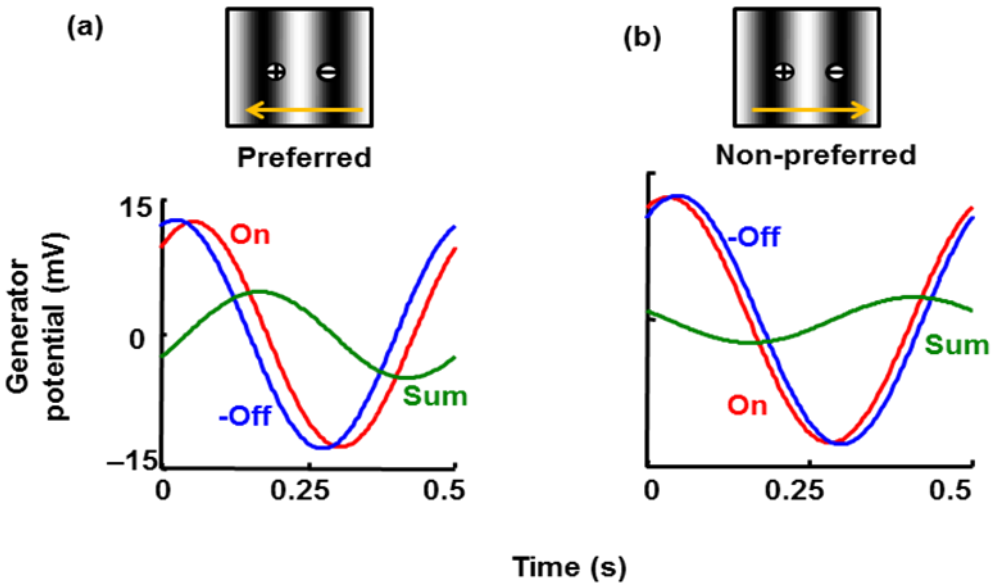

Figure 5.2: Direction selectivity mechanism. Geniculate generator potential in the on- and off-centre neurons, along with the sum, is shown in the a) preferred and b) non-preferred direction. A grating with optimal orientation and spatial frequency was drifted across the visual field. Only time-varying signals are shown and the off-centre signal is inverted for better comparison. The on- and off-inputs to a cortical cell are almost in phase in the non-preferred direction, resulting in cancellation and a smaller sum.

Figure 5.3 illustrates the response of the first-stage cortical cell whose receptive field lies midway between those of the sub-cortical channels. The generator potential in this cell is the result of weighting, summing, hyperpolarising, and low-pass filtering, of the two geniculate inputs in Figure 5.2. The generator potential amplitude for stimulus motion in the preferred direction is greater than that for the non-preferred direction, but not markedly so. The difference is much clearer after thresholding, to form the impulse rate shown in Figure 5.3b. Here the response for the preferred direction is much greater than for the non-preferred direction. This is largely due to the iceberg

effect, a phenomenon well documented from intracellular recordings of cortical cells (Carandini & Ferster, 2000).

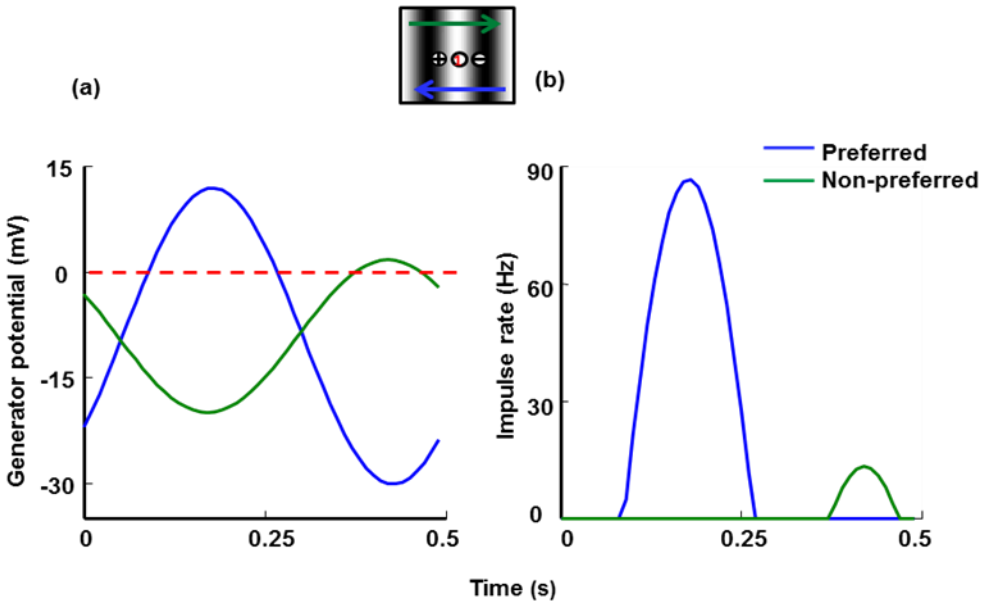

Figure 5.3: a) Comparison between generator potential in preferred and non-preferred direction for the centrally located neuron in cortical stage 1. b) Impulse rate of this cell. After thresholding, the response in the non-preferred direction is much smaller than that in the preferred direction.

The result of this individual cell compares well with the response of a simple cell in a physiological measurements (Figure 5.4). In one temporal cycle, both cells produce a high impulse rate in the preferred direction and little spike rate in the non-preferred direction (Priebe & Ferster, 2005).

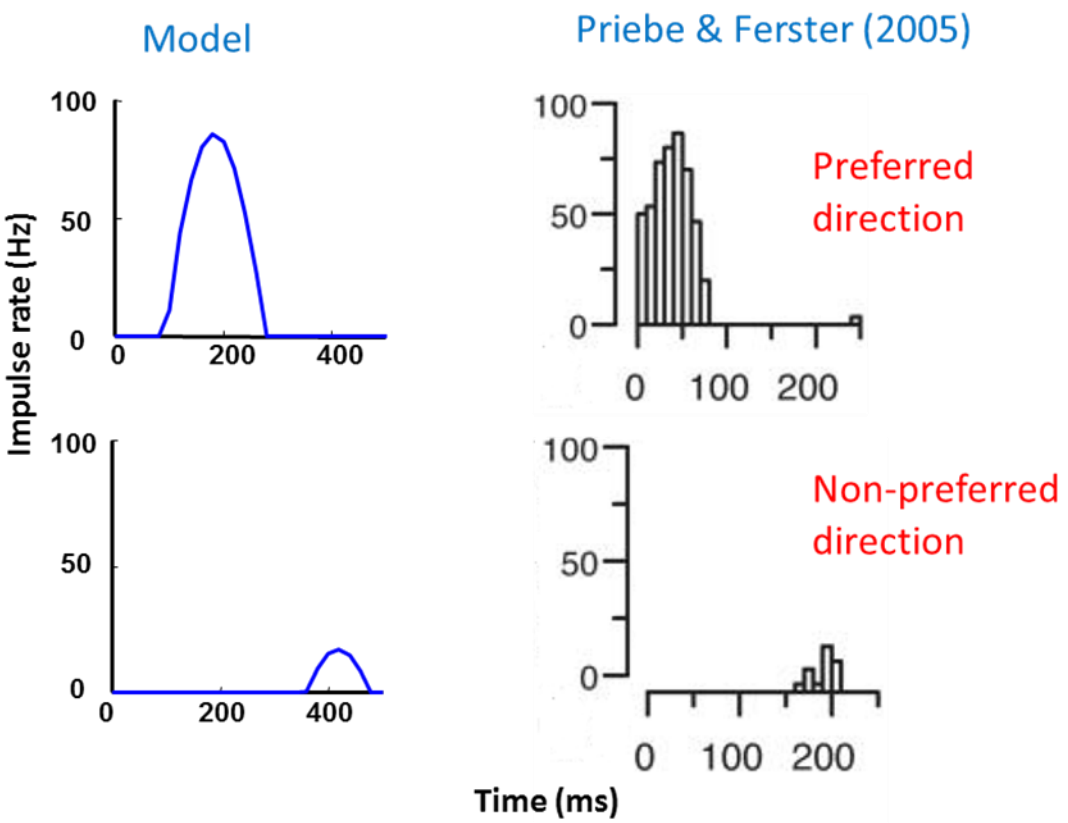

Figure 5.4: Verification of the direction selectivity of the model's result by comparison between a cortical cell response of the model and physiological data. The model response shows that the cortical cell has a high impulse rate in the preferred direction and a smaller response in the non-preferred direction, in accord with physiological data (temporal frequency: 4 Hz) (Priebe & Ferster, 2005).

Direction selectivity can be quantified with the direction selectivity index, which has a value of zero for non-directional cells and one for the most direction-selective cells. The direction selectivity index is calculated by drifting a grating across the receptive field and finding a spatial frequency and a direction that maximise the fundamental Fourier component of the response, where the response measure can be either membrane potential or impulse rate. The index is usually calculated as the difference of this fundamental component and the fundamental component when the same grating is drifted in the non-preferred direction, divided by the fundamental component in the preferred direction. The direction selectivity index calculated from

the membrane potential is substantially lower than the index from impulse rate (Jagadeesh et al., 1997).

The direction selectivity index over all active cortical cells in stage 1 of the basic model was computed from membrane potential (Figure 5.5a) and impulse rate (Figure 5.5b). All neurons in the basic model fall into a single bin, shown by an upward arrow. The comparison between model result and physiological result (Jagadeesh et al., 1997, Peterson et al., 2004) shows that the model cells are concentrated at the right end of the empirical data: the model is *too* direction selective.

To make the direction selectivity more realistic, I reduced the asymmetry between the two sub-cortical channels by decreasing their latency difference. The logic behind the procedure is as follows. The empirical data in Figure 5.5 come from many cells recorded across multiple cortical columns. It is to be expected that latency differences will vary from column to column. As such, I ran the basic model ten times, each time with a new value of the time constant difference between the two subcortical channels. In particular, I used differences uniformly distributed between 0 and 2 ms. The results for the multi-column model in Figure 5.4 closely match the empirical data. About 70% of the simple cells in the model are direction selective (index greater than 0.5) similar to the Peterson et al. (2004) data.

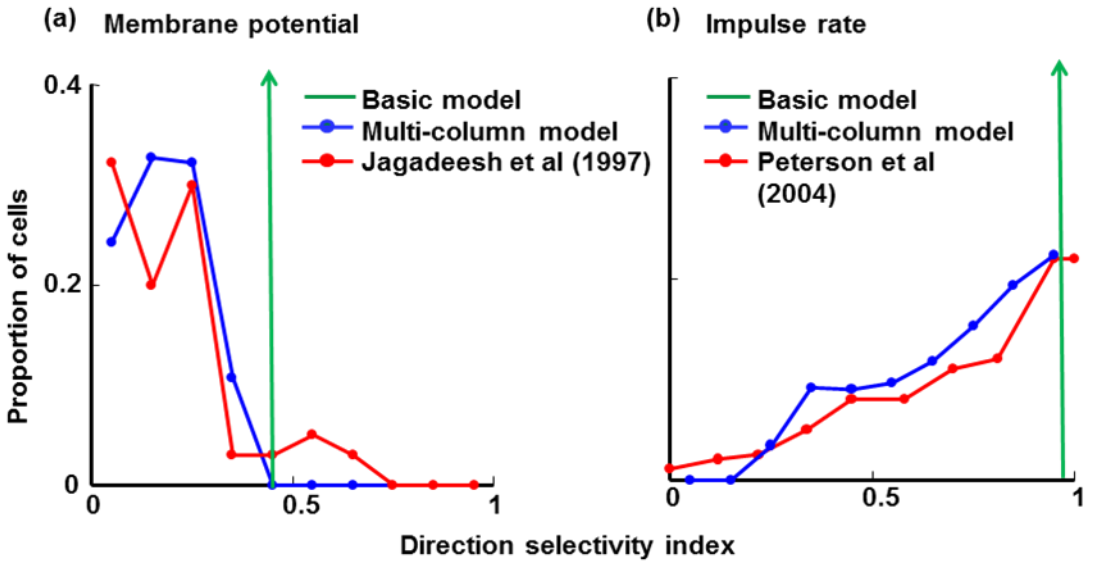

Figure 5.5: Comparison of direction selectivity index for cortical cells in the first cortical stage with empirical data. (a) Histogram of the direction selectivity index calculated from membrane potential (Equation 1.4) and compared with Jagadeesh et al. (1997). (b) Direction selectivity index calculated from the impulse rate (Equation 1.5). The basic model is too direction selective and all neurons fall into one bin. To have a more realistic situation, direction selectivity was calculated from 10 columns with different temporal latencies between on- and off-subcortical channels. The resulting histograms shown in blue are closer to their empirical counterparts.

5.4. Direction selectivity response: stationary stimuli

Direction selectivity was also investigated using stationary stimuli as shown in Figure 5.6. Spatiotemporal receptive field in the model were derived by presenting dark and bright bar stimuli at 16 locations across the 2°×2° visual field and measuring the impulse response of the cortical cells. Stimulus location changed only in the *x* dimension. The bar stimulus was optimally oriented with a duration of 40 ms, matching the duration used by DeAngelis et al. (1993b). The horizontal axis of the plot gives the location of a bar stimulus in the visual field and the vertical axis gives time from the onset of the bar.

Direction selective cells have different response time courses at different positions within the receptive field (Adelson & Burgen, 1985, DeAngelis, Ohzawa & Freeman, 1993a, DeAngelis et al., 1993b, Jagadeesh et al., 1993, Jagadeesh et al., 1997, Movshon et al., 1978a). Many direction-selective cells display spatiotemporal *inseparable* structure: response timing changes progressively from one position to the next across the receptive field, when tested with stationary stimulus. This property results in both a tilted spatiotemporal receptive field and direction selectivity (Jagadeesh et al., 1997, McLean & Palmer, 1994, Reid et al., 1991). In contrast, simple cells that are not direction selective are all space-time *separable*. Their receptive fields are not oriented in space-time (McLean & Palmer, 1994).

The basic model produces a inseparable receptive field with tilted subfields, confirming the previous results. To better understanding the separable and inseparable structure, the spatiotemporal receptive field of the middle cell in the first cortical stage is plotted for two states:

1) Equal temporal latency in subcortical channels, which produces a non-directional cell (Figure 5.6a)

2) Basic model: different temporal latency between the two subcortical channels generating a direction-selective cell (Figure 5.6b).

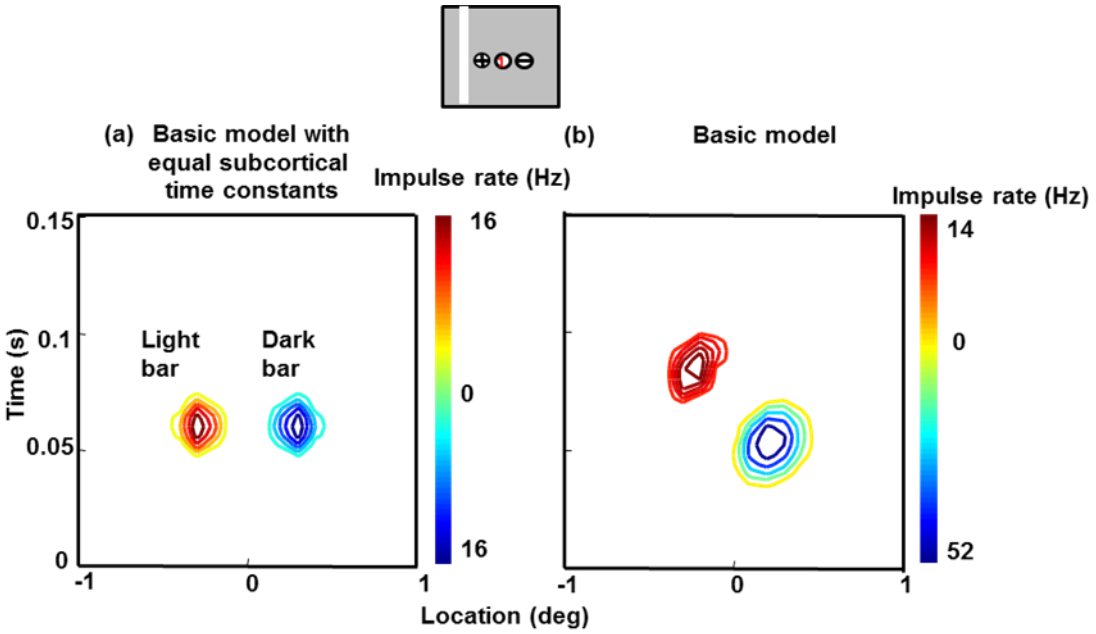

Figure 5.6: Comparison between separable and inseparable receptive fields in the middle cell of the first cortical stage of the model. The spatiotemporal receptive field was calculated for the centrally located cell in cortical stage 1 by presenting narrow bars of light and dark at a variety of locations as illustrated in the visual map. Bars were 0.3° wide and were presented at 16 locations evenly distributed across the visual field patch. (a) Equal temporal latency for on- and off-subcortical channels produces a non-directional cell with a separable receptive field profile. (b) A difference in latency between the two subcortical channels generates a direction-selective cell with tilted subfields.

Figure 5.7 demonstrates another comparison of direction selectivity in the model with empirical data. The six-channel model is used here because it produces more elongated contours than does the basic model. The model response can be understood by visualizing a vertical line through the zero spatial location. The response to the dark bar (blue contour) appears earlier than that to a light bar (red contour) because of the faster processing time in the off-channel. To the left of this line, the map is dominated by responses to light bars because these preferentially stimulate the on-channel, and to the right by dark bars, for which the off-channel dominates. The net effect is a set of contours slanted from lower left to upper right. The same tilting is seen in the empirical data (Figure 5.7b), which is a signature of direction-selective cells (DeAngelis et al., 1993b). As such, the model again reproduces the basic elements of laboratory observations.

One more consequence of the asymmetry of on- and off-channels should be noted from Figure 5.7a. The colour bar on the right side of the model plot shows the color coding of impulse rate. It is clear from the colour bar that the response to dark bars is larger than that to light bars. This corresponds to the empirical finding that simple cells close to the central area are off-dominated (Jin et al., 2008). Off-domination in the model occurs because the response in the off-centre channel is faster and therefore has a higher peak than that in the on-centre channel. The same effect is seen in the receptive fields plotted in Figure 4.2.

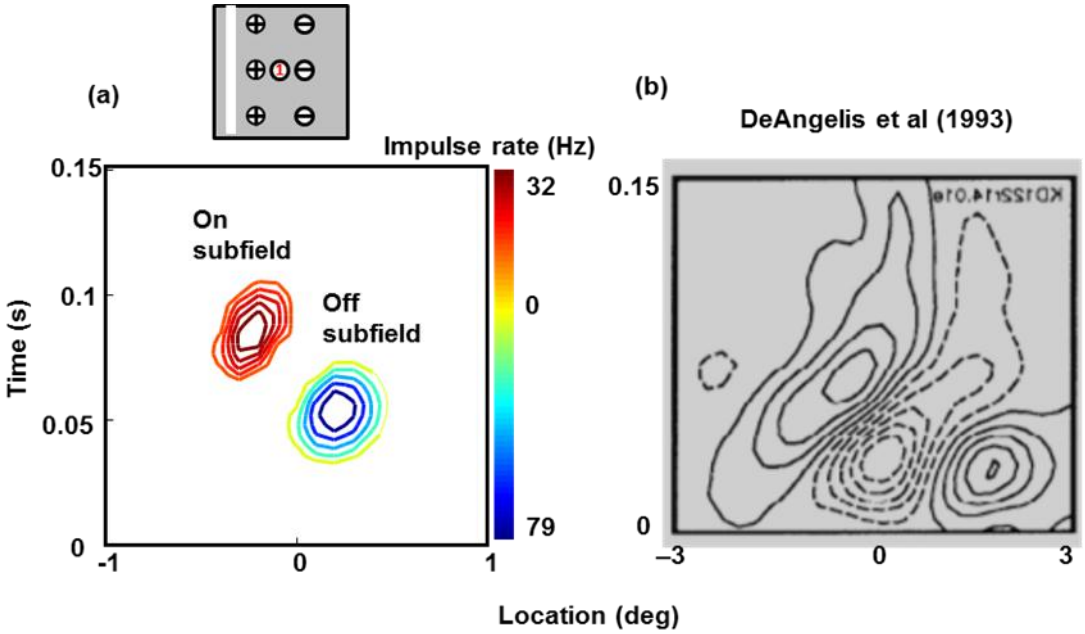

Figure 5.7: Spatiotemporal receptive field measured with a bar stimulus at different locations. A bar stimulus with 0.3° width was flashed for 40 ms in 16 locations across the visual field patch. The model produces slanted contours similar to the experimental data from DeAngelis et al. (1993b). The six-channel model is used here because it produces elongated contours.

Stationary gratings have also been used to study direction selectivity. The idea here is that if the signal processing is linear, the response to a moving stimulus should be predictable from the response to stationary stimuli presented at a series of locations across the receptive field (Movshon et al., 1978c, Reid et al., 1987). The filled circles in Figure 5.8 show the results of such an experiment (Murthy, Humphrey, Saul & Feidler, 1998). A simple cell was stimulated with a stationary contrast-reversing

grating. The horizontal axis gives the spatial phase of the grating and the left and right vertical axes give the amplitude and phase, respectively, of the response's fundamental Fourier component. The blue lines provide the same data for the basic model. The model was not adjusted to match the empirical data (apart from using a high grating contrast) and yet the model's temporal phase data match the laboratory data well. Also, like the simple cell, the model's amplitude data is always greater than zero and therefore shows no null.

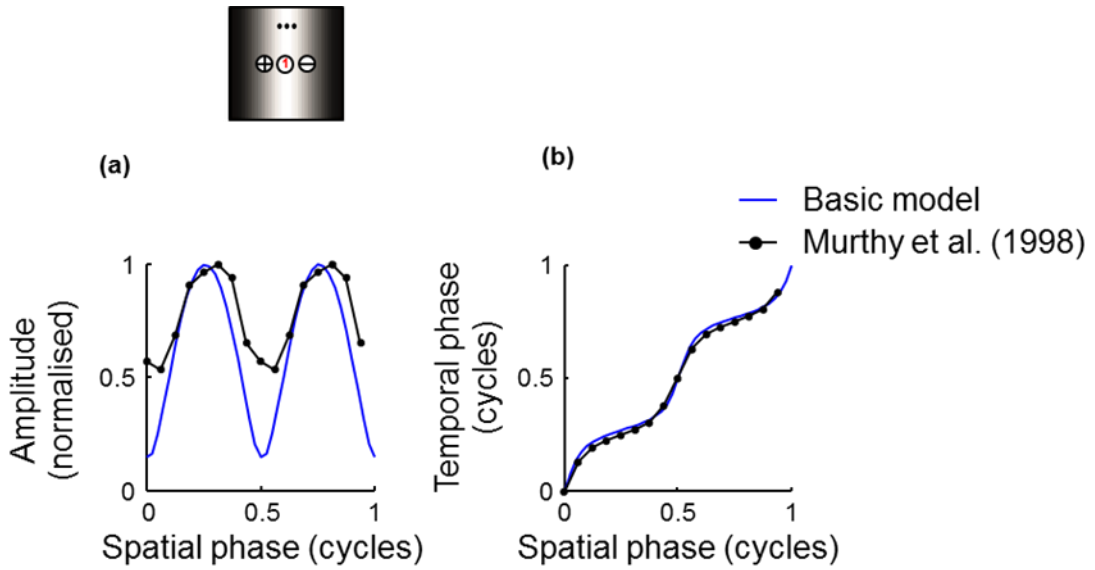

Figure 5.8: (a) Amplitude and (b) temporal phase of the middle cell in the first cortical stage to a contrast-reversing grating. The horizontal axis shows the spatial phase of a stationary grating whose contrast was varied sinusoidally in time; orientation and spatial frequency were optimal. The fundamental Fourier component in the resulting impulse rate was calculated. Results from the basic model, shown in blue, are compared with those from the cell in Figure 4A and B of Murthy et al. (1998). Grating contrast in the model was set at 1 to obtain the best match in amplitude data.

The temporal phase in Figure 5.8 (b) advances with the grating's spatial phase. This is another signature of direction selectivity (Movshon et al., 1978c, Reid et al., 1987) and a strong predictor of the direction to which a cell responds best: the preferred direction of a moving stimulus is that which "activates receptive field positions with progressively shorter latencies" (Murthy et al., 1998). This is also true of the model.

Increased spatial phase displaces a grating away from the off-centre input and towards the on-centre input, the preferred direction. This is a counter-intuitive finding in that the same displacement shifts the peak of the grating away from the low latency (off-) input and towards the high latency (on-) input. The mechanism underlying this result is shown in Figure 5.9. Grating responses are shown on a vector diagram, where the length of vector represents the (fundamental Fourier) amplitude in response to a contrast-reversing grating, and the direction of the vector represents temporal phase. The response of the on-input is arbitrarily pointed rightward and the off-response is almost 180° out of phase, but has a slight phase advance representing its shorter processing time. The sum of these two vectors approximates the response of a cortical cell that sums these two inputs. When the grating is displaced in the preferred direction it activates the on-input more and the off-input less, producing a phase advance in the sum vector.

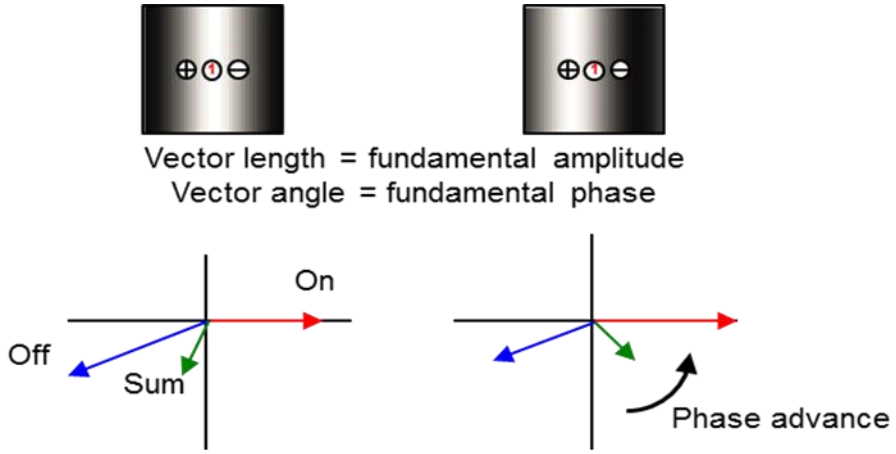

Figure 5.9: As shown in Figure 5.8, the model's spatial phase advances as the grating is shifted away from the off-centre input and towards the on-centre input. The vector diagram explains this finding. Vector length and angle give response amplitude and phase, respectively. Shifting the grating has the opposite effects on the amplitude of the off- and on-centre inputs, advancing the phase of their sum. The sum represents the synaptic drive to the first-stage cortical cell at the middle of the receptive field patch, and the phase of this cell's impulse rate therefore advances as the grating shifts.

5.5. Discussion and conclusions

There is no consensus about the mechanisms underlying direction selectivity in the primary visual cortex. A retinal study (Barlow & Levick, 1965) suggested that direction selectivity is mainly due to suppression in the non-preferred direction rather than facilitation in the preferred direction. Experimental (Saul & Humphrey, 1990, Saul & Humphrey, 1992) and computational (Ursino et al., 2007) studies suggested that direction selectivity originates from convergence of lagged and non-lagged LGN cells which fire about a quarter of a cycle out of phase, resulting in a relative delay of 40 to 120 ms. However, Peterson et al. (2004) found that the delay between directionally-unselective inputs was smaller than that between lagged and non-lagged inputs to cortex.

In the present study, I developed a simple feed-forward model for motion sensitivity of the cortical cells in a single column. The model incorporates two important factors for direction selectivity: 1) spatial difference 2) temporal delay between geniculate inputs. The crucial aspect of the model is that the direction selectivity arises from thalamic cells with a relative temporal delay. This delay is essential to achieve destructive summation when movement occurs in the non-preferred direction (Figure 5.1 and 5.2). Consistent with recent physiological evidence (Jin et al., 2009, Jin et al., 2011a), the off-centre geniculate inputs to cortex precede the on-centre inputs by a small delay, and it is this difference that confers direction selectivity on model neurons. The difference between responses in two opposite directions is more obvious after applying a threshold to generate firing rate (Figure 5.3). According to the model therefore, integration of synaptic inputs is linear and thresholding increases the difference between spike rates in the two directions relative to the difference in membrane potential responses (Jagadeesh et al., 1993, Jagadeesh et al., 1997, Priebe & Ferster, 2005).

Moreover, the model produced high direction selectivity indices over a population of first stage cells. In fact, the direction selectivity index was too high compared with physiological data. This discrepancy was removed by calculating over multiple

cortical columns, some of which had reduced inter-input delays. The direction selectivity of the model was confirmed with tilted spatiotemporal receptive fields and the results of stationary grating spatial phase. Further, I showed that, similar to empirical findings (Jin et al., 2008), the dark bar response is larger than the bright bar response due to faster processing time in the off-centre channel.

Hence, the fundamental idea that model suggests is that the small latency between thalamic inputs is enough for generate the direction-selective cell. This is in agreement with empirical recording which shows there is about 4 ms time difference (difference is the rise-times at 40% maximum response) between the on- and off-inputs to cortical cells (Jin et al., 2009).

Chapter 6. Simple and Complex Cells

6.1. Aim

As it was mentioned in Chapter 1, there are two types of cells in the primary visual cortex: simple and complex cells. In the physiological measurements, these cells are distinguished in two ways: first, simple cells have separated subfields while complex cells have overlapped subfields (shown in Chapter 4); Second, simple cells respond to grating stimuli with strong modulation of their impulse rate compared with complex cells, which produce weakly modulated responses and elevated mean rates. Modulation ratio, which is the ratio of fundamental frequency to mean rate of response is used for the classification of simple and complex cells. This ratio is usually bigger than one for the simple cells and smaller than one for the complex cells.

In this chapter, I will describe the response of the cortical cells of the basic model to drifting gratings, and show the histogram of modulation ratio over all these cells. The results will be compared with physiological measurements from cat cortical cells. If there is any discrepancy between the model result and the physiological data, the model will be improved accordingly.

6.2. Response to drifting grating

Figure 6.1 shows membrane potential and impulse rate of the middle cells in each cortical stage. The stimulus was a grating drifting in the preferred direction, with optimal orientation and optimal spatial frequency (0.49 cycle/deg). The synaptic drive of the first stage is the weighted sum of two geniculate inputs. Cells fire only when membrane potential exceed threshold, and the cortical impulse rate is therefore strongly modulated in time. Cells in the second and third cortical stages have impulse rates that are less modulated for two reasons: 1) they receive rectified inputs from preceding stages and 2) the static polarisation in these stages is assumed to be depolarizing. The minimum firing rate progressively increases and the modulation amplitude decreases from stage 1 to stage 3.

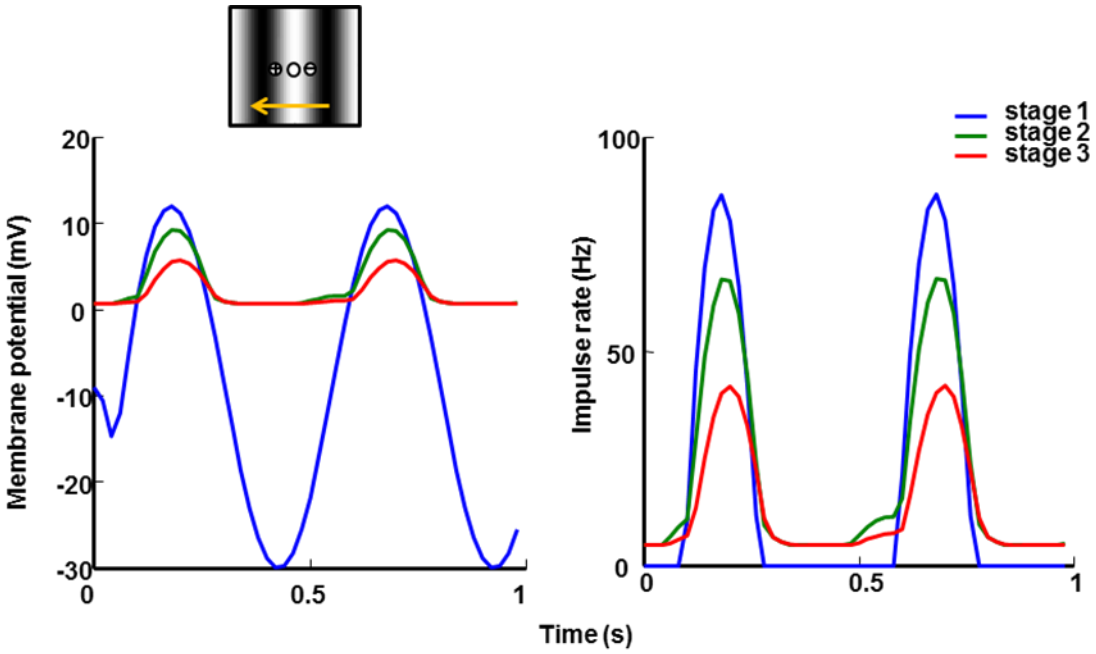

Figure 6.1: Membrane potential and spike rate of the middle cells in the three cortical stages in response to a grating drifting in the preferred direction. Synaptic inputs from the preceding stage are weighted and summed together to produce membrane potential. Impulse rate results from rectification of the membrane potential.

Figure 6.2 compares the response of the model with physiological data (Dean & Tolhurst, 1983). Cells in the first cortical stage are considered as simple cells for two reasons: 1) they have separate on- and off-subfields (Figure 4.7b, on the left) 2) the impulse rate is highly modulated with low mean firing rate. Cells in cortical stage 3 are complex-like cells because 1) they have overlapped on- and off-subfield (Figure 4.7b, middle and right) 2) the impulse rate is less modulated and they have high mean firing rate.

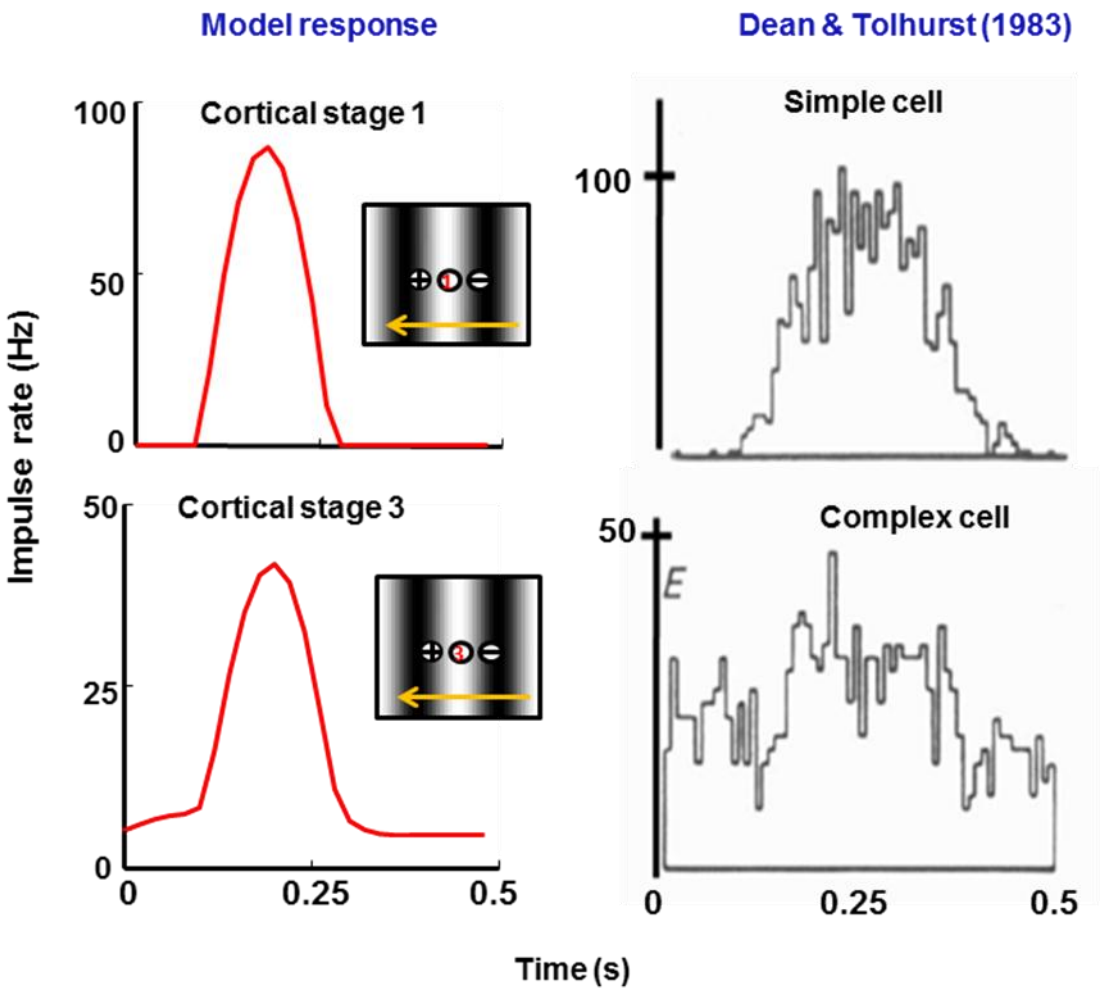

Figure 6.2: Comparison of the model response and physiological measurements. Model cells have receptive fields in the middle of the visual field patch.The cell in the first cortical stage of the model has a high modulated response, similar to the simple cell in the physiological measurement, and the cell in the third cortical stage has a low modulated response and high mean firing rate similar, to the complex cell.

6.3. Modulation ratio

There are many ways to quantitatively classify simple and complex cells as described in section 1.4.4. Among all of the different methods, modulation ratio has been chosen to classify a neuron as a simple or complex cell. Fourier analysis of the response to a drifting grating yields a fundamental component and mean rate, which quantify the modulated and unmodulated components, respectively. The modulation ratio is obtained by dividing the fundamental amplitude by the mean rate. Simple cells tend to

have a modulation ratio over 1 and complex cells have a modulation ratio less than 1 (Dean & Tolhurst, 1983).

The modulation ratio was calculated over all active cells in all stages, as shown in Figure 6.3. The modulation ratio is near 2 in the first cortical stage, similar to simple cells, and is less for the later stages.

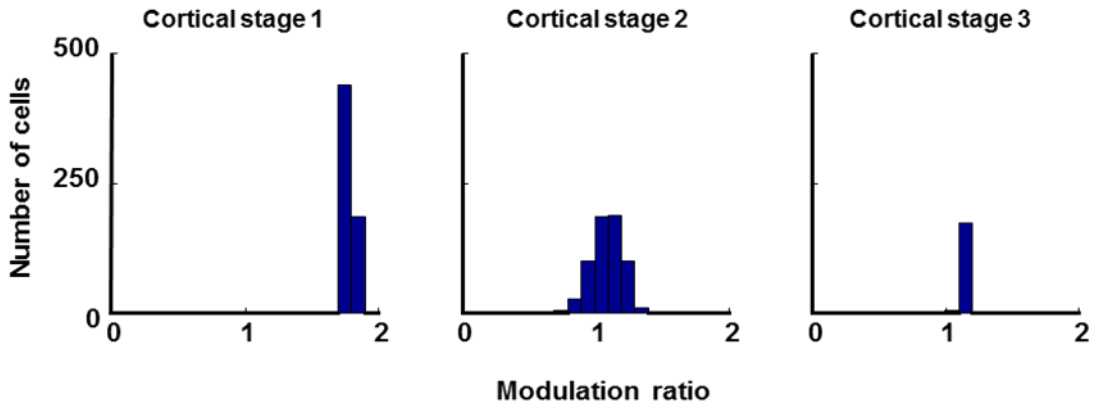

Figure 6.3: Modulation ratio of the cortical cells in all three stages. The modulation ratio is close to 2 for the first cortical stage, similar to simple cells, and this ratio is less for the second and third stage, representing complex-like behavior.

The frequency histogram of the modulation ratio pooled across all three stages is shown in Figure 6.4. There are two modes in the model's histogram. The mode on the right is due to cells in the first cortical stage, reinforcing their simple cell classification. The other mode, close to and less than 1, shows the tendency of the cells to be complex-like in the second and third cortical stages. Obviously, there are higher peaks and gap in the distribution of data from the model compared to the empirical counterpart (Dean & Tolhurst, 1983).

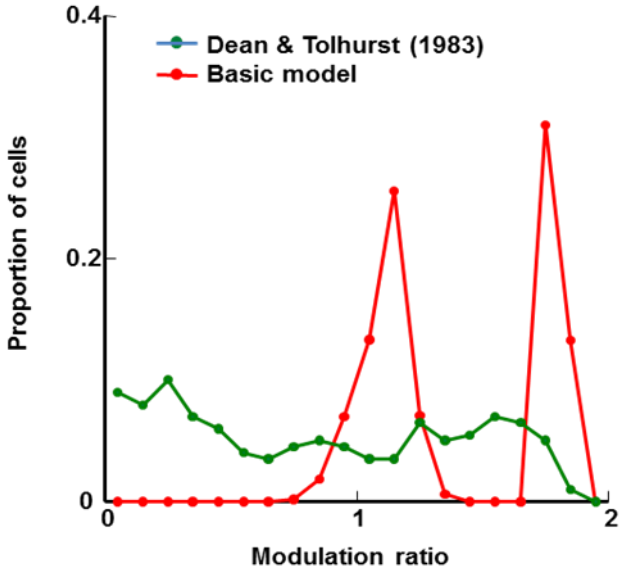

Figure 6.4: Comparison between model and empirical frequency histograms. The modulation ratio indicates that the model histogram has higher peaks than its empirical counterpart.

6.4. Improving the model

The basic model could predict the response to the grating stimulus for simple cells and complex-like cells. However, there is a discrepancy between the frequency histogram of the modulation ratio in the model and a physiological investigation. Given that the basic model assumes no subcortical rectification of impulse rate, I investigated whether the inclusion of subcortical rectification could reduce this discrepancy.

I suggest that adding rectification to the geniculate cells can substantially improve the result of the modulation ratio. The parameters described in Appendix B indicate that the geniculate cell centre mechanism has a maximum contrast sensitivity of 450 Hz/contrast-unit. The analytical solution of the model (Equation A.40 in Appendix A) predicts that surround antagonism at the optimal spatial frequency (0.49 cycle/deg) will lower this value to 280 Hz/contrast-unit. Given that X-type relay cells in the geniculate have an average spontaneous impulse rate of 14 Hz (Kaplan et al., 1978), a grating contrast of greater than 0.05 will result in rectification (280 Hz/contrast-unit ×

0.05 contrast-unit=14 Hz). Physiological studies almost always use a grating contrast greater than this value. As such, I suggest that LGN responses are typically rectified and that applying the rectification in the model may improve the histogram.

The modulation ratio was calculated over multiple cortical columns, assuming that these columns have different spontaneous activity in the geniculate neurons. Rectification was applied to the geniculate responses. The spontaneous activity was varied uniformly across columns from 14 Hz to an activity high enough to avoid rectification. Averaging modulation ratio across all columns produced the red curve in Figure 6.5 which is in better agreement with empirical data, producing a more distributed modulation ratio than the basic model.

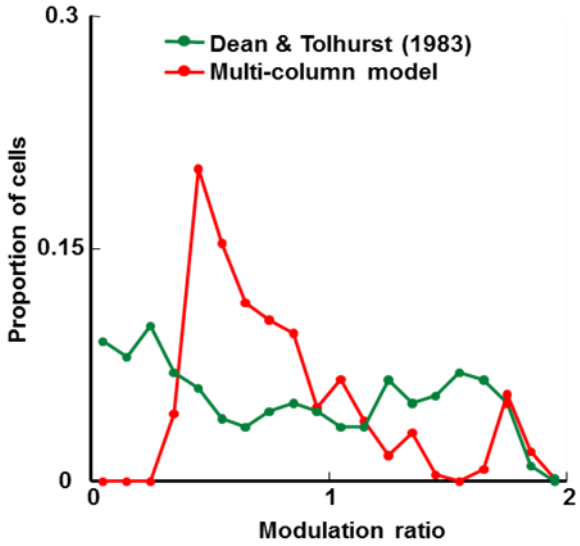

Figure 6.5: Comparison of the modulation ratio in the multi-column model with physiological results. The multi-column model consists of 10 columns with different spontaneous activities in the LGN neurons and rectified LGN responses.

6.5. Discussion and conclusions

Hubel and Wiesel (1962) categorised neurons in the primary visual cortex into simple and complex classes. One of the criteria for this categorisation was the form of the receptive field. Simple cells had subfields in which light increments evoked a response but decrements did not. These cells also had subfields in which a light decrement was required for a response, and on- and off-subfields were spatially separate. By contrast, a response could be obtained to both light on and off at each location in the complex cell receptive field. I have shown in Figure 4.7 that neurons at least partially replicate this behaviour. Cells in cortical stage 1 have clearly separated on- and off-subfields whereas cells in stage 2 and stage 3 have partially overlapped subfields. Cells in the first cortical stage are therefore simple in character, corresponding to the finding that cortical cells connected monosynaptically to the geniculate are simple (Reid & Alonso, 1995). Cells in stages 2 and 3 are more complex-like. Although improvement of the model creates better responses, properties of complex cells such as completely overlapped on- and off-subfields can't be achieved with a simple feedforward model, suggesting that 'complex' properties do not arise from purely feed-forward model.

The use of drifting gratings provides another method for separating simple from complex cells (Movshon et al., 1978b). Simple cells respond to a drifting grating with a modulated impulse rate: the rate rises and falls as each light bar crosses the receptive field. Complex cells respond with an increased impulse rate that is less modulated with time. Stage 1 cortical cells fire only when the geniculate input exceeds threshold and the cortical impulse rate is therefore strongly modulated in time. Second and third-stage cells have an unmodulated component in their impulse rates, for two reasons: they receives only rectified inputs from earlier stages, and the static polarisation in stages 2 and 3 is assumed to be depolarising.

Grating responses are used to classify active cells in cortical stages as simple and complex cells using the modulation ratio. Clearly from Figure 6.4, cells are divided into two groups: stage 1 cells had a modulation ratio close to two and stage 2 and 3 modulation ratio was around one reinforcing their clustering into two groups. The

model histogram, however, had higher peaks than the empirical data. Incorporation of geniculate rectification in the model improved the results. The recalculations of the modulation ratio over 10 cortical columns, which differ in the spontaneous activity of the geniculate inputs, produced a better agreement with physiological data. It should be noted that the aim was not an excat match between the distribution of ratios of the experimental data and the model. The objective was determining a mechanism which generates responses close to empirical data.

Chapter 7. Spatial Frequency Selectivity

7.1. Aim

Another fundamental cortical property is selectivity for spatial frequency. Cortical cells inherit spatial frequency selectivity from geniculate cells (So and Shapley 1981), which acquire this selectivity from retinal ganglion cells. The ganglion cell's selectivity is due to the centre-surround organisation of its receptive field (Enroth-Cugell & Robson, 1966, Kuffler, 1953, Troyer et al., 1998). Cortical cells, however, are more sharply tuned to stimulus spatial frequency than are geniculate cells.

This chapter investigates the response of the model for this property and compares the model's performance with responses measured from cortical cells. In addition, the frequency histogram of the bandwidth of the model's tuning function is compared with the empirical results.

7.2. Spatial frequency tuning

Empirically, this property is examined by drifting an optimally oriented grating across the receptive field at a variety of spatial frequencies. The usual response measure is the fundamental Fourier amplitude of the impulse rate. The typical result (Movshon et al., 1978b), is that the neuron has an optimal spatial frequency, and that the response falls away rapidly on either side of the optimal value.

Neurons in the first cortical stage of the basic model produce a similar result, as illustrated in the Figure 7.1a.This Figure indicates the spatial frequency selectivity of the cell at the middle of the visual field patch. The peak of the curve is the response of the neuron for the optimal spatial frequency (0.49 cycle/deg) and the response falls monotonically on either side of the peak. The existence of an optimal value is easily understood. When the light bar of the grating is over the on-subfield and the dark bar is simultaneously over the off-subfield the two phases of the grating contribute constructively in modulating the cell's impulse rate.

The tightness of tuning to spatial frequency can be assessed from the bandwidth of the tuning curve at half height. A histogram of the spatial frequency tuning bandwidth for all active cells in the first cortical stage is plotted in Figure 7.1b (see the Methods chapter for the definition of active). Neurons in the basic model have bandwidths above 1.5 octaves, which is broader than their empirical counterparts (Movshon et al. 1978b). I speculated that the poor tuning is due to the lack of a surround mechanism in the subcortical stages. In particular, very low spatial frequencies produce substantial surround signals that antagonise centre signals (Enroth-Cugell and Robson, 1966). This should be noted that the majority of neurons in the Movshon study (Movshon et al. 1978b) were within 5 degree eccentricity and the model results are simulated at an eccentricity of 11 degree. This may account for some of the lack of agreement between model and empirical data.

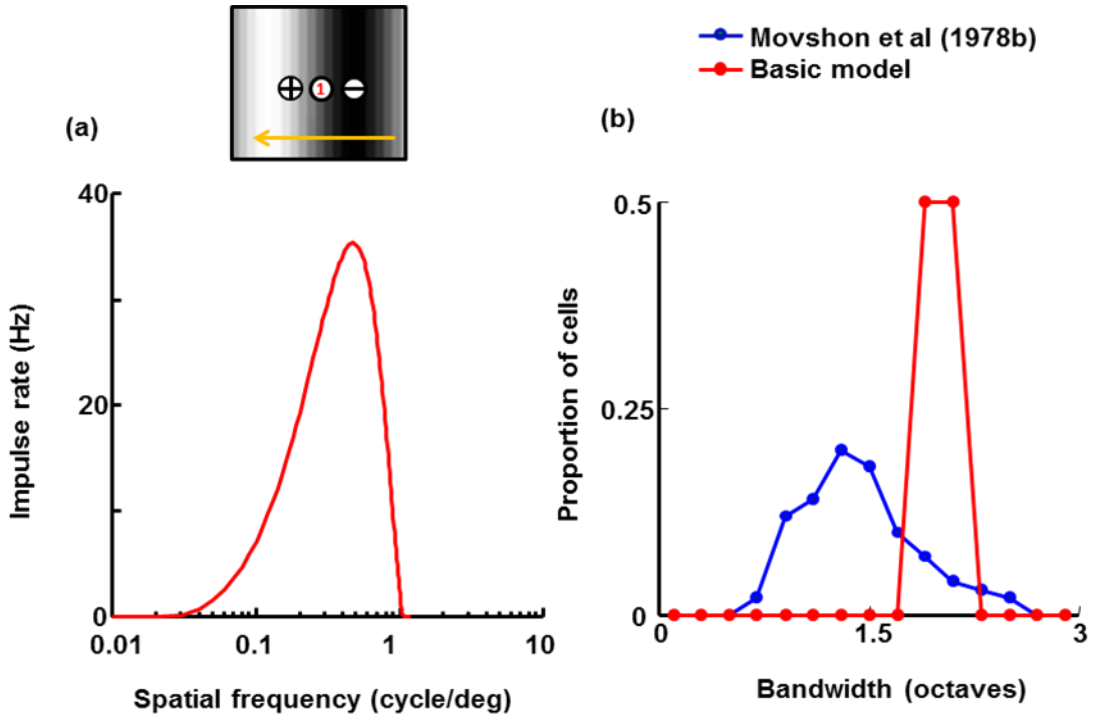

Figure 7.1: Spatial frequency selectivity. (a) Spatial frequency tuning curve of the middle cell in the first cortical stage. A grating stimulus was drifted across the visual field patch and the fundamental frequency component of the response plotted against grating spatial frequency. The optimal spatial frequency for this cells is 0.49 cycle/deg and the bandwidth is 2.1 octaves. (b) Comparison of the bandwidth of the spatial frequency for active neurons in the first cortical stage of the basic model with simple cells (Movshon et al. 1978b).

7.3. Improving the model

The histogram of the tuning bandwidth for the neurons in the first cortical stage indicated that the basic model is poorly tuned compared to physiological data. Many studies show that the spatial frequency tuning inherited from retinal ganglion cells is due to centre-surround organisation (Enroth-Cugell and Robson, 1966; Kuffler, 1953; Rodieck, 1965). The basic model includes no surround mechanism for ganglion and geniculate cells and the model was therefore modified by adding surround mechanism to the subcortical stages. With this modification, spatial frequency tuning became narrower (Figure 7.2a) due to suppression from the surround. Cortical cells are typically narrowly tuned with a bandwidth at half-height of 1.5 octaves (Movshon et al. 1978b) and the mean of the bandwidth for the cortical cells in the first stage is 1.3 octaves, close to the empirical data (Figure 7.2b).

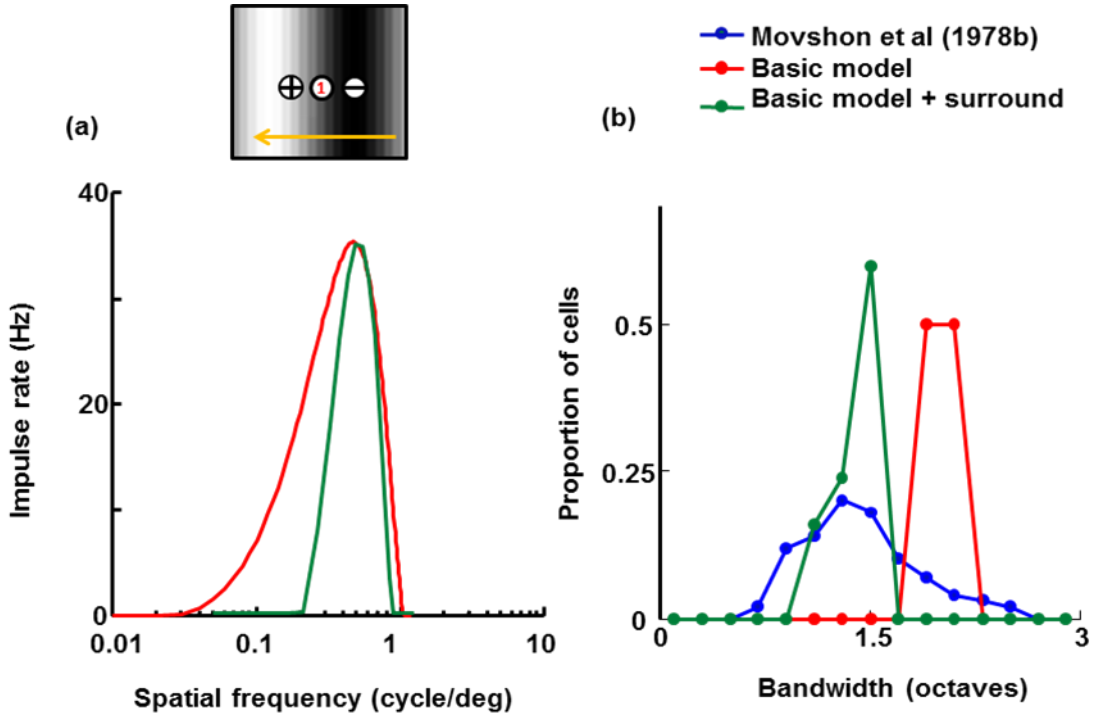

Figure 7.2: (a) The green curve shows the spatial frequency tuning of the middle cell in the first cortical stage after adding a surround to the subcortical cells. The optimal spatial frequency is barely changed but the bandwidth of the selectivity is 1.1 octaves after adding surround mechanism. The red curve is the previous result from the basic model, for comparison. (b) The population histogram of bandwidth is in better agreement with empirical data (Movshon et al. 1978b).

7.4. Discussion and conclusions

The model can reproduce the spatial frequency selectivity of cortical cells. The basic model showed a broadly tuned spatial frequency curve compared to physiological data. In order to rectify this problem, a surround mechanism was added to the basic model, making the cortical cells more sharply tuned for spatial frequency, similar to laboratory data. The model therefore fits with the idea that cortical spatial frequency selectivity comes from the convergence of the LGN inputs which they have centre-surround organisation. Some studies indicated that intracortical inhibition also plays a role in generating this selectivity (Zhu et al. 2010, Bauman and Bonds 1991). The static hyperpolarisation in the first cortical stage is the counterpart of this inhibition in this model. Most likely, intracortical inhibition is the source of this static hyperpolarisation as discussed in greater extent in section 8.3.

Chapter 8. Discussion

The present work was designed with two main objectives. The first objective was to reproduce fundamental properties of cortical cells such as direction selectivity, orientation selectivity, spatial frequency selectivity, and simple and complex-like responses, in a simple model. The second objective was to reproduce the population response for these properties. Many studies have explained and discussed these properties in individual models (Adelson & Burgen, 1985, Ahmed et al., 1994, Barlow & Levick, 1965, Ben-Yishai et al., 1995, Hubel & Wiesel, 1962, Peters & Payne, 1993, Reichardt, 1961, Somers et al., 1995, Torre & Poggio, 1978, Ursino et al., 2007). A novelty of the work in this thesis is explaining all of these features in a single model. The design and development of the model aimed to overcome limitations of present literature by using the simplest possible model and by using parameters taken from physiological measurements of the visual system. As documented in Chapters 4 to 7, the present model, despite its simplicity, is able to simulate and mimic several fundamental properties of the cortical cells in the primary visual cortex. In particular:

- The model provides a mechanism for direction selectivity that is firmly based on empirical observations.
- This model reproduces four fundamental properties – orientation selectivity, spatial frequency selectivity, direction selectivity, and the emergence of complex-like cells – in a single model.
- The model also shows that neurons sampled within and between columns possess these properties to varying extents, and that the model's population statistics largely match those measured in the laboratory.

- I show that dark stimuli tend to produce larger responses than do light stimuli, and that this off-domination follows naturally from the faster responses of off-centre geniculate inputs to cortex.

In what follows I discuss the geniculocortical synapse, direction selectivity, the role of inhibition in the model, the idea that simple cell responses are derivatives of their inputs, and sub-cortical connections.

8.1. Geniculocortical synapse

The pivotal piece of circuitry in the model is the geniculocortical synapse. It is at this synapse that the model's orientation and direction selectivity both arise. Further, both of these properties depend on the convergence of on-centre and off-centre geniculate axons onto the same cortical cells. There are two important pieces of evidence supporting this assumption of convergence. First, Wässle et al. (1981) showed that the anatomical substrate is available: the nearest neighbour of an X-type ganglion cell is nearly always of the opposite sign. Second, Reid and Alonso (1995) showed that where an on-centre geniculate cell connects monosynaptically to a cortical cell, the geniculate centre mechanism and cortical on-subfield are almost invariably co-localised. Off-centre geniculate centre mechanisms and cortical off-subfields are similarly co-localised. The one piece of evidence remaining, then, is a direct demonstration that on- and off-centre geniculate cells project to the same cortical cell. In a tour de force of experimental technique, two laboratories (Alonso et al., 1996, Tanaka, 1983) have provided such evidence for simple cells.

8.2. Direction selectivity

There is no current consensus on the mechanism by which direction selectivity arises in primary visual cortex. It has been recognised for many years that a temporal delay of one cortical input relative to other inputs could provide the basis for this selectivity (Adelson and Bergen, 1985; Watson and Ahumada, 1985). Saul and Humphrey (1990) suggested that lagged geniculate cells could provide the necessary delayed input. Peterson et al. (2004) measured the responses of direction selective cells and

modelled their data by assuming non-directional inputs with a relative delay. They found that the required delay was smaller than that between lagged and non-lagged inputs to the cortex. The use of a relatively small inter-input delay is consistent with this work. More recent models (Ursino et al., 2007) have suggested a role for intracortical inhibition in the production of direction selectivity. Given the demonstration that even a small variability in the timing of sub-cortical inputs can lead to strong selectivity, however, it is difficult to see how sub-cortical timing cannot be involved.

8.3. Inhibition

Inhibitory connections are not clearly evident in the model circuit, but inhibition plays a crucial role at two locations. The first is the sign-inverting synapse between photoreceptors and on-centre bipolar cells. It is this sign inversion that provides for the subsequent cancellation between on- and off-centre signals at cortical stage 1. The second role of inhibition is in hyperpolarising the cells in the same stage. It is this hyperpolarisation that sharpens selectivity through the iceberg effect. One piece of evidence for the assumed hyperpolarisation is that simple cells have little or no spontaneous activity (Rose & Blakemore, 1974). Indeed, when a grating is used as stimulus, grating contrast has to be raised to a threshold level before any response is evoked from a simple cell (Dean, 1981). Evidence that is more direct comes from intracellular recordings of simple cells, which show a hyperpolarised membrane potential in the absence of a stimulus (Carandini & Ferster, 2000). It seems highly likely that this hyperpolarisation results from intracortical inhibition. Given the role of this inhibition in sharpening selectivity, it is not surprising that the blockade of inhibition results in a reduction of orientation selectivity (Sillito, 1975) . Adding surround suppression in cortical cells may improve the model, but for the sake of simplicity, this is not included in the model.

8.4. Cortex as differentiator

The assumption that on- and off-centre geniculate afferents converge onto the same cortical cell has a fascinating corollary, illustrated in Figures 8.1 and 8.2. The cortical cell adds the two opposite-signed inputs and is therefore effectively differencing

similar spatial profiles. It is estimated in the Methods that the distance between neighbouring on- and off-centre receptive fields is 0.1° at the eccentricity of interest (11°), as shown in the figure 8.1a. This is substantially less than the centre mechanism radius of a geniculate afferent, $r = 0.4°$. Accordingly, the cortical receptive field spatial profile is the difference between similar spatial profiles separated by a relatively small distance, and is therefore approximately proportional to the spatial derivative of a single geniculate centre mechanism. The black curves in Figure 8.1b show the sum of the on- and off-inputs, and the (centred) derivative of one of them. The two curves overlie each other. The blue curve, showing the membrane potential of the first-stage cortical cell briefly stimulated with light bars (as in Figure 5.7), matches well with the black curves. The centre mechanism is assumed to have a Gaussian profile; computing its derivative shows that the cortical cell's on- and off-subfields are separated by $\sqrt{2}r = 0.57°$, as shown. This calculation helps to explain why the subfield separation in the cortex is substantially larger than the spacing of neighbouring retinal cells.

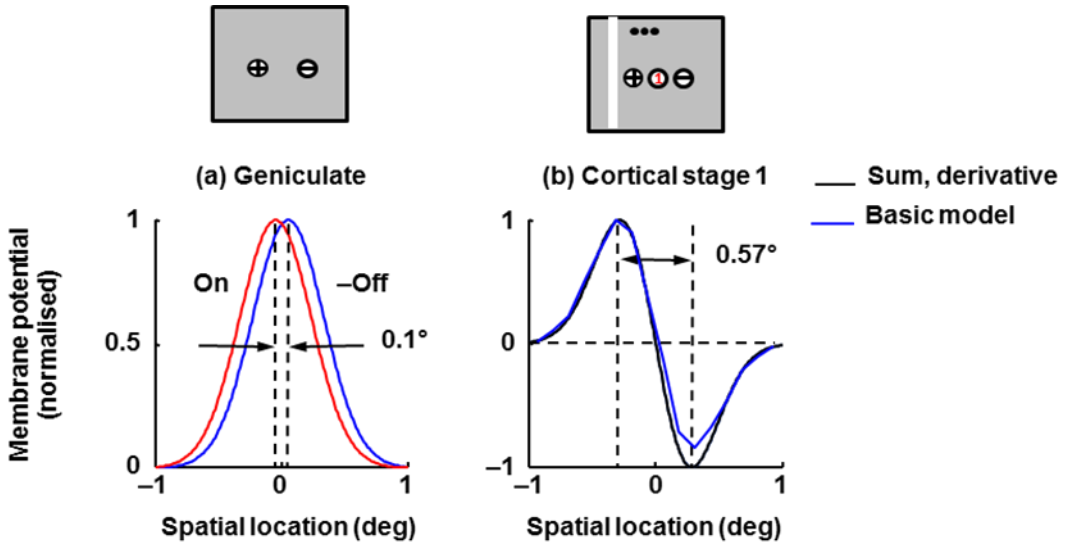

Figure 8.1: Spacing of on- and off-subfields. (a**)** The receptive field spatial profiles for the two sub-cortical channels in the basic model are shown. The distance between peaks is set equal to the distance between neighbouring on- and off-centre X-type ganglion cells, and the off-centre signal is inverted. **(b)** This graph shows the sum of the two sub-cortical profiles and the spatial derivative of one of them (shifted so that the zero-crossing is centred). The sum and derivative are indistinguishable. The response of the centrally located neuron in cortical stage 1 of the basic model is also shown. It was calculated with a bar stimulus with a width of 0.3° and a duration of 40 ms, and the response is the generator potential 70 ms after bar onset. There is a good match between all three curves.

This idea extends to the temporal domain. The impulse responses of the on-centre and off-centre geniculate cells are plotted in Figure 8.2a. These responses are gamma densities with shape factor $z = 4$ because they result from a cascade of four first-order low-pass filters. The on- and off-centre functions have time constants of 11 and 9 ms, respectively, and because of the closeness of these values the difference between them can be approximated by differentiating one of them with respect to time constant. Figure 8.2b shows, in black, the sum of the two geniculate inputs and the derivative of a gamma density with a time constant midway between that of the two inputs, $\tau = 10$ ms. The distance between the trough and peak (calculated by differentiating with respect to time) is $2\sqrt{z}\tau = 40$ ms.

Also shown, in blue, is the membrane potential of the first-stage cortical cell at the middle of the visual field patch. This approximation to the basic model's impulse

response was generated by presenting an optimally oriented bar very briefly at the middle of the patch. This response is similar in shape to the derivative function but is slower because it gives the cell's output rather that its synaptic drive, and therefore includes extra low-pass temporal filtering. These results together explain a counter-intuitive result. Whereas the off-input to cortex precedes the on-input by only a few milliseconds, the off-peak in the spatiotemporal receptive field (Figure 5.7) leads the on-peak by tens of milliseconds.

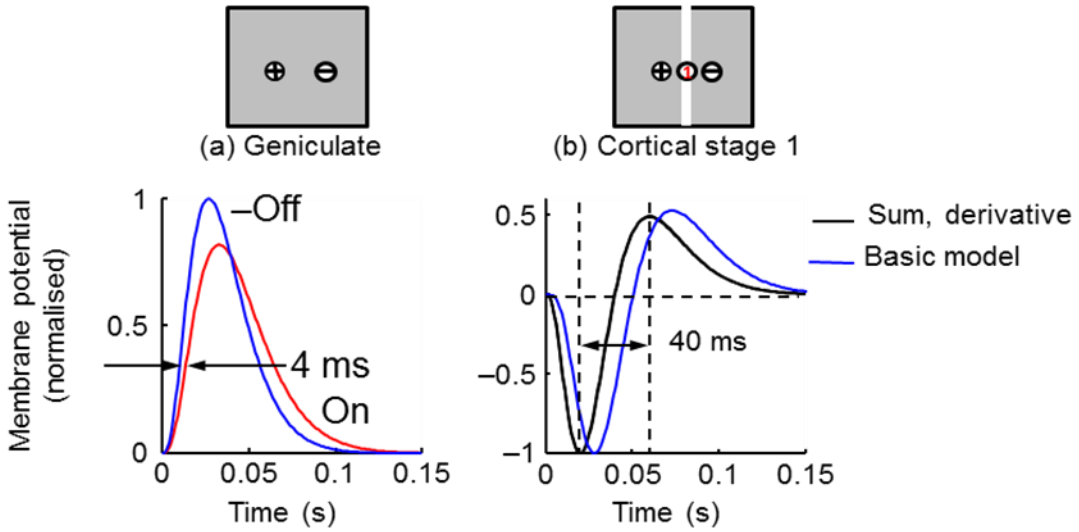

Figure 8.2: (a) Impulse responses for the on- and off-centre geniculate cells in the basic model, with the off-centre curve inverted for ease of comparison. (b) The sum of the on- and off-centre responses is shown in black, along with the derivative of one of the responses (computed with the mean of the on- and off-centre time constants); the sum and derivative are indistinguishable. Also shown, in blue, is the time course of the membrane potential in the first-stage cortical cell at the middle of the receptive field patch. Its impulse response was calculated by delivering a very brief bar of light (width = 0.25°) at the middle of the patch. The black lines give the synaptic drive to the cortical cell and the blue line is relatively delayed because the cortical cell acts as a low-pass filter.

8.5. Subcortical connections

According to the calculations in the Appendix B, there are over 200 X-type ganglion cells in the 2° × 2° visual field patch used here. The connection of just two (or six) of those cells to the first cortical stage of the model is therefore highly selective, a selection that will enhance orientation selectivity in cortex. Alonso et al. (2001) have

shown that layer 4 cells connect to only about one third of the geniculate relay cells available to them. Given the narrow orientation of these cells, it is natural to assume that the choice of connection is that which enhances orientation selectivity. How is the choice made? One possibility is the following. During the developmental period, the first two relay cells making a connection are likely to be driven by nearest neighbours in the retina, which almost certainly have centres of opposite sign. These two connections will establish broad orientation tuning. Other retinal neighbours will then attempt to contact the cortical cell via a relay cell. If Hebbian principles operate they will only succeed if their own firing enhances impulse rate in the cortical target. Only connections that enhance the existing orientation tuning will survive.

The receptive field of a cortical stage 3 neuron, shown in Figure 4.2b, indicates that the on- and off-subfields only partially overlap. This fails to match the complete overlap in the complex cell subfields of the physiological data shown in Figure 1.14. The reason for the incomplete overlap in the model is clear: on-centre sub-cortical inputs are segregated from off-centre inputs, regardless of the number of channels. It has recently been shown, by contrast, that on-centre inputs to a given cortical column are dispersed among the off-centre inputs (Jin, Wang, Swadlow & Alonso, 2011b). It would be of considerable interest to discover whether the Hebbian process described above can produce intermixing of on- and off-inputs in the model, and complete overlap of stage 3 subfields.

References

Adelson, E.H., & Burgen, J.R. (1985). Spatiotemporal energy models for the perception of motion. *The Journal of the Optical Society of America A 2*(2), 284-299.

Ahmed, B., Anderson, J.C., Douglas, R.J., Martin, K.A., & Nelson, J.C. (1994). Polyneuronal innervation of spiny stellate neurons in cat visual cortex. *The Journal of Comparative Neurology, 341* (1), 39-49.

Albrecht, D.G., & Geisler, W.S. (1991). Motion selectivity and the contrast-response function of simple cells in the visual cortex. *Visual Neuroscience, 7* (6), 531-546.

Alonso, J.M., & Martinez, L.M. (1998). Functional connectivity between simple cells and complex cells in cat striate cortex. *Nature Neuroscience, 1* (5), 395-403.

Alonso, J.M., Usrey, W.M., & Reid, R.C. (1996). Precisely correlated firing in cells of the lateral geniculate nucleus. *Nature, 383* (6603), 815-819.

Alonso, J.M., Usrey, W.M., & Reid, R.C. (2001). Rules of connectivity between geniculate cells and simple cells in cat primary visual cortex. *The Journal of Neuroscience, 21* (11), 4002-4015.

Anderson, J., Lampl, I., Reichova, I., Carandini, M., & Ferster, D. (2000a). Stimulus dependence of two-state fluctuations of membrane potential in cat visual cortex. *Nature Neuroscience, 3* (6), 617-621.

Anderson, J.S., Carandini, M., & Ferster, D. (2000b). Orientation tuning of input conductance, excitation, and inhibition in cat primary visual cortex. *Journal of Neurophysiology, 84* (2), 909-926.

Andrews, B.W., & Pollen, D.A. (1979). Relationship between spatial frequency selectivity and receptive field profile of simple cells. *The Journal of Physiology, 287*, 163-176.

Barlow, H.B., Hill, R.M., & Levick, W.R. (1964). Retinal ganglion cells responding selectively to direction and speed of image motion in the rabbit. *The Journal of Physiology, 173*, 377-407.

Barlow, H.B., & Levick, W.R. (1965). The mechanism of directionally selective units in rabbit's retina. *The Journal of Physiology, 178* (3), 477-504.

Bauman, L.A., & Bonds, A.B. (1991). Inhibitory refinement of spatial frequency selectivity in single cells of the cat striate cortex. *Vision Research, 31* (6), 933-944.

Beaulieu, C., & Colonnier, M. (1983). The number of neurons in the different laminae of the binocular and monocular regions of area 17 in the cat, Canada. *J Comp Neurol, 217* (3), 337-344.

Ben-Yishai, R., Bar-Or, R.L., & Sompolinsky, H. (1995). Theory of orientation tuning in visual cortex. *Proceedings of the National Academy of Sciences of the United States of America, 92* (9), 3844-3848.

Berman, N.E., Wilkes, M.E., & Payne, B.R. (1987). Organization of orientation and direction selectivity in areas 17 and 18 of cat cerebral cortex. *Journal of Neurophysiology, 58* (4), 676-699.

Binzegger, T., Douglas, R.J., & Martin, K.A. (2004). A quantitative map of the circuit of cat primary visual cortex. *The Journal of Neuroscience, 24* (39), 8441-8453.

Binzegger, T., Douglas, R.J., & Martin, K.A. (2007). Stereotypical bouton clustering of individual neurons in cat primary visual cortex. *The Journal of Neuroscience, 27* (45), 12242-12254.

Bonds, A.B. (1989). Role of inhibition in the specification of orientation selectivity of cells in the cat striate cortex. *Visual Neuroscience, 2* (1), 41-55.

Borst, A., & Egelhaaf, M. (1989). Principles of visual motion detection. *Trends in Neurosciences, 12* (8), 297-306.

Boycott, B.B., & Wässle, H. (1974). The morphological types of ganglion cells of the domestic cat's retina. *The Journal of Physiology, 240* (2), 397-419.

Bullier, J., & Henry, G.H. (1979). Laminar distribution of first-order neurons and afferent terminals in cat striate cortex. *Journal of Neurophysiology, 42* (5), 1271-1281.

Campbell, F.W., Cleland, B.G., Cooper, G.F., & Enroth-Cugell, C. (1968). The angular selectivity of visual cortical cells to moving gratings. *The Journal of Physiology, 198* (1), 237-250.

Carandini, M., & Ferster, D. (2000). Membrane potential and firing rate in cat primary visual cortex. *The Journal of Neuroscience, 20* (1), 470-484.

Carandini, M., Heeger, D.J., & Senn, W. (2002). A synaptic explanation of suppression in visual cortex. *The Journal of Neuroscience, 22* (22), 10053-10065.

Chung, S., & Ferster, D. (1998). Strength and orientation tuning of the thalamic input to simple cells revealed by electrically evoked cortical suppression. *Neuron, 20* (6), 1177-1189.

Cleland, B.G., Dubin, M.W., & Levick, W.R. (1971). Sustained and transient neurones in the cat's retina and lateral geniculate nucleus. *J Physiol, 217* (2), 473-496.

Cleland, B.G., & Levick, W.R. (1974). Brisk and sluggish concentrically organized ganglion cells in the cat's retina. *The Journal of Physiology, 240* (2), 421-456.

Daw, N. (2012). How Vision Works: The Physiological Mechanisms Behind What We See. (Oxford University Press.

De Valois, K.K., & Tootell, R.B. (1983). Spatial-frequency-specific inhibition in cat striate cortex cells. *The Journal of Physiology, 336,* 359-376.

De Valois, R.L., Albrecht, D.G., & Thorell, L.G. (1982). Spatial frequency selectivity of cells in macaque visual cortex. *Vision Research, 22* (5), 545-559.

Dean, A.F. (1981). The variability of discharge of simple cells in the cat striate cortex. *Experimental Brain Research, 44* (4), 437-440.

Dean, A.F., & Tolhurst, D.J. (1983). On the distinctness of simple and complex cells in the striate cortex of the cat. *The Journal of Physiology, 344,* 305-325.

DeAngelis, G.C., Anzai, A., Ohzawa, I., & Freeman, R.D. (1995). Receptive field structure in the visual cortex: does selective stimulation induce plasticity? *Proceedings of the National Academy of Sciences of the United States of America, 92* (21), 9682-9686.

DeAngelis, G.C., Ohzawa, I., & Freeman, R.D. (1993a). Spatiotemporal organization of simple-cell receptive-fields in the cats striate cortex .1. General-characteristics and postnatal-development. *Journal of Neurophysiology, 69* (4), 1091-1117.

DeAngelis, G.C., Ohzawa, I., & Freeman, R.D. (1993b). Spatiotemporal organization of simple-cell receptive-fields in the cats striate cortex .2. linearity of temporal and spatial summation. *Journal of Neurophysiology, 69* (4), 1118-1135.

Enroth-Cugell, C., & Robson, J.G. (1966). The contrast sensitivity of retinal ganglion cells of the cat. *The Journal of Physiology, 187* (3), 517-552.

Ferster, D., Chung, S., & Wheat, H. (1996). Orientation selectivity of thalamic input to simple cells of cat visual cortex. *Nature, 380* (6571), 249-252.

Ferster, D., & Koch, C. (1987). Neuronal connections underlying orientation selectivity in cat visual cortex. *Trends in Neurosciences, 10*, 6.

Ferster, D., & Lindstrom, S. (1983). An intracellular analysis of geniculo-cortical connectivity in area 17 of the cat. *The Journal of Physiology, 342*, 181-215.

Ferster, D., & Miller, K.D. (2000). Neural mechanisms of orientation selectivity in the visual cortex. *Annual Review of Neuroscience, 23*, 441-471.

Finn, I.M., Priebe, N.J., & Ferster, D. (2007). The emergence of contrast-invariant orientation tuning in simple cells of cat visual cortex. *Neuron, 54* (1), 137-152.

Frishman, L.J., Freeman, A.W., Troy, J.B., Schweitzer-Tong, D.E., & Enroth-Cugell, C. (1987). Spatiotemporal frequency responses of cat retinal ganglion cells. *The Journal of General Physiology, 89* (4), 599-628.

Gabbott, P.L., & Somogyi, P. (1986). Quantitative distribution of GABA-immunoreactive neurons in the visual cortex (area 17) of the cat. *Experimental brain research. Experimentelle Hirnforschung. Experimentation cerebrale, 61* (2), 323-331.

Ganz, L., & Felder, R. (1984). Mechanism of directional selectivity in simple neurons of the cat's visual cortex analyzed with stationary flash sequences. *Journal of Neurophysiology, 51* (2), 294-324.

Gardner, J.L., Anzai, A., Ohzawa, I., & Freeman, R.D. (1999). Linear and nonlinear contributions to orientation tuning of simple cells in the cat's striate cortex. *Visual Neuroscience, 16* (6), 1115-1121.

Gil, Z., Connors, B.W., & Amitai, Y. (1999). Efficacy of thalamocortical and intracortical synaptic connections: quanta, innervation, and reliability. *Neuron, 23* (2), 385-397.

Gilbert, C.D. (1977). Laminar differences in receptive field properties of cells in cat primary visual cortex. *The Journal of Physiology, 268* (2), 391-421.

Gilbert, C.D., & Wiesel, T.N. (1979). Morphology and intracortical projections of functionally characterised neurones in the cat visual cortex. *Nature, 280* (5718), 120-125.

Gizzi, M.S., Katz, E., Schumer, R.A., & Movshon, J.A. (1990). Selectivity for orientation and direction of motion of single neurons in cat striate and extrastriate visual cortex. *Journal of Neurophysiology, 63* (6), 1529-1543.

Goodwin, A.W., Henry, G.H., & Bishop, P.O. (1975). Direction selectivity of simple striate cells: properties and mechanism. *Journal of Neurophysiology, 38* (6), 1500-1523.

Hamilton, D.B., Albrecht, D.G., & Geisler, W.S. (1989). Visual cortical receptive fields in monkey and cat: spatial and temporal phase transfer function. *Vision Research, 29* (10), 1285-1308.

Hammond, P., & Andrews, D.P. (1978). Orientation tuning of cells in areas 17 and 18 of the cat's visual cortex. *Experimental Brain Research, 31* (3), 341-351.

Hammond, P., & MacKay, D.M. (1975). Proceedings: Response of cat visual cortical cells to kinetic contours and static noise. *The Journal of Physiology, 252* (2), 43P-44P.

Hammond, P., Pomfrett, C.J., & Ahmed, B. (1989). Neural motion after-effects in the cat's striate cortex: orientation selectivity. *Vision Research, 29* (12), 1671-1683.

Heeger, D.J. (1993). Modeling simple-cell direction selectivity with normalized, half-squared, linear operators. *Journal of Neurophysiology, 70* (5), 1885-1898.

Hirsch, J.A., Alonso, J.M., & Reid, R.C. (1995). Visually evoked calcium action potentials in cat striate cortex. *Nature, 378* (6557), 612-616.

Hirsch, J.A., Alonso, J.M., Reid, R.C., & Martinez, L.M. (1998). Synaptic integration in striate cortical simple cells. *The Journal of Neuroscience, 18* (22), 9517-9528.

Hirsch, J.A., Martinez, L.M., Alonso, J.M., Desai, K., Pillai, C., & Pierre, C. (2002). Synaptic physiology of the flow of information in the cat's visual cortex in vivo. *The Journal of Physiology, 540* (Pt 1), 335-350.

Hoffman, K.P., & Stone, J. (1971). Conduction velocity of afferents to cat visual cortex: a correlation with cortical receptive field properties. *Brain Research, 32* (2), 460-466.

Hubel, D.H. (1959). Single unit activity in striate cortex of unrestrained cats. *The Journal of Physiology, 147*, 226-238.

Hubel, D.H., & Wiesel, T.N. (1961). Integrative action in the cat's lateral geniculate body. *The Journal of Physiology, 155*, 385-398.

Hubel, D.H., & Wiesel, T.N. (1962). Receptive fields, binocular interaction and functional architecture in the cat's visual cortex. *The Journal of Physiology, 160*, 48.

Hubel, D.H., & Wiesel, T.N. (1963). Receptive Fields of Cells in Striate Cortex of Very Young, Visually Inexperienced Kittens. *Journal of Neurophysiology, 26*, 994-1002.

Hughes, A. (1976). A supplement to the cat schematic eye. *Vision Research, 16* (2), 149-154.

Humphrey, A.L., & Saul, A.B. (1998). Strobe rearing reduces direction selectivity in area 17 by altering spatiotemporal receptive-field structure. *Journal of Neurophysiology, 80* (6), 2991-3004.

Jagadeesh, B., Wheat, H.S., & Ferster, D. (1993). Linearity of summation of synaptic potentials underlying direction selectivity in simple cells of the cat visual cortex. *Science, 262* (5141), 1901-1904.

Jagadeesh, B., Wheat, H.S., Kontsevich, L.L., Tyler, C.W., & Ferster, D. (1997). Direction selectivity of synaptic potentials in simple cells of the cat visual cortex. *Journal of Neurophysiology, 78* (5), 2772-2789.

Jin, J.Z., Wang, Y., Lashgari, R., Swadlow, H.A., & Alonso, J.M. (2009). Visual responses are faster in OFF than ON Visual channels. *Society for Neuroscience,*

Jin, J.Z., Wang, Y., Lashgari, R., Swadlow, H.A., & Alonso, J.M. (2011a). Faster thalamocortical processing for dark than light visual targets. *Journal of Neuroscience, 31*, 17471-17479.

Jin, J.Z., Wang, Y., Swadlow, H.A., & Alonso, J.M. (2011b). Population receptive fields of ON and OFF thalamic inputs to an orientation column in visual cortex. *Nature Neuroscience, 14*, 232-238.

Jin, J.Z., Weng, C., Yeh, C.I., Gordon, J.A., Ruthazer, E.S., Stryker, M.P., Swadlow, H.A., & Alonso, J.M. (2008). On and off domains of geniculate afferents in cat primary visual cortex. *Nature Neuroscience, 11* (1), 88-94.

Jones, J.P., & Palmer, L.A. (1987). An evaluation of the two-dimensional Gabor filter model of simple receptive fields in cat striate cortex. *Journal of Neurophysiology, 58* (6), 1233-1258.

Kandel, E.R., Schwartz, J.H., & T.M., J. (1991). Principles of Neural Science. (New York: McGraw-Hill.

Kaplan, E., Purpura, J., & Shapley, R.M. (1978). Contrast affects the transmission of visual information through the mammalian lateral geniculate nucleus *The Journal of Physiology, 391*, 21.

Kuffler, S.W. (1953). Discharge patterns and functional organization of mammalian retina. *Journal of Neurophysiology, 16* (1), 37-68.

Kuhlmann, L., & Vidyasagar, T.R. (2011). A computational study of how orientation bias in the lateral geniculate nucleus can give rise to orientation selectivity in primary visual cortex. *Frontiers in Systems Neuroscience, 5*, 81.

Levick, W.R. (1975). Form and function of cat retinal ganglion cells. *Nature, 254* (5502), 659-662.

Levick, W.R., Cleland, B.G., & Dubin, M.W. (1972). Lateral geniculate neurons of cat: retinal inputs and physiology. *Investigative Ophthalmology & Visual Science, 11* (5), 302-311.

Levick, W.R., & Thibos, L.N. (1980). Orientation bias of cat retinal ganglion cells. *Nature, 286* (5771), 389-390.

Malpeli, J.G. (1983). Activity of cells in area 17 of the cat in absence of input from layer a of lateral geniculate nucleus. *Journal of Neurophysiology, 49* (3), 595-610.

Malpeli, J.G., Lee, C., Schwark, H.D., & Weyand, T.G. (1986). Cat area 17. I. Pattern of thalamic control of cortical layers. *Journal of Neurophysiology, 56* (4), 1062-1073.

Martin, K.A., & Whitteridge, D. (1984). The relationship of receptive field properties to the dendritic shape of neurones in the cat striate cortex. *The Journal of Physiology, 356*, 291-302.

Martinez, L.M., & Alonso, J.M. (2001). Construction of complex receptive fields in cat primary visual cortex. *Neuron, 32* (3), 515-525.

Martinez, L.M., Alonso, J.M., Reid, R.C., & Hirsch, J.A. (2002). Laminar processing of stimulus orientation in cat visual cortex. *The Journal of Physiology, 540* (Pt 1), 321-333.

Martinez, L.M., Wang, Q., Reid, R.C., Pillai, C., Alonso, J.M., Sommer, F.T., & Hirsch, J.A. (2005). Receptive field structure varies with layer in the primary visual cortex. *Nature Neuroscience, 8* (3), 372-379.

Mastronarde, D.N. (1987a). Two classes of single-input X-cells in cat lateral geniculate nucleus. I. Receptive-field properties and classification of cells. *Journal of Neurophysiology, 57* (2), 357-380.

Mastronarde, D.N. (1987b). Two classes of single-input X-cells in cat lateral geniculate nucleus. II. Retinal inputs and the generation of receptive-field properties. *Journal of Neurophysiology, 57* (2), 381-413.

McLean, J., & Palmer, L.A. (1994). Organization of simple cell responses in the three-dimensional (3-D) frequency domain. *Visual Neuroscience, 11* (2), 295-306.

McLean, J., Raab, S., & Palmer, L.A. (1994). Contribution of linear mechanisms to the specification of local motion by simple cells in areas 17 and 18 of the cat. *Visual Neuroscience, 11* (2), 271-294.

Movshon, J.A. (1978). Hypercomplexities in the visual cortex. *Nature, 272* (5651), 305-306.

Movshon, J.A., Thompson, I.D., & Tolhurst, D.J. (1978a). Receptive field organization of complex cells in the cat's striate cortex. *The Journal of Physiology, 283*, 79-99.

Movshon, J.A., Thompson, I.D., & Tolhurst, D.J. (1978b). Spatial and temporal contrast sensitivity of neurones in areas 17 and 18 of the cat's visual cortex. *The Journal of Physiology, 283*, 101-120.

Movshon, J.A., Thompson, I.D., & Tolhurst, D.J. (1978c). Spatial summation in the receptive fields of simple cells in the cat's striate cortex. *The Journal of Physiology, 283*, 53-77.

Murthy, A., Humphrey, A.L., Saul, A.B., & Feidler, J.C. (1998). Laminar differences in the spatiotemporal structure of simple cell receptive fields in cat area 17. *Visual Neuroscience, 15* (2), 239-256.

Ohzawa, I., & Freeman, R.D. (1986a). The binocular organization of complex cells in the cat's visual cortex. *Journal of Neurophysiology, 56* (1), 243-259.

Ohzawa, I., & Freeman, R.D. (1986b). The binocular organization of simple cells in the cat's visual cortex. *Journal of Neurophysiology, 56* (1), 221-242.

Orban, G.A., Kennedy, H., & Maes, H. (1981). Response to movement of neurons in areas 17 and 18 of the cat: direction selectivity. *Journal of Neurophysiology, 45* (6), 1059-1073.

Palmer, L.A., & Davis, T.L. (1981). Receptive-field structure in cat striate cortex. *Journal of neurophysiology, 46* (2), 260-276.

Peters, A., & Payne, B.R. (1993). Numerical relationships between geniculocortical afferents and pyramidal cell modules in cat primary visual cortex. *Cerebral Cortex, 3* (1), 69-78.

Peterson, M.R., Li, B., & Freeman, R.D. (2004). The derivation of direction selectivity in the striate cortex. *The Journal of Neuroscience, 24* (14), 3583-3591.

Priebe, N.J., & Ferster, D. (2005). Direction selectivity of excitation and inhibition in simple cells of the cat primary visual cortex. *Neuron, 45* (1), 133-145.

Reichardt, W. (1961). Autocorrelation, a principle for evaluation of sensory information by the central nervous system. In: W.A. Rosenblith (Ed.) *Sensory communications* (pp. 303-318). New York: Wiley.

Reid, C., & Usrey, M. (2004). Functional connectivity in the pathway from retina to striate cortex. In: L.M. Chalupa, & J.S. Werner (Eds.), *The Visual Neuroscience* (London, England: The MIT press.

Reid, R.C., & Alonso, J.M. (1995). Specificity of monosynaptic connections from thalamus to visual cortex. *Nature, 378* (6554), 281-284.

Reid, R.C., Soodak, R.E., & Shapley, R.M. (1987). Linear mechanisms of directional selectivity in simple cells of cat striate cortex. *Proceedings of the National Academy of Sciences of the United States of America, 84* (23), 8740-8744.

Reid, R.C., Soodak, R.E., & Shapley, R.M. (1991). Directional selectivity and spatiotemporal structure of receptive fields of simple cells in cat striate cortex. *Journal of Neurophysiology, 66* (2), 505-529.

Romo, P.A., Wang, C., Zeater, N., Solomon, S.G., & Dreher, B. (2011). Phase sensitivities, excitatory summation fields, and silent suppressive receptive fields of single neurons in the parastriate cortex of the cat. *Journal of Neurophysiology, 106* (4), 1688-1712.

Rose, D., & Blakemore, C. (1974). An analysis of orientation selectivity in the cat's visual cortex. *Experimental Brain Research, 20* (1), 1-17.

Saul, A.B., & Humphrey, A.L. (1990). Spatial and temporal response properties of lagged and nonlagged cells in cat lateral geniculate nucleus. *Journal of Neurophysiology, 64* (1), 206-224.

Saul, A.B., & Humphrey, A.L. (1992). Temporal-frequency tuning of direction selectivity in cat visual cortex. *Visual Neuroscience, 8* (4), 365-372.

Schiller, P.H., Finlay, B.L., & Volman, S.F. (1976). Quantitative studies of single-cell properties in monkey striate cortex. I. Spatiotemporal organization of receptive fields. *Journal of Neurophysiology, 39* (6), 1288-1319.

Schiller, P.H., Sandell, J.H., & Maunsell, J.H. (1986). Functions of the ON and OFF channels of the visual system. *Nature, 322* (6082), 824-825.

Sclar, G., & Freeman, R.D. (1982). Orientation selectivity in the cat's striate cortex is invariant with stimulus contrast. *Experimental Brain Research, 46* (3), 457-461.

Sillito, A.M. (1975). The contribution of inhibitory mechanisms to the receptive field properties of neurones in the striate cortex of the cat. *J Physiol, 250* (2), 305-329.

Skottun, B.C., Bradley, A., Sclar, G., Ohzawa, I., & Freeman, R.D. (1987). The effects of contrast on visual orientation and spatial frequency discrimination: a comparison of single cells and behavior. *Journal of Neurophysiology, 57* (3), 773-786.

Skottun, B.C., De Valois, R.L., Grosof, D.H., Movshon, J.A., Albrecht, D.G., & Bonds, A.B. (1991). Classifying simple and complex cells on the basis of response modulation. *Vision Research, 31* (7-8), 1079-1086.

Skottun, B.C., & Freeman, R.D. (1984). Stimulus specificity of binocular cells in the cat's visual cortex: ocular dominance and the matching of left and right eyes. *Experimental brain research Experimentelle Hirnforschung Experimentation cerebrale, 56* (2), 206-216.

Solomon, S.G., & Lennie, P. (2007). The machinery of colour vision. *Nature Reviews Neuroscience, 8* (4), 276-286.

Somers, D.C., Nelson, S.B., & Sur, M. (1995). An emergent model of orientation selectivity in cat visual cortical simple cells. *The Journal of Neuroscience, 15* (8), 5448-5465.

Sompolinsky, H., & Shapley, R. (1997). New perspectives on the mechanisms for orientation selectivity. *Current Opinion in Neurobiology, 7* (4), 514-522.

Soodak, R.E. (1986). Two-Dimensional Modeling of Visual Receptive-Fields Using Gaussian Subunits. *Proceedings of the National Academy of Sciences of the United States of America, 83* (23), 9259-9263.

Stein, J.J., Johnson, S.A., & Berson, D.M. (1996). Distribution and coverage of beta cells in the cat retina. *The Journal of Comparative Neurology, 327* (4), 10.

Stone, J., & Dreher, B. (1982). Parallel processing of information in the visual pathways: A general principle of sensory coding? *Trends in Neurosciences, 5*, 441-446.

Stone, J., Dreher, B., & Leventhal, A. (1979). Hierarchical and parallel mechanisms in the organization of visual cortex. *Brain Research, 180* (3), 345-394.

Stone, J., & Fukuda, Y. (1974). Properties of cat retinal ganglion cells: a comparison of W-cells with X- and Y-cells. *Journal of Neurophysiology, 37* (4), 722-748.

Stone, J., & Hoffmann, K.P. (1972). Very slow-conducting ganglion cells in the cat's retina: a major, new functional type? *Brain Research, 43* (2), 610-616.

Tanaka, K. (1983). Cross-correlation analysis of geniculostriate neuronal relationships in cats. *Journal of Neurophysiology, 49* (6), 1303-1318.

Thompson, P.G., & Movshon, J.A. (1978). Storage of spatially specific threshold elevation. *Perception, 7* (1), 65-73.

Torre, V., & Poggio, T. (1978). A synaptic mechanism possibly underlying directional selectivity to motion. *Proceedings of the Royal Society of London. Series B, Biological Sciences, 202* (1148), 409-416.

Troyer, T.W., Krukowski, A.E., Priebe, N.J., & Miller, K.D. (1998). Contrast-invariant orientation tuning in cat visual cortex: thalamocortical input tuning and correlation-based intracortical connectivity. *The Journal of Neuroscience, 18* (15), 5908-5927.

Tusa, R.J., Palmer, L.A., & Rosenquist, A.C. (1978). The retinotopic organization of area 17 (striate cortex) in the cat. *J Comp Neurol, 177* (2), 213-235.

Ursino, M., La Cara, G.E., & Ritrovato, M. (2007). Direction selectivity of simple cells in the primary visual cortex: comparison of two alternative mathematical models. I: response to drifting gratings. *Computers in Biology and Medicine, 37* (3), 398-414.

Usrey, W.M., Reppas, J.B., & Reid, R.C. (1999). Specificity and strength of retinogeniculate connections. *Journal of Neurophysiology, 82* (6), 3527-3540.

Vidyasagar, T.R., & Heide, W. (1984). Geniculate orientation biases seen with moving sine wave gratings: implications for a model of simple cell afferent connectivity. *Experimental brain research. Experimentelle Hirnforschung. Experimentation cerebrale, 57* (1), 176-200.

Vidyasagar, T.R., Pei, X., & Volgushev, M. (1996). Multiple mechanisms underlying the orientation selectivity of visual cortical neurones. *Trends in Neurosciences, 19* (7), 272-277.

Wässle, H., Boycott, B.B., & Illing, R.B. (1981). Morphology and mosaic of on- and off-beta cells in the cat retina and some functional considerations. *Proceedings of the Royal Society B: Biological Sciences, 212* (1187), 177-195.

Watson, B.A., & Ahumada, J., Jr. Albert (1985). Model of human visual-motion sensing *Optics InfoBase: Journal of the Optical Society of America A, 2* (2), 21.

Wehmeier, U., Dong, D., Koch, C., & Van Essen, D. (1989). Modeling the visual system. In: C. Koch, & I. Segev (Eds.), *Methods in neuronal modeling* (Cambridge, MA: MIT Press.

Worgotter, F., & Koch, C. (1991). A detailed model of the primary visual pathway in the cat: comparison of afferent excitatory and intracortical inhibitory connection schemes for orientation selectivity. *The Journal of Neuroscience, 11* (7), 1959-1979.

Xu, X., Ichida, J., Shostak, Y., Bonds, A.B., & Casagrande, V.A. (2002). Are primate lateral geniculate nucleus (LGN) cells really sensitive to orientation or direction? *Visual Neuroscience, 19* (1), 97-108.

Appendix A. Equations

A.1. Model

Each neuron in the model is simulated as a low-pass temporal filter defined, in its simplest form, by:

$$\tau \frac{dO}{dt} = I - O \tag{A.1}$$

where:
O is the output of the neuron
I is the input of the neuron
τ is the time constant
t is time

The main variable in the model is membrane potential, p, at the initial segment of a neuron's axon. This is the potential that generates action potentials and is therefore referred here to as the generator potential. Equation A.1 can be rewritten using the generator potential as the output of the neuron and postsynaptic potential as the inputs (equation A.2). The growth rate of the generator potential depends on the postsynaptic potential, v_i, from k synapses driving the neuron ($i=1,2,\ldots,k$). The contribution of each postsynaptic potential is weighted by a constant, g_i, which reduces with the distance between the receptive fields of the neuron and its presynaptic driver. The generator potential growth rate also depends on a static polarisation, p_s, which is independent of the visual stimulus. The static polarisation is responsible, for example, for the high spontaneous firing rate in subcortical neurons and for the hyperpolarisation that produces the iceberg effect in the simple cells. Equation A.1 then becomes:

$$\tau \frac{dp}{dt} = \sum_{i=1}^{k} g_i v_i + p_s - p \tag{A.2}$$

The conversion from generator potential, *p*, to action potential rate, *a*, is shown in Figure 3.3 (taken from Carandini and Ferster (2000)) and can be described by equation A.3. This equation requires that action potential rate be proportionally related to positive generator potentials and zero for negative potentials:

$$\begin{aligned} a &= [g_{rect}\, p]^{+} \\ &= \begin{cases} g_{rect}\, p & p \geq 0 \\ 0 & p < 0 \end{cases} \end{aligned} \tag{A.3}$$

where a = action potential rate

p = generator potential (the difference between membrane potential and action potential threshold)

g_{rect} = gain of generator function (7.2 impulse/(s.mV))

Assume that Equation A.2 applies to a neuron in stage *z* of the model. I need to relate it to generator potentials in the previous stage, *z-1*. I make the simplest assumption: postsynaptic potential is proportional to impulse rate in the presynaptic neuron, and the conversion function is the inverse of that in Equation A.3 (any difference in the proportionality constants at the initial segment and the synapse can be absorbed into the gain g_i). The conversion from generator potential in a neuron at stage *z-1* to postsynaptic potential in the target neuron at stage *z* is then given by:

$$v(z) = [p(z-1)]^{+} \tag{A.4}$$

Equation A.2 then becomes:

$$\tau \frac{dp(z)}{dt} = \sum_{i=1}^{k} g_k [p_k(z-1)]^{+} + p_s(z) - p(z) \tag{A.5}$$

This equation can be generalized by including the dependency on time (*t*), and visual field location *(x, y)*, and by showing the sum term as a spatial convolution.

$$\tau(x,y,z) \frac{dp(t,x,y,z)}{dt} = g(x,y,z) * [p(t,x,y,z-1)]^{+} + p_s(z) - p(t,x,y,z) \tag{A.6}$$

where

$$g(x,y,z)*[p(t,x,y,z-1)]^{+}=\int_{w=-\infty}^{\infty}\int_{u=-\infty}^{\infty}g(x-u,y-w,z)[p(t,u,w,z-1)]^{+}dudw \quad \text{(A.7)}$$

The gain function, *g*, takes several forms depending on the stage. For the sub-cortical stages, this gain is the difference between centre and surround Gaussians. For computational simplicity, all sub-cortical spatial convergence is folded into the first stage. The gain function for the cortical stage is a single Gaussian function. The only difference between cortical stages is the gain constant. For the first cortical stages, this gain is the geniculocortical gain (g_{GC}) and for the later stages is the cortiocortical gain (g_{cort}). Thus:

$$g(x,y,z)=\begin{Bmatrix} g_{cen}e^{-(x^2+y^2)/r_{cen}^2}-g_{sur}e^{-(x^2+y^2)/r_{sur}^2} & z=1 \\ \delta(x)\delta(y) & z=2,3,4 \end{Bmatrix} \quad \text{(A.8)}$$

$$g(x,y,z)=\begin{Bmatrix} g_{GC}e^{-(x^2+y^2)/r_{cort}^2} & z=5 \\ g_{cort}e^{-(x^2+y^2)/r_{cort}^2} & z=6,7 \end{Bmatrix} \quad \text{(A.9)}$$

where g_{cen} and g_{sur} are the gain of the centre and surround mechanisms in the subcortical stages and r_{cen} and r_{sur} are the radius of the centre and surround, respectively. r_{cort} stands for the radius of receptive fields in the cortical stages. δ is the Dirac delta function.

Equation A.6 needs some modifications for the sub-cortical stages. First, the input to photoreceptors is the visual stimulus, *s(t,x,y).* Second, the sign *n(x,y)*, of the driver depends on whether the neuron being modelled is on-centre or off-centre. Photoreceptors hyperpolarise to light and the first synapse for the on-centre channel is sign-inverting. For computational simplicity, I assume that the photoreceptors driving on-centre channels depolarise to light. The sign of the first term on the right of Equation A.10 is then positive for on-centre and negative for off-centre channels. Third, the neurons presynaptic to ganglion cells do not produce action potentials, so there is no rectification. Thus, substituting the sign and equation A.8 and A.9 in equation A.7, results in the following:

$$\tau(x,y,z)\frac{dp(t,x,y,z)}{dt}=\begin{Bmatrix} n(x,y)g(x,y,z)*s(t,x,y)+p_s(z)-p(t,x,y,z) & z=1 \\ p(t,x,y,z-1)+p_s(z)-p(t,x,y,z) & z=2,3 \\ [p(t,x,y,z-1)]^{+}+p_s(z)-p(t,x,y,z) & z=4 \end{Bmatrix} \quad \text{(A.10)}$$

The sub-cortical pathways can be divided into channels. Assume that there are *m* channels. The *i*th channel ($i=1,2,...,m$) is defined by the location of the middle of its receptive field, (x_i, y_i), its sign, $n_i = n(x_i, y_i)$, and its time constant:

$$\tau_i = \begin{Bmatrix} \tau_{on} & \text{on-centre} \\ \tau_{off} & \text{off-centre} \end{Bmatrix} \quad \text{(A.11)}$$

It is convenient, then, to recast the equations for the sub-cortical stages using subscripts rather than function arguments:

$$\tau_i \frac{dp_i(t,z)}{dt}=\begin{Bmatrix} n_i g(x_i,y_i,z)*s(t,x_i,y_i,z)+p_s(z)-p_i(t,z) & z=1 \\ p_i(t,z-1)+p_s(z)-p_i(t,z) & z=2,3 \\ [p_i(t,z-1)]^{+}+p_s(z)-p_i(t,z) & z=4 \end{Bmatrix} \quad \text{(A.12)}$$

The input to the cortex is then spatially discrete:

$$p(t,x,y,4)=\sum_{i=1}^{m} p_i(t,4)\delta(x-x_i)\delta(y-y_i) \quad \text{(A.13)}$$

A further simplification can be achieved by considering sub-cortical steady-state potentials. I assume that these potentials are above threshold in order to produce the spontaneous impulse rate observed in ganglion and geniculate cells (Kaplan et al., 1978, Stone & Fukuda, 1974) and that the steady-state potentials are the same for all stages. Steady-state potential is calculated by setting the stimulus and time derivatives to zero. Solution of equation A.12 then yields:

$$p_s(z)=0 \quad z=2,3,4 \quad \text{(A.14)}$$

Denoting the cortical time constant as τ_{cort}, the model's defining equations can then be stated in their final form:

$$\tau_i \frac{dp_i(t,z)}{dt} = \begin{Bmatrix} n_i g(x_i, y_i, z) * s(t, x_i, y_i, z) + p_s(z) - p_i(t,z) & z = 1 \\ p_i(t, z-1) - p_i(t,z) & z = 2,3 \\ [p_i(t, z-1)]^+ - p_i(t,z) & z = 4 \end{Bmatrix} \qquad \text{(A.15)}$$

$$\tau_{cort} \frac{dp_i(t,x,y,z)}{dt} = g(x,y,z) * [p(t,x,y,z-1)]^+ + p_s(z) - p(t,x,y,z) \quad z = 5,6,7$$

A.2. Resting activity

Resting activity in a neuron is an important parameter because it determines whether signals passing through the neuron are rectified. Resting impulse rate in each stage of the model is determined, in part, by the static depolarisation, p_s. The following values are assigned to this parameter:

$$p_s(z) = \begin{cases} p_{photo} & z = 1 \\ 0 & z = 2,3,4 \\ p_{hyp} & z = 5 \\ p_{dep} & z = 6 \\ 0 & z = 7 \end{cases} \qquad \text{(A.16)}$$

where p_{photo} and p_{dep} are assumed to be positive and p_{hyp} to be negative. Resting activity can be determined by setting both the stimulus and derivatives to zero in equation A.15.

$$0 = \begin{Bmatrix} 0 + p_s(z) - p_i(\infty, z) & z = 1 \\ p_i(\infty, z-1) - p_i(\infty, z) & z = 2,3 \\ [p_i(\infty, z-1)]^+ - p_i(\infty, z) & z = 4 \end{Bmatrix} \qquad \text{(A.17)}$$

$$\Rightarrow p_i(\infty, z) = p_{photo} \quad z = 1,2,3,4$$

$$\begin{aligned} &0 = g(x,y,z) * p_{photo} + p_{hyp} - p(\infty, x, y, z) \quad \Rightarrow \\ &p(\infty, x, y, z) = g(x,y,z) * p_{photo} + p_{hyp} \\ &p(\infty, x, y, z) = g_{GC} p_{photo} \sum_i e^{-((x_i - x)^2 + (y_i - y)^2)/r_{cort}^2} + p_{hyp}(x,y) \quad z = 5 \end{aligned} \qquad \text{(A.18)}$$

The static hyperpolarisation p_{hyp} in stage 5 is set sufficiently negative that the resting potential is also negative. This ensures that cells in that stage, the first cortical stage,

have no spontaneous impulse rate, in keeping with most simple cells (Rose & Blakemore, 1974). Thus, term $[p(t,x,y,z-1)]^+$ in Equation A.15 is zero:

$$p(\infty,x,y,z)=\begin{Bmatrix} p_{dep} & z=6 \\ g(x,y,z)*p_{dep}=\pi r_{cort}^2 g_{cort} p_{dep} & z=7 \end{Bmatrix} \quad \text{(A.19)}$$

From Equation A.3, the resting impulse rate in those cells that produce action potentials is:

$$a(\infty,x,y,z)=\begin{Bmatrix} 0 & z=1,2 \\ g_{rect} p_{photo} & z=3,4 \\ 0 & z=5 \\ g_{rect} p_{dep} & z=6 \\ \pi r_{cort}^2 g_{cort} g_{rect} p_{dep} & z=7 \end{Bmatrix} \quad \text{(A.20)}$$

A.3. Stimuli

There is no surround antagonism in the basic model. By way of compensation, stimuli are defined in terms of local contrast rather than luminance. Local contrast is obtained by finding the difference between local and background luminance, and dividing the difference by background luminance. Three types of stimulus are used: gratings, spots, and bar stimuli.

Grating stimuli

The equation for a grating is:

$$s(t,x,y)=\begin{Bmatrix} c\cos(\omega_t t+\sin(\theta)\omega_s x+\cos(\theta)\omega_s y) & \text{drifting} \\ c\cos(\omega_t t)\cos(\sin(\theta)\omega_s x+\cos(\theta)\omega_s y+\phi) & \text{contrast-reversing} \end{Bmatrix} \quad \text{(A.21)}$$

where

c = contrast

ω_s = spatial frequency (radians/deg)

ω_t = temporal frequency (radians/s)

θ = orientation (radians)

φ = spatial phase (radians)

Bar and spot stimulus

These stimuli are rectangular functions of time, and are presented in different locations in the visual field. So, the stimulus is equal to the contrast during the stimulus presentation and in the visual field area covered by the stimulus, otherwise it is zero:

$$s(t, x, y) = c \tag{A.22}$$

A.4. Analytical solution

The static polarisation in the sub-cortical channels is assumed to elevate the generator potential above threshold. There is a range of contrasts, therefore, for which the impulse rate is positive and signals up to, and including, the generator potential in first-stage cortical cells are linearly processed. The equations representing this processing can be solved analytically. I here derive the solution because it provides a check on the numerical solution, and because it proves important is estimating the gain, g_{GC} , from geniculate to cortex. I start by evaluating the convolution of the stimulus with the sub-cortical spatial weighting function (Equation A.15). Assume that the stimulus is a drifting grating with optimal orientation:

$$s(t, x, y) = c\cos(\omega_t t + \omega_s x) \tag{A.23}$$

and that the sub-cortical pathway of interest is channel *i*. Consider first the centre mechanism:

$$g(x, y, 1) = g_{cen} e^{-(x^2+y^2)/r_{cen}^2} \tag{A.24}$$

The convolution is:

$$\begin{aligned} conv_{cen} &= g(x_i, y_i, 1) * s(t, x_i, y_i) \\ &= \int_{-\infty}^{\infty}\int_{-\infty}^{\infty} g(x_i - x, y_i - y, 1) s(t, x, y) dx dy \\ &= cg_{cen} \int e^{-(x_i - x)^2 / r_{cen}^2} \cos(\omega_t t + \omega_s x) dx \int e^{-(y_i - y)^2 / r_{cen}^2} dy \\ &= c\sqrt{\pi} r_{cen} g_{cen} \int e^{-(x_i - x)^2 / r_{cen}^2} \cos(\omega_t t + \omega_s x) dx \end{aligned} \tag{A.25}$$

Changing the integration variable to $u = x - x_i$ and expanding the resulting cosine term yields:

$$\begin{aligned} conv_{cen} &= c\sqrt{\pi} r_{cen} g_{cen} \cos(\omega_t t + \omega_s x_i) \int e^{-u^2 / r_{cen}^2} \cos(\omega_s u) du \\ &= c\pi r_{cen}^2 g_{cen} \cos(\omega_t t + \omega_s x_i) e^{-(r_{cen}\omega_s)^2 / 4} \end{aligned} \tag{A.26}$$

Including the surround, the convolution is:

$$conv = cg_{sub} \cos(\omega_t t + \omega_s x_i) \tag{A.27}$$

where

$$g_{sub} = \pi r_{cen}^2 g_{cen} e^{-(r_{cen}\omega_s)^2/4} - \pi r_{sur}^2 g_{sur} e^{-(r_{sur}\omega_s)^2/4} \tag{A.28}$$

is the subcortical contrast sensitivity. The first line of Equation A.15 then becomes

$$\tau_i \frac{dp_i(t,1)}{dt} = p_{photo} + cg_{sub} n_i \cos(\omega_t t + \omega_s x_i) - p_i(t,1) \tag{A.29}$$

Given that the sub-cortical channel is a cascade of temporal filters, it is convenient to switch from the time to the frequency domain. Denoting temporal frequency by ω the Fourier transform of $\cos(\omega_t t + \omega_s x_i)$ is

$$\begin{Bmatrix} e^{j\omega_s x_i} \pi\delta(\omega - \omega_t) & \omega \geq 0 \\ e^{-j\omega_s x_i} \pi\delta(\omega + \omega_t) & \omega < 0 \end{Bmatrix} \tag{A.30}$$

where $j = \sqrt{-1}$. The transform for negative ω is the conjugate of that for positive ω (in common with all real functions of time), and it is therefore sufficient to consider

only the latter. Denoting Fourier transforms in upper case, the transform of Equation A.29 is:

$$j\tau_i \omega P_i(\omega,1) = p_{photo}\pi\delta(\omega) + cg_{sub} n_i e^{j\omega_s x_i}\pi\delta(\omega-\omega_t) - P_i(\omega,1) \tag{A.31}$$

Thus

$$P_i(\omega,1) = \frac{p_{photo}\pi\delta(\omega) + cg_{sub} n_i e^{j\omega_s x_i}\pi\delta(\omega-\omega_t)}{1+j\tau_i\omega} \tag{A.32}$$

Similarly, the transform of Equation A.15 for the remaining sub-cortical stages is given by

$$\frac{P_i(\omega,z)}{P_i(\omega,z-1)} = \frac{1}{1+j\tau_i\omega} \quad z = 2,3,4 \tag{A.33}$$

Multiplying the left sides of the four transformed equations yields

$$\begin{aligned} P_i(\omega,4) &= \frac{p_{photo}\pi\delta(\omega) + cg_{sub} n_i e^{j\omega_s x_i}\pi\delta(\omega-\omega_t)}{(1+j\tau_i\omega)^4} \\ &= p_{photo}\pi\delta(\omega) + \frac{cg_{sub} n_i e^{j\omega_s x_i}\pi\delta(\omega-\omega_t)}{(1+j\tau_i\omega)^4} \end{aligned} \tag{A.34}$$

because the first term is non-zero only at $\omega=0$. From Equation A.13, the input to stage 5 is

$$P(\omega,x,y,4) = \sum_{i=1}^{m} P_i(\omega,4)\delta(x-x_i)\delta(y-y_i) \tag{A.35}$$

Transforming Equation A.15 and then applying Equation A.35, generator potential in the first cortical stage is

$$\begin{aligned} P(\omega,x,y,5) &= p_{hyp}\pi\delta(\omega)\frac{g(x,y,5)*P(\omega,x,y,4)}{1+j\tau_{cort}\omega} \\ &= p_{hyp}\pi\delta(\omega) + \frac{\sum g(x-x_i,y-y_i,5)P_i(\omega,4)}{1+j\tau_{cort}\omega} \end{aligned} \tag{A.36}$$

Substituting Equation A.9 gives

$$P(\omega,x,y,5) = p_{hyp}\pi\delta(\omega) + \frac{\sum g_{GC} g_i P_i(\omega,4)}{1+j\tau_{cort}\omega} \tag{A.37}$$

where the attenuation due to cortical spatial factors is

$$g_i = e^{-((x-x_i)^2+(y-y_i)^2)/r_{cort}^2} \tag{A.38}$$

Substitution of Equation A.34 into Equation A.37 then yields

$$\begin{aligned} P(\omega,x,y,5) &= p_{hyp}\pi\delta(\omega) + \sum \frac{g_{GC} g_i}{1+j\tau_{cort}\omega} \frac{p_{photo}\pi\delta(\omega) + cg_{sub} n_i e^{j\omega_s x_i}\pi\delta(\omega-\omega_t)}{(1+j\tau_i\omega)^4} \\ &= (p_{hyp} + p_{photo}\sum g_{GC} g_i)\pi\delta(\omega) + \sum \frac{cg_{sub} n_i e^{j\omega_s x_i} g_{GC} g_i \pi\delta(\omega-\omega_t)}{(1+j\tau_i\omega)^4(1+j\tau_{cort}\omega_t)} \end{aligned} \tag{A.39}$$

The Fourier transform thus has two components:

$$P(\omega,x,y,5) = \left\{ \begin{array}{ll} p_{photo} g_{GC} \sum g_i + p_{hyp} & \text{Mean } (\omega=0) \\ \dfrac{cg_{sub} g_{GC}}{1+j\tau_{cort}\omega_t} \sum \dfrac{g_i n_i e^{j\omega_s x_i}}{(1+j\tau_i\omega_t)^4} & \text{Fundamental } (\omega=\omega_t) \end{array} \right\} \tag{A.40}$$

Appendix B. Parameter Settings

Model parameters were estimated from empirical studies of the cat's visual system at an eccentricity of 11°. I chose this eccentricity because the centre and surround dimensions of the sub-cortical cells are derived from Saul and Humphrey (1990), who used a mean eccentricity of 11°. The following sections describe the model parameters and how they were set. Table B.1 provides a glossary of the parameters and their values.

B.1. Spatial parameters

Size of visual field patch

I assume a visual field patch of $2^{\circ} \times 2^{\circ}$ centred on the horizontal meridian. This size is intended to span a substantial fraction of a typical receptive field in primary visual cortex.

Retinal magnification factor

I use this value to convert from degrees of visual angle to a linear unit. Each degree equal 0.2 mm (Hughes, 1976). For example, the retinal patch has an eccentricity of 11 × 0.2 =2.2 mm.

Size of centre and surround mechanisms

Saul and Humphrey (1990) measured the receptive field size of non-lagged X-type geniculate neurons in cat, at a mean eccentricity of 11°. The centre and surround radii were found to be 0.4° and 1.13° respectively.

Distance between same sign X-type ganglion cells

The distance between same-sign X cells and between opposite-sign cells were calculated from Stein et al. (1996) and Wässle et al. (1981). Stein et al. (1996) estimated the density of beta cells along the nasotemporal axis of the retina (Figure B.1). The density of beta cells in this Figure at 11° (2.2 mm) eccentricity is 1275

cells/mm^2 or 51 cells/deg^2 (1275 x (0.2)^2=51 cells/deg^2). Assuming there are equal numbers of the two signs of cells, there are $\sqrt{51/2} = 5$ same-sign X cells in one degree. Therefore, the distance between same-sign cells is 1/5=0.2 degree.

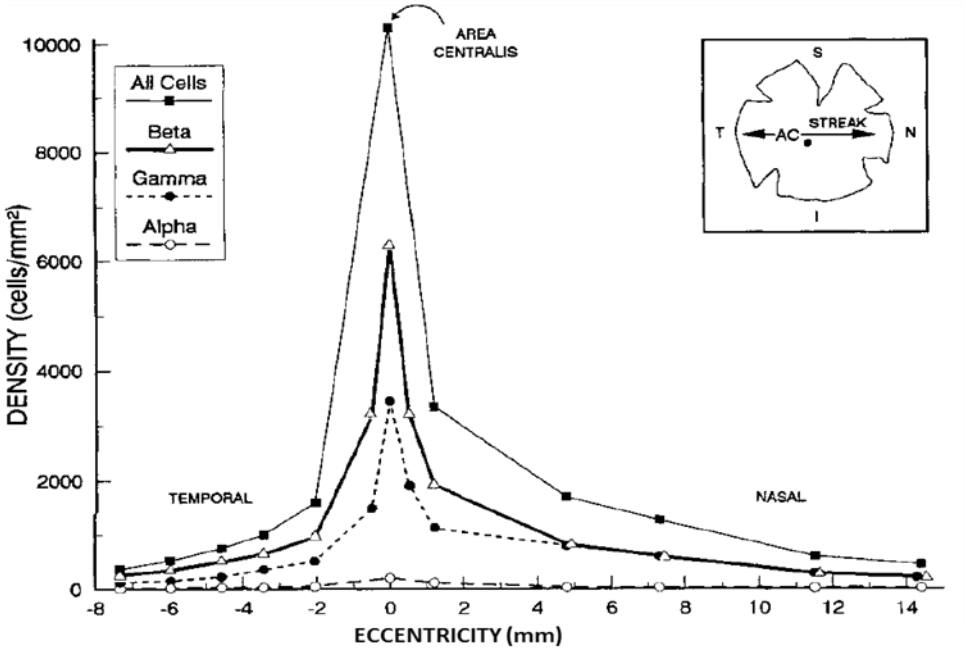

Figure B.1: Density of all types of ganglion cells versus eccentricity (Stein et al., 1996). This graph is used to calculate the distance between beta ganglion cells at an eccentricity of 11° (2.2 mm).

The 6-channel model assumes 3 ganglion cells of the same centre sign and 3 cells of the opposite sign. The distance between ganglion cells of the same sign can be as small as 0.2°, as described above, but can also be much larger, as indicated by the radius of the cortical cell receptive field. I chose a compromise distance of 0.75°: this produces an elongated subfield that largely fits into the 2° × 2° receptive field patch.

Distance between opposite-sign X-type ganglion cells

Wässle et al. (1981) measured nearest neighbour distances for both on- and off-centre beta cells. The mean distance between nearest neighbours was 43 µm, between on-centre cells 90 µm, and between off-centre cells 85 µm, at an eccentricity of 33˚ (Figure B.2).

Their results show that the distance between same-sign cells is almost independent of sign while the distance between two opposite-sign cells is about half of the distance between same-sign cells. If I assume that there is the same relationship between cells at the eccentricity of 11°, the distance between opposite-sign cells is 0.1°.

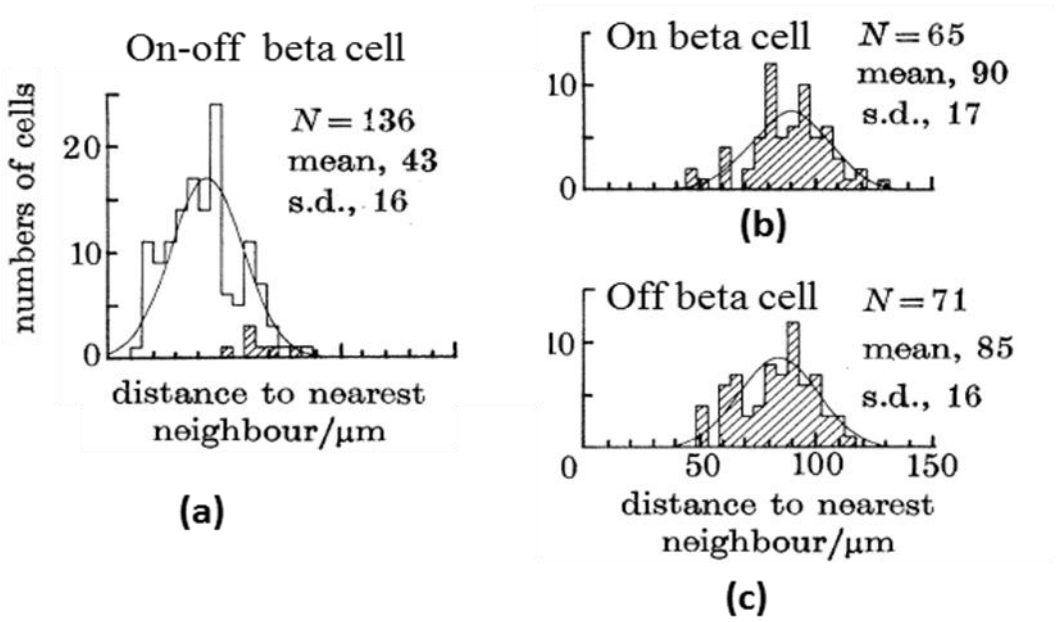

Figure B.2: Distribution of the distance of each retinal ganglion cell from its nearest neighbor in a morphological study. (a) Nearest neighbour beta (X) cells and (b,c) same-signed beta cells. Almost all nearest neighbours are of opposite sign (Wässle et al., 1981).

Length of cortical cell receptive field

Spatial spread of the Gaussian function from LGN stage to first cortical stage and between cortical stages was based on the length of the cortical cell receptive field measured by Gardner et al. (1999) work. The mean value of the measured subfields from Figure B.3 is 5.5°, giving a radius of 2.75°.

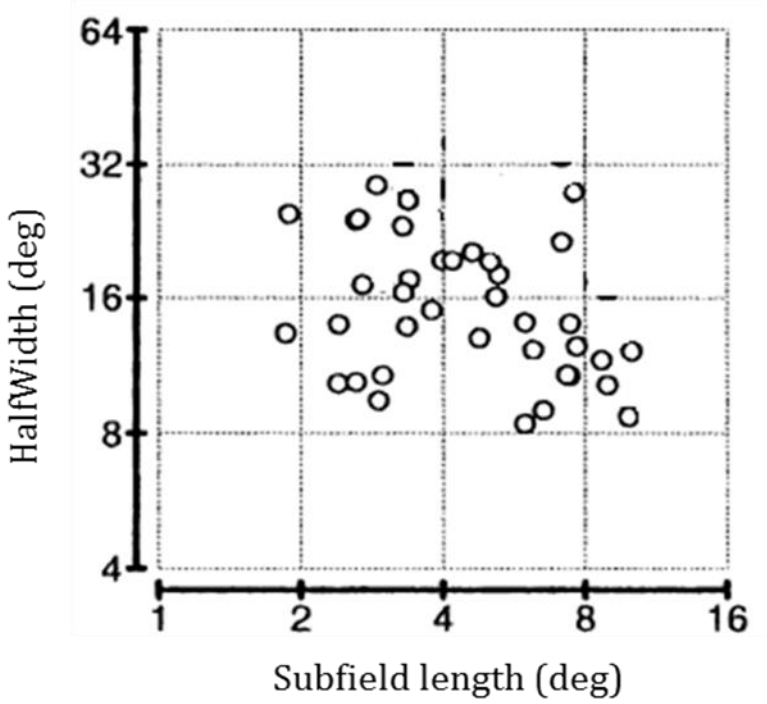

Figure B.3: Orientation tuning halfwidth versus measured length of the subfield for simple cells (Gardner et al., 1999). The geometric mean of the subfield length is calculated from this graph to set the length of the cortical neurons of the model.

Cortical magnification factor

This factor, 0.45 mm^2/deg^2 is taken from the measurements of Tusa et al. (Tusa, Palmer & Rosenquist, 1978) at 11° eccentricity along the horizontal meridian.

Cortical density of neurons

Beaulieu and Colonnier (Beaulieu & Colonnier, 1983) found 78,440 neurons under each mm^2 of binocular cortex. To obtain the linear cell density in the model we apply the following operations. First, this value is multiplied by the cortical magnification factor to convert it to degrees. Second, the model contains only excitatory neurons; assuming that all other neurons contain GABA, we multiply by 0.794 to eliminate them (Gabbott & Somogyi, 1986). Third, we divide by 3 to obtain the density per stage. Finally, we assume that neurons are arranged in a square array and therefore take the square root to find the linear density. The result is $\sqrt{78,440 \times 0.45 \times 0.794/\ 3} = 97$ cells deg^{-1} stage^{-1}.

B.2. Temporal parameters

Cortical time constant, τ

There is a problem in estimating the time constant for model cells: the modelled neurons are inhomogeneous in their temporal properties. Photo-transduction, for example, includes the time required for a series of reactions not present in following cells. I adopt, therefore, a pragmatic approach for finding the time constant of the neurons. The model is a series of a first-order low-pass filters and the time constant can be estimated from this series.

The Laplace transform of the differential equation (Equation A.1) is:

$$\frac{O}{I} = \frac{1}{1+\tau s} \tag{B.1}$$

For a series of *n* low-pass filters, the Laplace transform is:

$$\frac{O}{I} = (\frac{1}{1+\tau s})^n = \frac{(1/\tau)^n}{(\frac{1}{\tau}+s)^n} \tag{B.2}$$

The impulse response of this function is given by $I = 1$:

$$O = \frac{(1/\tau)^n}{(\frac{1}{\tau}+s)^n} \tag{B.3}$$

Or in the time domain:

$$O(t) = (\frac{1}{\tau})^n \frac{t^{n-1}}{(n-1)!} e^{-\frac{1}{\tau}t} \tag{B.4}$$

To find the peak of this function, the derivative is set to zero. So, the peak time of the impulse response is *τ(n-1)*. Simple cell impulse responses peak as early as 40 ms (DeAngelis et al., 1993a). Thus, for the first stage cortical cell (n=5), 4τ=40 ms which give a time constant of 10 ms for each stage. Therefore, the time constant of cortical cells was set at 10 ms.

Sub-cortical time constant

It has recently been shown that off-centre X-type geniculate cells lead their on-centre neighbours (Jin et al., 2009, Jin et al., 2011a). At an average of 7° eccentricity, the leading edge of the response of off-X LGN cells was, on average, 3 ms faster than on-X cell (Figure B.4). I set time constants in the two sub-cortical channels as follows: τ_{off} = 9 ms; τ_{on} = 11 ms. Examination of the response of the model in the LGN stage of the model (Chapter 5, impulse response) shows that the model approximates the empirical finding.

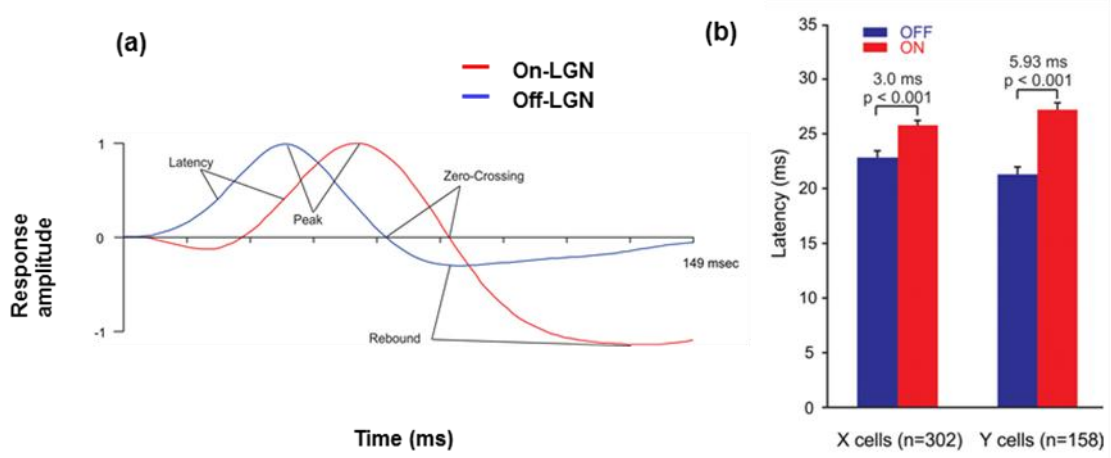

Figure B.4: (a) Time course response of an on- and off-channel X geniculate cell at an eccentricity of 7° with a spot stimulus. The off-geniculate cell is faster than the on-geniculate cell. (b) Off-geniculate cells have shorter response latency than on-geniculate cells. Average latency difference in the X-pathway is 3 ms (Jin et al., 2009, Jin et al., 2011a).

B.4. Intensive parameters

Generator gain

The form of the generator function (Figure 3.3) and its gradient, $g_{\text{rect}} = 7.2$ Hz/mV, are taken directly from the work of Carandini and Ferster (2000).

Geniculate contrast sensitivity

This parameter is defined as the peak sensitivity of the centre mechanism's spatial profile. It can be calculated by integrating the centre mechanism's spatial profile over both dimensions:

$$output = \int_{-\infty}^{\infty}\int S(x,y)G(x,y)dxdy \tag{B.5}$$

where

S(x,y): stimulus, which is uniform with an amplitude of *c*

G(x,y): weighting function representing the centre mechanism

The output is:

$$\begin{aligned} output &= \int_{-\infty}^{\infty}\int cg_{cen}e^{-(x^2+y^2)/r_{cen}^2}dxdy \\ &= cg_{cen}\int e^{-x^2/r_{cen}^2}dx\int e^{-y^2/r_{cen}^2}dx \\ &= cg_{cen}\sqrt{\pi}r_{cen}\sqrt{\pi}r_{cen} = cg_{cen}\pi r_{cen}{}^2 \end{aligned} \tag{B.6}$$

The contrast sensitivity of X-type ganglion cell centre mechanisms has a geometric mean of 620 Hz/contrast-unit (Figure B.5 (a)) for a 2 Hz stimulus. The contrast sensitivity of the LGN cells can be calculated by the attenuation between retina and geniculate at low contrast, 0.73 (Figure B.5 (b)). Contrast sensitivity is the amplitude of the fundamental Fourier component of the impulse rate divided by the stimulus contrast. As a result:

$$cg_{cen}\pi r_{cen}^{\ 2} = 620 \times 0.73 = 450$$
$$g_{cen} = \frac{450}{c\pi r_{cen}^{\ 2}} \text{Hz.contrast-unit}^{-1}.\text{deg}^{-2} \quad \text{(B.7)}$$

In order to convert this to potential, I need to divide the value by the slope of the conversion between membrane potential and impulse rate which is g_{rect} (Figure 3.3).

$$g_{cen} = \frac{450}{g_{rect} c\pi r_{cen}^{\ 2}} \text{mV.contrast-unit}^{-1}.\text{deg}^{-2} \quad \text{(B.8)}$$

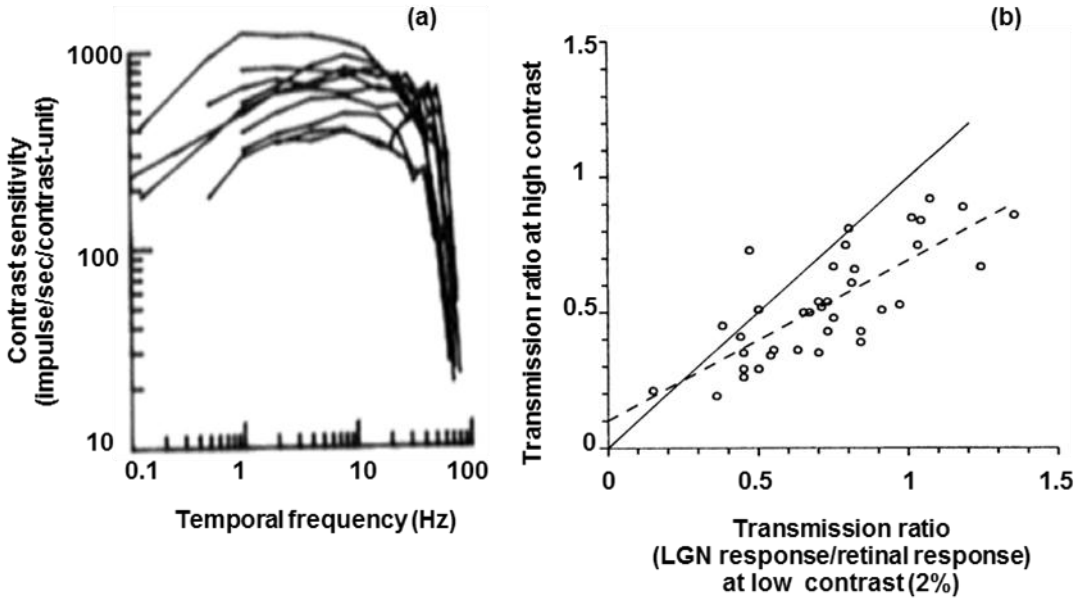

Figure B.5: (a) Centre mechanism response of X ganglion cells. The geometric mean of the contrast sensitivity of the centre mechanism of X ganglion cells is 620 Hz/contrast-unit (Frishman, Freeman, Troy, Schweitzer-Tong & Enroth-Cugell, 1987) (b) the ratio of the LGN response to retinal response at low contrast is the mean of all points projected on the horizontal axis, which is 0.73 (Kaplan et al., 1978)).

Cortical contrast sensitivity

The contrast sensitivity of stage 1 cortical cells is best determined from the responses of simple cells to gratings of optimal orientation and spatial frequency. I used the membrane potential measurements of Carandini and Ferster (2000) because they avoid the complications of action potential threshold (Figure B.6a). Data from these three cells are pooled together in Figure B.6b and the gradient of the regression line is

70 mV/contrast-unit. The geniculocortical gain, g_{GC} , was calculated by setting the fundamental amplitude in Equation A.40 to this value, and then solving for g_{GC} .

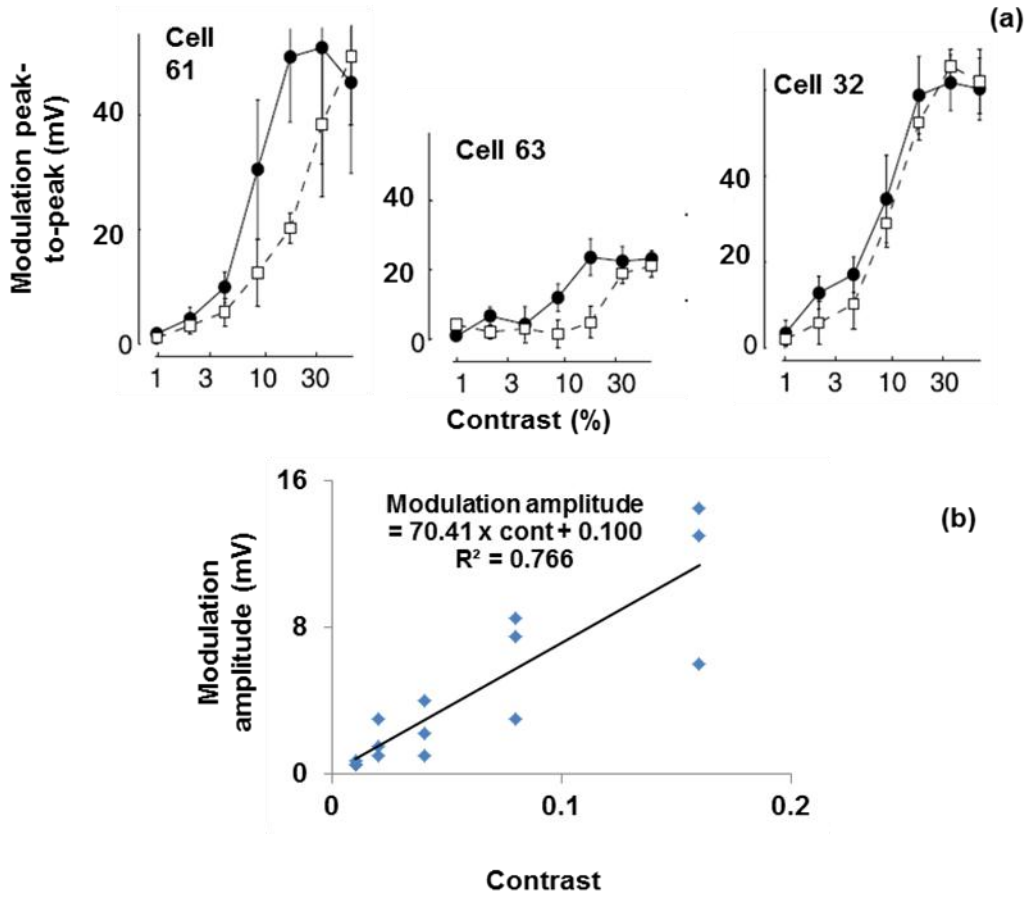

Figure B.6: (a) Contrast response of three simple cells for adaptation to low contrast of 1% (filled circle) and for adaptation to a high contrast of 47% (open circle) (Carandini & Ferster, 2000). (b) Data for the low contrast are pooled together to find the contrast sensitivity for simple cells in the first cortical stage of the model. This contrast sensitivity is used for finding the geniculocortical gain (g_{GC}).

Surround contrast sensitivity

I use Saul and Humphrey's (1990) measurements of mechanism strength, $(r_{sur}^2 g_{sur}) / (r_{cen}^2 g_{cen}) = 0.77$.

Static polarisation of subcortical levels

The constant value $p_s(z)$ in equation A.15 is the static polarisation, and equals the difference between resting membrane potential and threshold. This value was set to $14 / g_{rect} = 1.94$, which is the ratio of the spontaneous activity of LGN X-cells (Kaplan et al., 1978) to generator gain (Carandini & Ferster, 2000).

Static hyperpolarisation

This parameter was estimated from the work of Anderson et al. (2000b). From their Table 1, the median difference between threshold and resting potential in nine simple cells is -9 mV. Equation A.40 was solved for p_{hyp} by setting the left side $p(\infty, x, y, z)$ to this value.

Static depolarisation

Cells in primary visual cortex have a mean spontaneous impulse rate of 3.1 Hz (Rose and Blakemore, 1974). From Equation A.20, the mean impulse rate in model cortical cells is:

$$\frac{(1+g_{cort}\pi r_{cort}^2)p_{dep}g_{rect}}{3} = 3.1$$
$$\text{thus} \quad g_{dep} = \frac{3*3.1}{(1+g_{cort}\pi r_{cort}^2)g_{rect}} = 0.646 \tag{B.9}$$

Intracortical gain

There is little evidence for consistent contrast sensitivity differences between simple and complex cells (Dean, 1981). I therefore assumed unity gain between one cortical stage and the next. The parameter g_{cort} is then given by:

$$\iint g_{cort} e^{-(x^2+y^2)/r_{cort}^2} dxdy = \pi r_{cort}^2 g_{cort} = 1$$
$$\Rightarrow g_{cort} = 1/(\pi r_{cort}^2) \tag{B.10}$$

Table B.1. Glossary of symbols and their values

Symbol	Parameter	Value	Unit
c	Contrast	Variable	None
g_{cen}	Centre mechanism contrast sensitivity	62	mV contrast-unit^{-1}
g_{cort}	Intracortical gain	1	None
g_{GC}	Geniculocortical gain	4.21 (2 channels); 1.47 (6 channels)	None
g_{sur}	Surround mechanism contrast sensitivity	48	mV contrast-unit^{-1}
g_{rect}	Gain of generator function	7.2	Hz/mV
i	Index of sub-cortical channel	1, 2, …, m	None
m	Number of sub-cortical channels	Variable	None
n_i	Sign of ith sub-cortical channel	1 (on-channel); -1 (off-channel)	None
ω_s	Stimulus spatial frequency	Variable	radians/deg
ω_t	Stimulus temporal frequency	$2\pi \times 2$	radians/s
p	Generator potential	Variable	mV
p_{dep}	Static polarisation, cortical stages 2, 3	0.646	mV
p_{hyp}	Static polarisation, cortical stage 1	$-25.5 \quad (x = y = 0)$	mV
p_i	Generator potential in ith sub-cortical channel	Variable	mV
p_{photo}	Sub-cortical static polarisation	1.94	mV
p_s	Static polarisation	Variable	mV
r_{cen}	Radius of centre mechanism	0.4	deg
r_{cort}	Radius of cortical convergence	2.8	deg
r_{sur}	Radius of surround mechanism	1.1	deg
t	Time	Variable	s
τ_{cort}	Time constant of cortical cells	10	ms
τ_i	Time constant in ith sub-cortical channel	τ_{on} (on-channel); τ_{off} (off-channel);	ms
τ_{off}	Time constant of off-centre cells	9	ms
τ_{on}	Time constant of on-centre cells	11	ms
θ	Stimulus orientation	Variable	radians
x	Horizontal position in visual	Variable	deg

	field		
x_i	Horizontal position of channel *i*	Variable	deg
y	Vertical position in visual field	Variable	deg
y_i	Vertical position of channel *i*	Variable	deg
z	Index of processing stage	1, 2, …, 7	None

Appendix C. Publications

There follows a list of publications resulting from the work described in this thesis.

Journal papers

Hesam Shariati, N. Freeman A.W. (2012) A multi-stage model for fundamental functional properties in primary visual cortex. *PLoS ONE.*7(4). e34466

Abstracts and conference proceedings

Hesam Shariati, N. Freeman, A. W. Computational mechanisms underlying signal processing in primary visual cortex. *32nd Annual Meeting of Australian Neuroscience Society.* Feb 2012, Gold Coast, Australia.

Hesam Shariati, N. Freeman, A. W. A model for fundamental functional properties in primary visual cortex. 5th Australian Workshop on Computational Neuroscience, Dec 2011, Sydney, Australia.

Hesam Shariati, N. Freeman, A. W. A model for neuronal properties in primary visual cortex. *31st Annual Meeting of Australian Neuroscience Society.* Feb 2011, Auckland, New Zealand.

Hesam Shariati, N. Freeman, A. W. Modeling the functional properties of cells in primary visual cortex. *Bosch Young Investigator's Symposium*. Nov 2010, University of Sydney.

Freeman, A. W. Hesam Shariati, N. A model for functional diversity in primary visual cortex. *40th Meeting of the Society for Neuroscience*, Nov 2010, San Diego, USA.

Hesam Shariati, N. Freeman, A. W. A model for signal processing in primary visual cortex. *30th Annual Meeting of Australian Neuroscience Society.* Feb 2010, Sydney, Australia.

Hesam Shariati, N. Freeman, A.W. A model for orientation selectivity, direction selectivity, and complex cells, in primary visual cortex. *39th Meeting of the Society for Neuroscience*, Oct 2009, Chicago, USA.